AEROSOL PROPAGATION EFFECTS

G. E. Caledonia, et al

Physical Sciences, Incorporated

Prepared for:

Office of Naval Research
Advanced Research Projects Agency

13 September 1974

SECURITY CLASSIFICATION OF THIS PAGE (When Data Entered)

REPORT DOCUMENTATION PAGE		READ INSTRUCTIONS BEFORE COMPLETING FORM
1. REPORT NUMBER	2. GOVT ACCESSION NO.	3. RECIPIENT'S CATALOG NUMBER AD/A-006676
4. TITLE (and Subtitle) AEROSOL PROPAGATION EFFECTS		5. TYPE OF REPORT & PERIOD COVERED FINAL - 1/15/74-9/14/74
		6. PERFORMING ORG. REPORT NUMBER PSI TR-13
7. AUTHOR(s) G. E. Caledonia, J. D. Teare		8. CONTRACT OR GRANT NUMBER(s) N00014-74-C-0254
9. PERFORMING ORGANIZATION NAME AND ADDRESS Physical Sciences Inc., 18 Lakeside Office Park, Wakefield, MA 01880		10. PROGRAM ELEMENT, PROJECT, TASK AREA & WORK UNIT NUMBERS ARPA Order No. 2439
11. CONTROLLING OFFICE NAME AND ADDRESS Office of Naval Research, Department of the Navy, Arlington, Va. 22217		12. REPORT DATE September 13, 1974
		13. NUMBER OF PAGES 96
14. MONITORING AGENCY NAME & ADDRESS(if different from Controlling Office)		15. SECURITY CLASS. (of this report) Unclassified
		15a. DECLASSIFICATION/DOWNGRADING SCHEDULE

16. DISTRIBUTION STATEMENT (of this Report)

Approved for public release; distribution unlimited

17. DISTRIBUTION STATEMENT (of the abstract entered in Block 20, if different from Report)

18. SUPPLEMENTARY NOTES

19. KEY WORDS (Continue on reverse side if necessary and identify by block number)

Atmospheric Aerosols
Laser Propagation
Thermal Blooming
Vaporization
Thermal Conduction
Absorption

20. ABSTRACT (Continue on reverse side if necessary and identify by block number)

A model for the prediction of the temperature and vapor fields created about a small water droplet undergoing irradiation by a laser beam has been developed. Time dependent and steady state solutions of the model are discussed, as well as the possible effects of a number of aerosol properties not included in the model. Estimates of characteristic phase shifts to be expected in propagating through

DD FORM 1 JAN 73 1473 EDITION OF 1 NOV 65 IS OBSOLETE

UNCLASSIFIED

SECURITY CLASSIFICATION OF THIS PAGE (When Data Entered)

standard atmospheric aerosol distributions are also presented. While the model is quite general, the calculations in this report are limited to DF laser wavelengths.

AEROSOL PROPAGATION EFFECTS

FINAL REPORT

SEPTEMBER 13, 1974

by

G. E. CALEDONIA AND J. D. TEARE

Sponsored by

Advanced Research Projects Agency
ARPA Order No. 2439
Contract Number N00014-74-C-0254

PHYSICAL SCIENCES INC.
18 Lakeside Office Park
Wakefield, MA 01880

AEROSOL PROPAGATION EFFECTS

FINAL REPORT

SEPTEMBER 13, 1974

by

G. E. CALEDONIA AND J. D. TEARE

ARPA Order Number	2439
Program Code Number	62301E
Contract Number	N00014-74-C-0254
Contract Duration	15 January 1974 - 14 September 1974
Amount of Contract	$44,458.00
Scientific Officer	Director, Naval Research Lab. 6555 Overlook Avenue, SW Washington, D. C.
Principal Investigator	Kurt L. Wray (617) 245-7408

Sponsored by

Advanced Research Projects Agency

ARPA Order No. 2439

PHYSICAL SCIENCES INC.

The views and conclusions contained in this document are those of the authors and should not be interpreted as necessarily representing the official policies, either expressed or implied, of the Advanced Research Projects Agency of the U. S. Government.

ABSTRACT

A model for the prediction of the temperature and vapor fields created about a small water droplet undergoing irradiation by a laser beam has been developed. Time dependent and steady state solutions of the model are discussed, as well as the possible effects of a number of aerosol properties not included in the model. Estimates of characteristic phase shifts to be expected in propagating through standard atmospheric aerosol distributions are also presented. While the model is quite general, the calculations in this report are limited to DF laser wavelengths.

TABLE OF CONTENTS

		Page
I.	INTRODUCTION	1
II.	PROPERTIES OF ATMOSPHERIC AEROSOLS	3
III.	MODELING	13
IV.	MODEL PREDICTIONS	22
V.	"NON-IDEAL" DROPLET EFFECTS	58
VI.	BEAM PROPAGATION EFFECTS	79
VII.	SUMMARY	87
	REFERENCES	90

I. INTRODUCTION

There is considerable current interest in the effect of atmospheric aerosols on laser propagation[1-4]. In the case of propagation of low intensity radiation through the atmosphere the primary extinction mechanisms are absorption and scattering by both aerosols and molecules. As the radiation intensity increases the interaction between these extinction mechanisms and the radiation field can become important. The phenomenon of thermal blooming occurs when the laser energy absorbed by atmospheric aerosols or molecules is converted into translational energy of the surrounding air. The index of refraction of this heated air will differ from ambient which in turn can cause beam de-focusing and/or steering. The magnitude of this effect will depend upon both the laser pulse shape and the heating phenomenology.

The case of laser blooming resulting from molecular absorption has been treated in some detail[5] and is included in the larger laser propagation codes (for example, Ref. 6). The atmospheric heating due to molecular absorption may be treated relatively straightforwardly in that it occurs continuously and uniformly in space and the temperature increase at any one point is directly proportional to the local laser intensity. Recently, the heating resulting from the absorption of laser energy by aerosols has received some attention.[1-3, 7] The situation in this case is more complicated than that of molecular absorption in that the absorption and resulting heating occurs at discrete points rather than continuously and thus the temperature fields in the surrounding air are highly nonuniform. Blooming/scattering predictions have been presented[1-3] for the temperature fields resulting from the absorption of laser radiation by nonvaporizing aerosols. As will be discussed further in the text the main features of these heating models are that the rate of temperature increase of a given

aerosol is linearly proportional to the laser intensity and that the increase in temperature above ambient about the aerosol will scale inversely with distance from the aerosol out to some distance which is an increasing function of time.

The temperature fields resulting from the absorption of laser energy by a vaporizable aerosol have been discussed briefly in Ref. 7 and will be considered in more detail here. As discussed earlier[7] the temperature increase of the aerosol need no longer scale linearly with laser intensity and, furthermore, the temperature increase in the air around the aerosol will not necessarily decrease inversely with radius. The subsequent prediction of blooming/scattering resulting from such temperature fields necessarily becomes more complex than for the case of nonvaporizing aerosols.

This report is concerned with the prediction of the temperature and vapor fields arising from the interaction of a laser beam with hygroscopic aerosols at sea level. Although the modeling presented is quite general the discussion will be limited to DF laser wavelengths. Section II provides a brief description of atmospheric aerosols and their optical properties. The details of the mathematical model describing the interaction of a laser beam with an aerosol (taken as pure H_2O) are presented in Section III. Simplified analytic solutions to the model as well as detailed computer predictions for a matrix of laser intensities and aerosol sizes are given in Section IV. A number of real aerosol effects not included in the modeling are discussed in Section V. These include nonuniform aerosol heating, original solute effects and ebullition. Section VI provides a brief discussion on the effect of the laser-aerosol interaction on laser propagation. Lastly, a summary of the report is presented in Section VII.

II. PROPERTIES OF ATMOSPHERIC AEROSOLS

A. Aerosol Particle Size Distributions

The particle size distribution, mass loading and composition of natural sea level aerosols vary considerably depending upon such factors as time of day, geographical location, weather, etc.[8] The "standard" continental distribution[4,9] will be used in this section for computational purposes because of the simplicity of its mathematical form. This distribution is defined by the relationship

$$dN_A/dR,\ cm^{-4} = \frac{0.32 \times 10^{-12}}{R^4}\ ;\quad 10^{-5}\ cm < R < 5 \times 10^{-3}\ cm \qquad (1)$$

where N_A is the number of particles/cc of radius R. The R^{-4} dependence of the distribution has been verified by a number of measurements[10]; however, the functional form can be somewhat misleading. Assuming an average aerosol material density of 1.5 gms/cc the total mass of the aerosol distribution represented by Eq. (1) is a modest 12 $\mu gm/m^3$. Furthermore, the distribution corresponds to a total particle density of 110 part/cc (10^{-5} cm < R < 5×10^{-3} cm.)

Oceanic aerosol distributions are not as well defined as the continental; however, there is a "standard" maritime distribution[4,9] which, although somewhat different in shape than the continental distribution, also corresponds to a mass loading of approximately 12 $\mu gm/m^3$. There can be a large number of particles with radius < 10^{-5} cm in both the continental and maritime environments; however, for most situations these will not constitute a significant fraction of the total aerosol mass loading and have been neglected in the present analysis.

The variation in aerosol mass loading from the "standard" distributions can be quite large.[8] As examples, aerosol mass loadings in urban areas such as Los Angeles, are typically measured in hundreds of $\mu gm/m^3$ and sea salt concentrations in Pacific Ocean aerosols have been found to vary from 10 - 1000 $\mu gm/m^3$ depending on wind velocity.[11] Of course, scenarios involving mist, fog or even ship induced spray could result in still higher mass loadings.

B. Relative Humidity Effects

It has been demonstrated that hygroscopic aerosols increase in size with increasing relative humidity, this accretion resulting from the condensation of water vapor on the aerosol. A relationship widely used[4,9] to predict the factor F by which the radius of the aerosol increases with increasing relative humidity is

$$F = 1 - 0.9 \ln (1 - R.H./100) \qquad (2)$$

where R.H. is relative humidity. This relationship is obviously unsatisfactory for R.H. = 100; however, it is expected to provide reasonable estimates of aerosol growth at high relative humidities. Unfortunately there is little experimental data available to provide validation for Eq. (2). Recently DeBary et al[12] presented measurements on the growth of sea spray aerosols with relative humidity. No details of the measurement technique were given. These measurements are shown in Fig. 1 along with the growth curve predicted by Eq. (2). As can be seen the data fall somewhat below the prediction over the full range of relative humidity. This difference corresponds to approximately a factor of two in aerosol volume at 98% relative humidity. Note there is a hysteresis effect in the aerosol growth measurements at relative humidities less than 80% (i.e. the growth parameter varies depending upon whether the measurement was made with increasing or decreasing relative humidity).

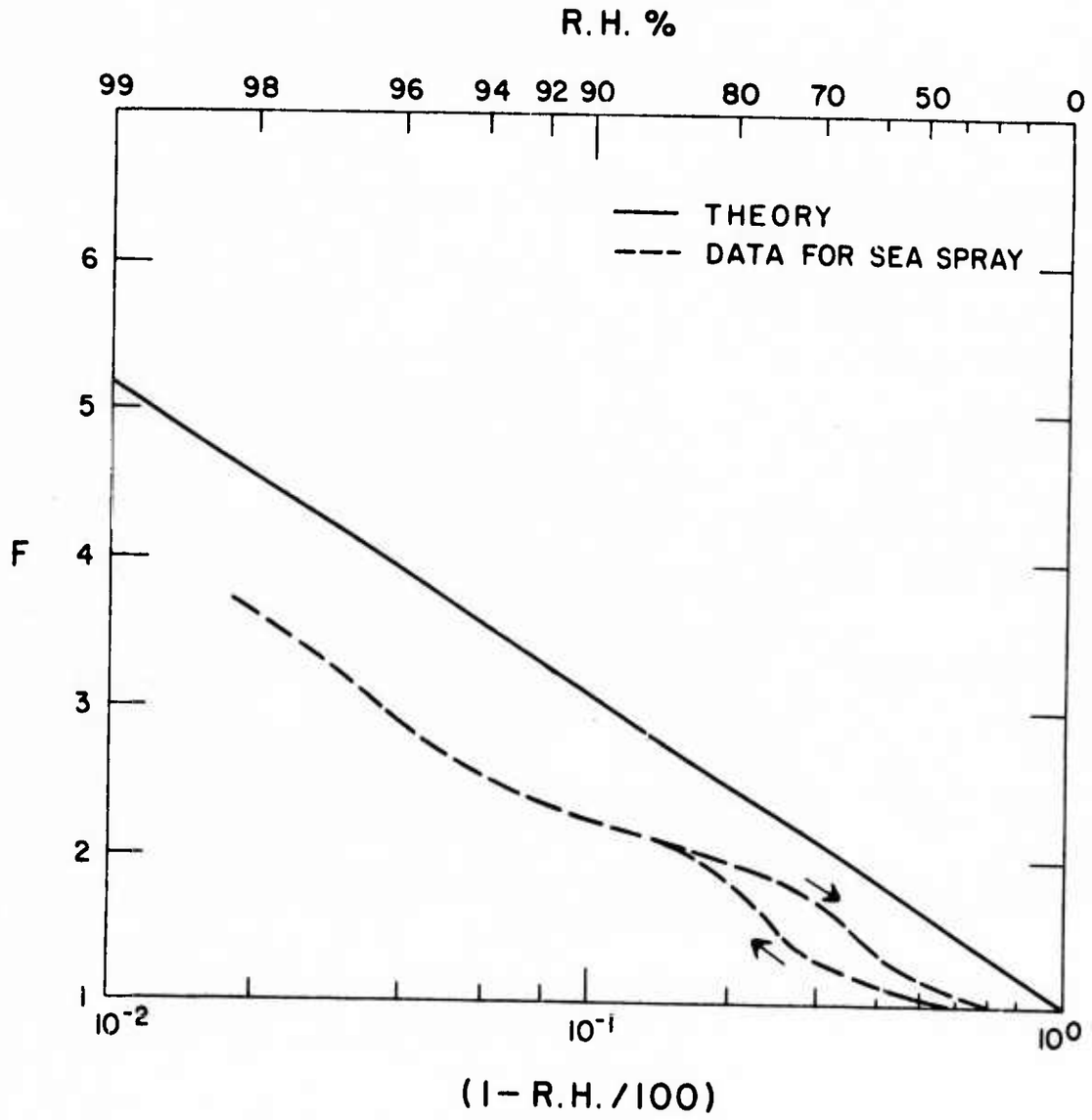

Fig. 1 Growth Factor for Hygroscopic Aerosols vs. Relative Humidity - - - -, Data for sea spray from Ref. 12, - Eq. (2) of text.

It should be noted that there is some theoretical justification for the use of Eq. (2). A pure water droplet cannot attain an equilibrium configuration unless the surrounding water vapor concentration corresponds to super-saturation. On the other hand salt solution aerosols can reach equilibrium configurations at relative humidities below 100% because of the reduction in the water vapor pressure at the droplet surface caused by the presence of the salt. A salt solution aerosol will reach a saturation level at a relative humidity somewhere below 100%. As the relative humidity is increased above this level the solution will be diluted and the particle will grow to a new equilibrium size. The resulting growth law will be a function of the solution properties and for the case of NaCl this growth is in reasonable agreement with the predictions of Eq. (2) at relative humidities above 80%, this latter condition corresponding to the saturated solution. The details of this phenomenon are given in Section V.

In any case this relationship only pertains to hygroscopic aerosols, and the percentage of aerosol mass loading corresponding to hygroscopic materials can vary significantly. Maritime aerosols can be dominantly hygroscopic whereas aerosols over urban areas may be composed largely of non-hygroscopic materials. (For example it has been reported that only 15% of the aerosol mass loading over Los Angeles is hygroscopic[13]). The remainder of this discussion will be limited to hygroscopic aerosols. It is clear for this case that relationship (2) provides for a dramatic variation in aerosol mass density (or volume) with relative humidity. For example at 98% relative humidity the total aerosol mass density for the continental distribution would be 740 $\mu gm/m^3$ as compared to 12 $\mu gm/m^3$ on a dry day. It should be emphasized that this apparently high mass loading still corresponds to a relatively clear day, the scattering coefficient for visible light being $< 10^{-1}\ km^{-1}$.

C. Particle Absorption Cross Sections

If the aerosol particles are assumed to be spheres their absorption cross sections may be calculated by use of Mie Theory (particle radius of

same order as laser wavelength.). Thus the absorption cross section is a complicated function of the complex index of refraction of the absorbing material, $m = n - in'$, and the ratio of particle size to wavelength, R/λ.

The simplest case corresponds to when $|m - 1| << 1$ and $4\pi n' R/\lambda < 1$ whence it can be shown[14] that the absorption cross section is given by

$$Q = 4/3\ \pi R^3 \left(\frac{4\pi n'}{\lambda}\right) \tag{3}$$

with the quantity $4\pi n'/\lambda$ defined as α, the bulk absorption coefficient. This limit is generally referred to as volume absorption. Unfortunately, real aerosol materials exhibit values of n ranging from 1.34 to 1.5 in the infrared and prediction of the absorption cross section requires use of the full Mie theory.

Such predictions have been made for the case of water droplets, with $m = 1.364 - 0.0034i$, for a wavelength of 3.8 μm (corresponding to a strongly transmitting DF laser line). These predictions, normalized by particle volume, are shown vs. aerosol radius in Fig. 2. Shown for comparison are the normalized absorption cross sections resulting from volume absorption, Eq. (3), and that predicted by geometric optics, which of course is only valid when $\lambda << R$. As can be seen, over much of the aerosol size range of interest the Mie theory prediction is larger than that due to volume absorption. At larger particle sizes the absorption coefficient falls off because of self absorption and at the smallest radii asymptotes to the Rayleigh limit[14], i.e.

$$Q \approx - \frac{8\pi^2 R^3}{\lambda} \mathrm{Im}\left(\frac{m^2 - 1}{m^2 + 2}\right) \tag{4}$$

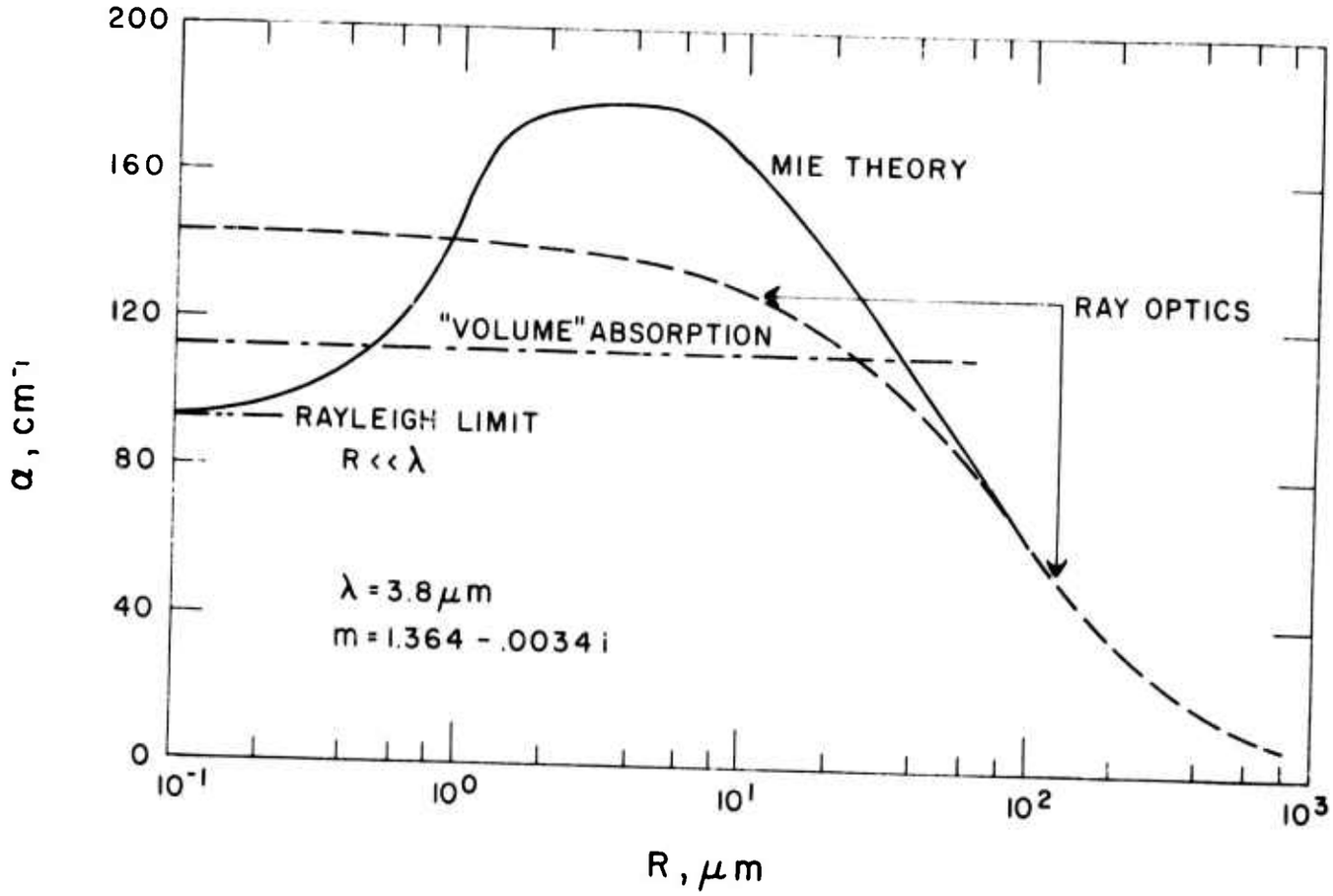

Fig. 2 The Absorption Cross Section Normalized by Particle Volume vs. Particle Radius for Water Droplets at $\lambda = 3.8\ \mu m$.

At approximately R = 60 μm the Mie theory and geometric optics predictions converge. It should be noted that the geometric prediction rises above that of volume absorption because of nonuniform absorption within the aerosol resulting from focusing effects. It may be that the increase in the Mie theory absorption cross section over that of volume heating may also result from nonuniform absorption within the aerosol. (This can only be verified by an examination of the electro-magnetic field within the aerosol as predicted by Mie theory). In any event in the modeling to be presented in Sections III and IV uniform absorption has been assumed for simplicity. A discussion of possible effects arising from nonuniform absorption is presented in Section V.

D. Atmospheric Aerosol Absorption Coefficients

The total atmospheric aerosol absorption coefficient is defined by

$$k = \int_{R_1}^{R_2} Q\,(R, \lambda, n', n)\,(dN_A/dR)\,dR \qquad (5)$$

where dN_A/dR is now the aerosol distribution function, Eq. (1), with the effects of relative humidity included, (Eq. (2)). For simplicity the aerosol has been taken to be composed completely of hygroscopic material having the complex index of refraction of water. This approximation is most relevant to a marine environment on a humid day. (It has been previously demonstrated[4] that the "standard" continental and maritime distributions result in similar absorption coefficients for $\lambda \approx 4$ μm).

There is still some uncertainty in the imaginary part of the index of refraction of liquid water at 3.8 μm. In two recent reviews the values of 3.4×10^{-3} and 6×10^{-3} have been recommended (Refs. 15 and 16, respectively). Absorption coefficients for both values of n' have been calculated in order to bound the actual aerosol absorption coefficient. For simplicity the calculations were performed assuming volume heating, Eq. (3), and the

prediction for $n' = 6 \times 10^{-3}$ was increased by a factor of 1.5 as a crude correction factor for Eq. (3) to account for the fact that $m \approx 1.36$.

These predictions are shown vs. relative humidity in Fig. 3 along with similar predictions for an aerosol distribution with ten times the mass loading. The shaded area between each set of curves approximately represents the uncertainty in the absorption coefficient. It is to be noted that these predictions are much lower than those presented by Hodges[4] for the same aerosol distribution function. The cause for this discrepancy is not clear.

An important consideration is the determination of the conditions under which absorption will dominate molecular absorption. McClatchey and Selby[17] have made predictions of atmospheric laser attenuation for a number of important HF and DF laser lines. An example of a strong DF laser line with weak molecular absorption is the v = 2-1, J = 8 line at 3.8 μm for which McClatchey and Selby predict a sea level absorption coefficient of 7.3×10^{-3} km^{-1} for a mid-latitude summer day (R.H. = 80%). This is shown as the circled point on Fig. 3. The dominant molecular absorber for this case was found to be HDO.

Recently Burch[18] has found evidence for a water vapor continuum absorption band in the 4 μm region. The continuum appears to be due to a pressure broadening phenomenon, with N_2 found to be 1/8 as efficient as H_2O as a collision partner.

There is still some uncertainty in the magnitude of this continuum absorption in that the measurements were made at temperatures > 338^{o} K and extrapolated to room temperature. Nonetheless, the water vapor continuum would appear to be a prominent absorption mechanism in the 4 μm region. A prediction of the absorption coefficient due to this water vapor continuum is shown vs. R.H. in Fig. 3.

As can be seen by reference to Fig. 3 molecular absorption will dominate aerosol absorption for the "standard" continental aerosol distribution. On the other hand much larger aerosol mass loadings are commonly observed in a variety of scenarios, and these in turn will provide the

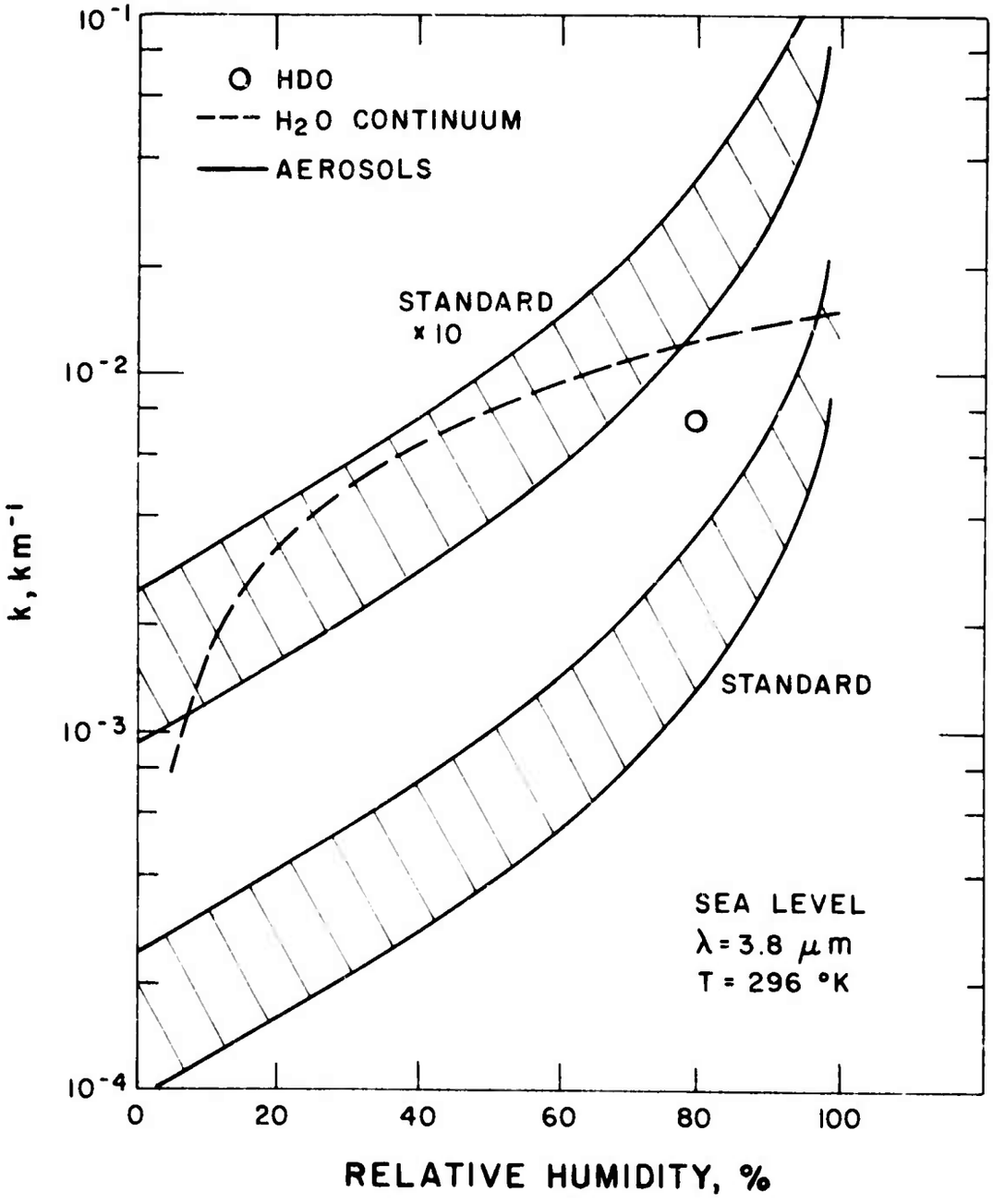

Fig. 3 Predicted Absorption Coefficients vs. Relative Humidity for Sea Level Molecular and Aerosol Absorption.

dominant absorption loss mechanism for DF laser radiation. This absorption can be particularly severe under conditions corresponding to mist, heavy maritime winds, etc.

It should be pointed out that the main interest in this phenomenon is not beam attenuation, indeed scattering from aerosols will attenuate the laser beam more rapidly than absorption, but rather the resulting effects on beam quality due to thermal blooming. Unlike molecular absorption, absorption by aerosols results in nonuniform atmospheric heating with strongly localized temperature gradients. The resulting effects on beam quality can be significantly different from those arising from uniform heating. In the next section a model is presented for the prediction of the atmospheric perturbations resulting from the absorption of laser radiation by aerosols.

III. MODELING

The phenomenon to be modeled here is the time and spatial variation of the temperature and vapor fields about a water droplet undergoing laser irradiation. This problem, in its aggregate form, has been considered by Sutton[19] and Glickler[20] (among others) in their analysis of laser propagation through fogs and clouds, respectively. The steady state solutions for an individual droplet, developed under the assumption of constant density, have been discussed by Williams.[21] The fully time dependent solutions for an individual droplet have not appeared in the open literature.

The phenomenology of the present problem is that the aerosol droplet absorbs energy and is heated. As the droplet temperature rises above ambient the droplet conducts heat energy to the surrounding air and undergoes surface vaporization. The vapor leaves the droplet with a directed velocity and a pressure wave is induced in the surrounding gas in response to the mass and heat addition. (If the rate of energy absorption were sufficiently large the droplet would "explode", creating a shock wave; the laser intensity/particle size range at which this occurs has been discussed by Sutton[19]. The present analysis will be limited to laser intensities and droplet sizes such that the directed velocity of the vapor leaving the droplet surface is much less than the local sound speed). An additional feature which must be included in the analysis is the fact that the droplet radius decreases with time due to mass loss resulting from vaporization.

A. Gas Equations

A number of approximations have been made to simplify the solution of this problem. The most prominent of these is that the gas is taken to be at constant pressure. As pointed out above, pressure gradients are induced in the gas because of the mass and heat addition from the droplet. However,

if the pressure equilibrates on a time scale fast relative to the times for conduction and diffusion then the heat and mass transfer may be assumed to be occurring in a constant pressure gas. The characteristic time for water vapor to diffuse a distance L in air is approximately

$$\tau_D \approx L^2/D \tag{6}$$

where D is the diffusion coefficient. The characteristic time for heat conduction in air is

$$\tau_C \approx L^2 \rho C_{P_A}/k_A \tag{7}$$

where ρ is the density, C_{P_A} the specific heat and k_A the thermal conductivity of air. Lastly, the characteristic time for pressure equilibration is

$$\tau_P \approx L/c \tag{8}$$

where c is the sound speed in air. Evaluating these expressions with $D = 0.24\ cm^2/sec$, $\rho_A = 1.2 \times 10^{-3}$ gms/cc, $C_{P_A} = 0.24$ cal./gm-^oK, $k_A = 6.2 \times 10^{-5}$ cal./cm-sec-^oK and $c \approx 3 \times 10^4$ cm/sec results in

$$\tau_D \sim \tau_C \gg \tau_P \tag{9}$$

for $L \gtrsim 1\ \mu m$. The characteristic droplet sizes of interest in this work are a few tenths μm to 50 μm, and for the typical atmospheric aerosol distributions of interest the average spacing between droplets, which would be the heating range of interest, is approximately one mm. Thus, it would appear that the approximation of a constant pressure gas is reasonable.

Another simplifying approximation used is that the gas properties are taken to be those of clean air. Although this approximation would suggest that the defining equations would not be valid for high water vapor concentrations

this is not the case, as will be demonstrated later in this section. Also, the coefficient of thermal conductivity, k_A and the product of the coefficient of diffusion and number density, DN, were taken to be constant. These quantities vary by $\lesssim$ 15% over the temperature range of interest, 0 - 100° C.

The last simplifications concern the fluid mechanics. The processes considered in the analysis are thermal conduction, diffusion and convection. The phenomena of thermal diffusion (Soret effect) and thermo-diffusion (Dufour effect) have not been included. Generally, these processes are insignificant in flow fields of the type under consideration. Furthermore, consideration must be given to gravitational effects. As the gas surrounding the droplet is heated it will rise. The characteristic time for the gas to rise a distance L is:

$$\tau_g \approx \left(2\, L/g \left[\Delta\rho/\rho \right] \right)^{1/2} \tag{10}$$

where g is the acceleration due to gravity, 980 cm/sec^2, and $\Delta\rho/\rho$ is the fractional difference in density between the heated gas and the surrounding medium. A strong lower bound on τ_g corresponds to $\Delta\rho/\rho \sim 0.3$. Even in this limit it can be shown that

$$\tau_D \sim \tau_C \ll \tau_g$$

for L less than one mm. Of course this effect might have to be included for long time ($t \gtrsim 0.01$ sec) irradiation. However, in this case it would perhaps be more appropriate to treat the aerosols as an aggregate rather than individually.

Within the framework of the above-mentioned approximations, the general relationships describing the system are

a) Conservation of mass

$$\partial\rho/\partial t = -\vec{\nabla} \cdot (\rho \vec{V}) \tag{11}$$

where $\vec{V}$ is the gas velocity,

b) Euler's equation

$$\partial \vec{V} / \partial t = - \vec{V} \cdot \vec{\nabla} \vec{V} \tag{12}$$

c) Conservation of energy

$$\partial (1/2 \rho V^2 + \rho C_v T)/\partial t = - \vec{\nabla} \cdot \left[\rho \vec{V} (1/2 V^2 + C_p T) - k_A \vec{\nabla} T \right] \tag{13}$$

where C_v is the specific heat at constant volume, and

d) The diffusion equation

$$\partial \rho_v / \partial t = \vec{\nabla} \cdot (D \vec{\nabla} \rho_v \vec{V} \tag{14}$$

where ρ_v is the water vapor density and D is the H_2O-air diffusion coefficient.

If the droplet is taken to be heated uniformly, the system will be spherically symmetric and it can be shown that the ordered kinetic energy terms drop out of the equations under the condition of constant pressure. The relevant gas equations for $r > R$, where R is the droplet radius, are

$$\partial T/\partial t = - V \partial T/\partial r + \frac{k k_A A T}{r^2 C_{P_A} P M_A} \frac{\partial}{\partial r} (r^2 \partial T/\partial r), \tag{15}$$

$$\partial X_v/\partial t = - V \partial X_v/\partial r + \frac{k T (DN)}{P r^2} \frac{\partial}{\partial r} (r^2 \partial X_v/\partial r), \tag{16}$$

$$\partial V/\partial r = - 2 V/r + \frac{k k_A A}{r^2 C_{P_A} P M_A} \frac{\partial}{\partial r} (r^2 \partial T/\partial r), \tag{17}$$

where k is Boltzmann's constant, A is Avogadro's number, P is the total

pressure taken as one atm., M_A is the molecular weight of air, N is the total number density, and X_v is the mole fraction of water vapor.

These equations have been formulated in terms of number density rather than mass density, since in a constant pressure flow of two gases with different molecular weights the quantity NT, rather than ρ T, remains constant. As mentioned earlier, these equations were derived under the assumption $X_v \ll 1$. In reality, the quantity $C_{P_A} M_A$ should be replaced by the expression

$$C_{P_A} M_A (1 - X_v) + C_{P_v} M_v X_v$$

where the subscript v refers to water vapor, and the diffusion coefficient should be replaced by that for full binary diffusion. However, over the temperature and water vapor ranges of interest in this problem these latter two quantities are reasonably constant and well represented by $C_{P_A} M_A$ and D, respectively. Thus Eqs. (15) - (17) are approximately valid for water vapor concentrations approaching unity.

B. Droplet Equations

In the following analysis the temperature field across the droplet is taken to be constant. As will be seen (Sections IV and V) this approximation is reasonable until the droplet temperature approaches the boiling point, if the absorption is volumetric. (As pointed out in Section II the absorption will not necessarily be volumetric. Specifically, as is evident from Fig. 2, there can be significant laser attenuation within the droplet for large sizes. Ameliorating this effect somewhat is the fact that heat conduction within the droplet will tend to smooth out temperature irregularities resulting from nonuniform absorption).

The basic equation connecting the droplet and gas dynamics is conservation of energy in the droplet.

$$4/3\,\pi R^3 I\alpha = 4/3\,\pi R^3 \rho_D C_{P_D} d T_D/dt$$

$$+ 4\pi R^2 k_A (-\partial T/\partial r \,|_R) \qquad (18)$$

$$+ 4\pi R^2 \Delta H_v \frac{M_v}{A} (NV)\,|_R$$

The LHS of Eq. (18) is the rate of absorption of energy, where I is the laser intensity, and the RHS represents the energy deposition into droplet heating, conduction and vaporization respectively. The quantity ΔH_v is the change in enthalpy required to proceed from liquid to gaseous state and the subscript D refers to droplet properties. Note that the temperature is continuous across the droplet surface; i.e. $T_D = T(R)$. The terms involving the ordered kinetic energy of the vapor are negligible for the present considerations and have been left out of Eq. (18).

The vapor concentration at the surface of the droplet has been related to the droplet temperature by the Clausius-Clapeyron relationship,

$$\left.\frac{d \ln X_v}{d T}\right|_P = \frac{\Delta H_v}{R_v T^2} \qquad (19)$$

where R_v is the ideal gas constant per unit mass of water vapor. It has been demonstrated[21] that this relationship properly describes the surface vapor pressure of a water droplet when the vapor velocity is less than the sound speed and the droplet radius is sufficiently large ($> 0.05\ \mu m$) so that surface tension effects may be neglected. In the present analysis Eq. (19) has been used in its integral form

$$X_v(R) = X_{v_\infty} \exp\left[\frac{\Delta H_v}{R_v}\frac{\left(T_D - T_\infty\right)}{T_D\, T_\infty}\right] \qquad (20)$$

where the subscript ∞ refers to ambient conditions. Eq. (20) is derived under the assumption that ΔH_v is a constant. Indeed ΔH_v varies by less than 10% between 0 - 100°C and has been taken to have the constant value of 585 cal/gm.

The last equation connecting the droplet and gas behavior is the conservation of mass of the vapor. If a spherical shell of thickness ΔR is constructed about the droplet, then it is required that the rate of mass loss of the droplet be balanced by the rate of increase of vapor within the shell plus the rate of vapor leaving the exterior of the shell. With some straightforward mathematical manipulation this leads to the relationship

$$(NV)_R = - (1 - X_v(R))^{-1} DN \, \partial X_v / \partial r \Big|_R . \qquad (21)$$

Note that X_v as given by Eq. (20) could exceed unity for sufficiently high temperature. However, if this occurred, the vaporization rate as given by Eq. (21) would become negative. This is a consequence of assuming a constant pressure gas and limits the droplet temperature that can be attained to 100°C.

It was assumed in the derivation of Eq. (21) that the vaporization rate at the surface is controlled by diffusion. Actually vaporization at the surface is a kinetic process obeying Knudsen's equation with diffusion taking control approximately a mean free path (~ 0.06 μm at 1 atm) away from the droplet. It can readily be shown[22] that if the vaporization coefficient for water, α_v, were unity Eq. (21) would adequately represent this phenomenon for particle radii $\gtrsim 0.5$ μm. At the time that this research was in progress the value of $\alpha_v = 1$ appeared to be preferred[22-24]; however, very recently a measurement of $\alpha_v = 0.033$ has been reported[25] in agreement with several earlier measurements. If this latter value of 0.033 is correct then Eq. (21) would provide an overestimate of the vaporization rate for the droplet sizes considered.

The computer predictions to be presented in Section IV were made using Eq. (21). The computer code can be readily adjusted to include the more general vaporization rate as is discussed in Section V. In general, a smaller value of α_v will provide more heat conduction for a given configuration at the expense of vaporization.

C. Effect of Varying Droplet Size

So far in the analysis the effect of decreasing droplet size has not been considered. This effect can be uncoupled because the rate of change of droplet size is small compared to the rate of change of the gas parameters (because of the large difference between liquid and gas densities). Of course, it has been implicitly assumed that the time varying, rather than initial, value of R will be used in the solution of the equations.

The governing equations have been recast in terms of the variable

$$Z = R\,(t)/r \tag{22}$$

In terms of this variable the equations may be written as

$$\partial T/\partial t = R^{-1}\,(Q Z^4 - Z\, dR/dt)\,\partial T/\partial Z + \frac{k\,k_A\,A}{C_{P_A} P M_A} T R^{-2} Z^4\,\partial^2 T/\partial Z^2 \tag{23}$$

$$\partial X_v/\partial t = R^{-1}\,(Q Z^4 - Z\, dR/dt)\,\partial X_v/\partial Z + \frac{k\,DN}{P} T R^{-2} Z^4\,\partial^2 X_v/\partial Z^2 \tag{24}$$

$$\partial Q/\partial Z = -\frac{k\,k_A\,A}{C_{P_A} P M_A} R^{-1}\,\partial^2 T/\partial Z^2 \tag{25}$$

where

$$dR/dt = -\frac{P M_v}{A \rho_D\, k\, T} Q\,(Z = 1) \tag{26}$$

and

$$Q = V/Z^2 \tag{27}$$

The transformed boundary conditions at r = R (Z = 1) are

$$I\alpha = \rho_D C_{P_D} \partial T/\partial t \Big|_{Z=1} + 3 R^{-2} k_A \partial T/\partial Z \Big|_{Z=1}$$

$$+ 3 R^{-1} \frac{M_v \Delta H_v P}{A k T} Q (Z = 1) , \tag{28}$$

$$Q (Z = 1) = R^{-1} \frac{k T DN}{P} \left[1 - X_v (Z = 1)\right]^{-1} \partial X_v/\partial Z \Big|_{Z=1} \tag{29}$$

and the Clausius-Clapeyron relationship, Eq. (20).

Note that the quantities I and α enter only as a product in the problem, Eq. (28). As shown in Fig. 2 the effective value of α as determined by Mie theory can vary by close to a factor of two for particles of radius between 0.1 and 100 μm. Thus the absorption efficiency of a droplet can vary as the particle vaporizes (and thus decreases in size). Given the uncertainty in the imaginary part of the index of refraction of water and the desire to present generalized solutions this effect was not included in the computations of Section IV.

IV. MODEL PREDICTIONS

No analytic solution has been found for the system of Eqs. (20), (23) - (29). A computer program has been developed for their numerical evaluation which employs a fully implicit Crank-Nicolson finite difference scheme. A complication in using the Z co-ordinate is that a constant grid size in Z space results in a limited number of grid points at large r, where the solution may be most interesting. This complication has been circumvented by modifying the finite difference scheme to allow for a change in grid spacing at small Z. In the present mode of operation the grid spacing for $0.00 \leq Z \leq 0.05$ is an order of magnitude finer than that for $0.05 \leq Z \leq 1.00$.

A matrix of computer solutions for the Eqs. (20), (23) - (29) has been completed. Simultaneously a steady state solution of the equations has been performed in order to analytically predict the effects of varying fundamental parameters such as particle radius and laser intensity. The latter analysis is useful not only as a check for the computer solutions but also in that it presents a broad overview of the laser-aerosol interaction.

A. Steady State Solutions

In the limit where the velocity term in Eqs. (23) and (24) can be neglected, the equations effectively uncouple, and it can be readily demonstrated that the steady state solutions for $\Delta T = T - T_\infty$ and $\Delta X_v = X_v - X_{v_\infty}$ scale inversely with r, i.e.,

$$\Delta T(r) = (R/r)\,\Delta T(R) \tag{30}$$

and

$$\Delta X_v(r) = (R/r)\,\Delta X_v(R) \tag{31}$$

Indeed, even the time dependent solutions, which may be found in standard texts (for example, Ref. 26) vary approximately as r^{-1} for $r < 2 (k_A t/\rho C_{P_A})^{1/2}$. Thus, in the limit of low velocity the gradients appearing in the equation for droplet energy conservation, Eq. (28), may be evaluated by use of Eq. (30) and (31).

If this is done, use of Eqs. (20), (28) and (29) results in

$$d(\Delta T_D)/dt = \frac{3}{R^2 \rho_D C_{P_D}} \left\{ \frac{R^2 I\alpha}{3} - k_A \Delta T_D - \frac{\Delta H_v M_v}{A} D N (1 - X_v(R))^{-1} (X_v(R) - X_{v_\infty}) \right\} \qquad (32)$$

where

$$X_v(R) - X_{v_\infty} = X_{v_\infty} \left\{ \exp \left[\frac{\Delta H_v \Delta T_D}{R_v (\Delta T_D + T_\infty) T_\infty} \right] - 1 \right\}$$

Although this differential equation is separable, it affords no simple analytic solution. One feature of interest is the maximum value of ΔT_D which is reached when the time derivative is zero. Equation (32) in this limit reduces to a transcendental equation for $\Delta T_{D\text{-max}}$ which may be evaluated as a function of the parameter $R^2 I\alpha$. The solution to this equation is shown in Fig. 4 over a range of 5 orders of magnitude in the parameter $R^2 I\alpha$. Shown for comparison are the predicted maximum droplet temperatures for the related cases of "heat conduction only" and "vaporization only". These calculations were performed for initial conditions of $T_\infty = 293^\circ K$, $X_{v_\infty} = 2.1 \times 10^{-2}$.

Note that for the full range of $R^2 I\alpha$ shown the $\Delta T_{D\text{-max}}$ predicted for the case of heat conduction alone is significantly higher than that predicted when both heat conduction and vaporization were included. On the

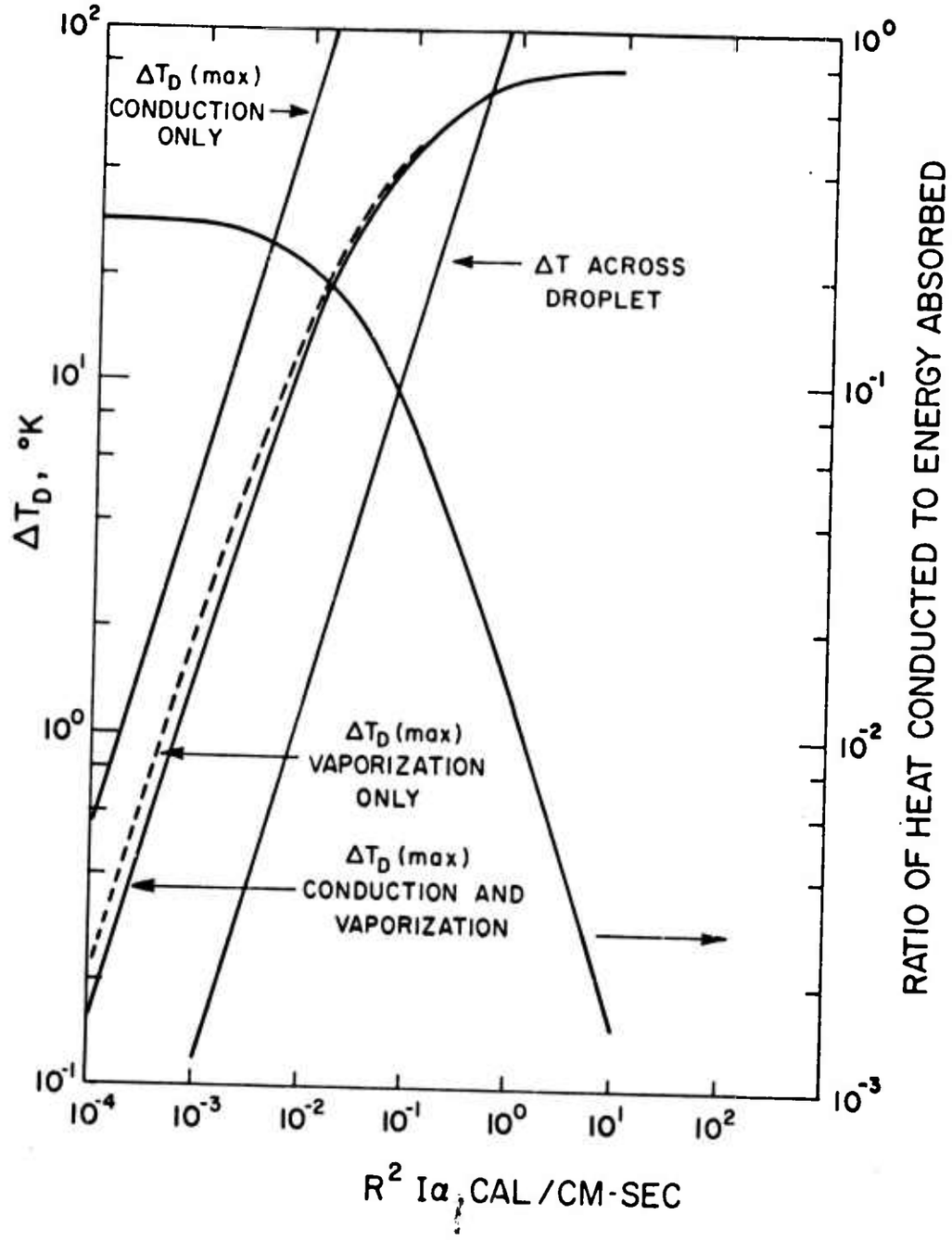

Fig. 4 Maximum Increase in Droplet Temperature vs. $R^2 I\alpha$. Also shown is the fraction of absorbed energy lost to heat conduction and the predicted variation in temperature across the droplet.

other hand, the predictions for the case of "vaporization only" are relatively close to the full solution. The reason for this is that the major portion of the absorbed energy goes into vaporization rather than heat conduction. This is shown explicitly in Fig. 4 where the fraction of the absorbed energy which is lost to heat conduction is plotted vs. $R^2 I\alpha$. For low $R^2 I\alpha$ this fraction asymptotes to ~ 0.3, and falls off rapidly with increasing $R^2 I\alpha$. This rapid fall-off occurs as the droplet temperature approaches the boiling point. This is because the vaporization rate increases exponentially in this region, whereas the rate of heat conduction approaches a constant. The relative value of this fraction is determined by the ratio of the last two terms on the RHS of Eq. (32). For small $\Delta T_{D\text{-max}}$ this ratio reduces to

$$\frac{\text{Power into heat conduction}}{\text{Power into vaporization}} = \frac{k_A R_v T_\infty^2 A (1 - X_{v_\infty})}{X_{v_\infty} DN (\Delta H_v)^2 M_v}$$

$$\approx 0.43 \qquad (33)$$

in agreement with the asymptotic value shown in Fig. 4 (i.e., 0.43/1.43≈0.3).

Note that Fig. 4 is somewhat misleading at large values of $R^2 I\alpha$ in that convective heat transfer will dominate conductive heat transfer in that range, i.e. the water vapor is heated prior to leaving the droplet. The fraction of the vaporization energy which goes to heating is

$$E_F = \frac{C_{P_{H_2O}} \Delta T_D}{\Delta H_v} \qquad (34)$$

which at 100°C is $E_F \sim 0.06$. The fraction of absorbed energy converted to heat will not fall below that value given by Eq. (34). Note further that the radial steady state solutions Eq. (30) - (31) are not strictly valid in the convection dominated regime. Williams[21] has discussed the steady state solution for this case under the assumption of constant density and showed

that the radial distribution is exponential with an argument preportional to the vaporization rate over radius. Nonetheless for the cases corresponding to high vaporization considered in the present work the computed radial derivatives of the temperature and water vapor distributions at r = R were typically within a factor of two of those predicted from Eqs. (30) - (31). Thus it is concluded that the present steady state analysis should adequately describe the gross phenomenology of the convection dominated regime.

One last point with reference to Fig. 4 is that although the solution for the case of "heat conduction only" is linearly proportional to laser intensity this is not the case for the more general solution. As vaporization begins to strongly dominate, the temperature increase scales more weakly with laser intensity. This occurs approximately at an $R^2 I\alpha$ of 1.5×10^{-2} cal/cm-sec which for a laser intensity of 10^4 watts/cm^2 and an α of **112 cm^{-1}** corresponds to a droplet size of $\sim 2\mu m$.

The fact that vaporization dominates heat conduction as an energy loss mechanism allows an approximate analytic formulation for several of the variables of interest in the problem. In particular, in steady state it can be readily shown from Eq. (32) that the rate of mass loss from the droplet can be expressed as

$$dm/dt = -4/3\ \pi R^3 I\alpha/\Delta H_v \tag{35}$$

or in terms of the droplet radius

$$dR/dt = -R I\alpha/(3\Delta H_v \rho_D) \tag{36}$$

From Eq. (36) it can be seen that the characteristic e-folding time for droplet radius is

$$\tau_R = 3\ \Delta H_v \rho_D / I\alpha \tag{37}$$

which is inversely proportional to $I\alpha$ and independent of initial particle size. Lastly, the gas velocity leaving the droplet surface is given by

$$V(R) \approx M_A R I\alpha / (3 M_v \rho \Delta H_v) \tag{38}$$

Note this latter quantity scales as $R I\alpha$ rather than $R^2 I\alpha$, and thus is less sensitive to changes in radius than the droplet temperature.

The relationships (33) - (38) are all valid after the droplet has reached its steady state temperature. It can be shown that prior to that time the major portion of the absorbed energy is consumed in heating the droplet. It was found through computer solutions of Eq. (32) that the e-folding time for the quantity $\Delta T_{D\text{-max}} - \Delta T_D$ was given by

$$\tau_D \sim \frac{0.65\ \Delta T_{D\text{-max}}\ \rho_L\ C_{P_L}}{I\alpha} \tag{39}$$

to within 20% for $R^2 I\alpha$ between 10^{-4} - 10^{1} cal./cm-sec. Note that τ_D is not independent of particle size since $\Delta T_{D\text{-max}}$ is a function of $R^2 I\alpha$. Indeed for $R^2 I\alpha \lesssim 1.5 \times 10^{-2}$ cal/cm-sec

$$\Delta T_{D\text{-max}} \sim 1.6 \times 10^{3} R^2 I\alpha \tag{40}$$

whence

$$\tau_D \sim 10^{3} \rho_L C_{P_L} R^2;\ R^2 I\alpha < 1.5 \times 10^{-2} \text{ cal/cm-sec} \tag{41}$$

independent of $I\alpha$. As a numerical example, for a droplet of radius 1μm the characteristic time to steady state as determined from Eq. (41) is 10^{-5} seconds. For values of $R^2 I\alpha$ larger than 1.5×10^{-2} cal/cm-sec the characteristic heating time must be determined from Eq. (39) in conjunction with the values of $\Delta T_{D\text{-max}}$ shown in Fig. 4.

A last point before leaving the discussion on steady state solutions concerns the importance of temperature gradients within the droplet. If one considers volume absorption followed by heat conduction as the only phenomenon occurring within the droplet, the defining steady state energy equation becomes

$$4/3\ \pi r^3 I\alpha = -4\pi r^2 k_D\ \partial T/\partial r \quad (r < R) \tag{42}$$

where k_D is the coefficient of thermal conductivity of liquid water, taken as 1.4×10^{-3} cal/cm-sec-^oK. Eq. (42) requires that

$$T_C - T_S = \frac{R^2 I\alpha}{6 k_D} \tag{43}$$

where the subscripts C and S refer to conditions at the droplet center and surface, respectively. This temperature variation is also shown in Fig. 4 and can be seen to be significantly lower than $\Delta T_{D\text{-max}}$ until the droplet approaches the boiling point. Of course, Eq. (43) is not necessarily realistic in that region since it requires droplet superheating. In reality, vaporization could occur within the droplet and original nuclei effects, etc. could be quite important. These points are discussed in Section V. In any event, it is clear that the approximation of a constant temperature field across the droplet is not appropriate at large values of $R^2 I\alpha$.

B. Time Dependent Solutions

Computer calculations have been performed for droplet radii between 0.5 - 50 μm and for values of $I\alpha$ = 27, 81, 270, 810, 2700 kcal/cc-sec. (For a nominal value of α = 113 cm^{-1} these correspond to I = 1, 3, 10, 30, 100 kwatts/cm^2). Only a few predictions have been made for the largest and smallest droplet sizes inasmuch as these require the largest amount of computer time.

Shown in Figs. 5 - 9 are the rise in droplet temperature vs. time for an $I\alpha$ of 270 kcal/cc-sec ($I = 10^4$ watts/cm^2 for an α of 113 cm^{-1}) and for particle radii of 0.5, 1., 3., 5. and 10. μm. The slope discontinuities appearing on the curves are not real but are a result of the plotting technique. As can be seen the time to reach steady state increases with increasing particle size as expected from Eq. (39) and (41). The decrease in droplet temperature with increasing time results from the decrease in radius due to vaporization. The predicted droplet temperatures for times corresponding to the point of maximum tempera- and beyond are in good agreement with the steady state predictions shown in Fig. 4.

The radial profiles of the temperature increase in the gas for these cases are shown in Figs. 10 - 14 at times of 1, 3 and 5 msec. These profiles scale inversely with radius out to distances roughly given by $r \sim 2 (k_A t/\rho C_{P_A})^{1/2}$ in agreement with the analytic solution for the case of heat conduction with no vaporization. (The magnitude of the increase is of course lower than the heat conduction case as is evident from Fig. 4). The decrease in temperature at small radius with increasing time is caused by the decreasing droplet temperature. At the larger distances the temperature is highest at the longest time because of the finite time required for heat conduction.

The radial profiles of the increase in water vapor mole fraction in the gas are quite similar in form to those for the temperature increase. Examples of this are shown in Figs. 15 and 16 for particle radii of 1 and 10 μm and an $I\alpha$ of 270 kcal/cc-sec. The profiles scale inversely with radius out to approximately the same distance as the respective profiles for the temperature increase in the gas as shown in Figs. 11 and 14. This is because the characteristic time for diffusion is approximately the same as that for heat conduction (See Eqs. (6) and (7)).

Similar predictions for an $I\alpha$ of 2700 kcal/cc-sec ($I = 10^5$ watts/cm^2 for an α of 113 cm^{-1}) and for particle radii of 0.5, 1., 3. and 5. μm are shown in Figs. 17-24. The rise in droplet temperature vs. time for various droplet sizes is shown for this $I\alpha$ in Figs. 17-20. Note the time scale to reach steady state again increases with radius. At the larger droplet sizes these times are considerably faster than those for the same droplet size at an $I\alpha$ of 270 kcal/cc-sec. This is as expected from Eq. (39). The fall-off in droplet temperature with increasing time is more rapid in this case than at the lower $I\alpha$ since the characteristic time for droplet shrinkage scales inversely with $I\alpha$ (Eq. (38)).

The increase in temperature of the gas vs. radius is shown in Fig. 21-24 at times of 0.2, 0.6 and 1.0 msec. Departures from an inverse radial dependence are obvious in these profiles particularly for the larger droplet radii. The corresponding predictions for the increase in water vapor mole fraction exhibit a similar behavior.

Predictions of the cumulative energy distribution vs. time are shown in Figs. 25-29 for a droplet radius of 5 μm and for five values of $I\alpha$ lying between 27 to 2700 kcal/cc-sec. Shown are the total absorbed energy, the amount of energy converted to heat of the surrounding gas by conduction and by convection and that lost to vaporization. Note that the five figures are not all plotted on the same time scale.

The first thing that can be seen is that the total energy absorbed does not scale linearly with $I\alpha$ over the time ranges shown. The reason for this is that the rate of droplet shrinkage increases with increasing $I\alpha$ and thus the effective absorption coefficient decreases. Also the percentage of the total absorbed energy which is conducted away as heat energy decreases with increasing $I\alpha$ as expected from the steady state analysis discussed in Section A. Indeed the heat flow resulting from convection exceeds that from conduction at an $I\alpha$ of 2700 kcal/cc-sec.

It should be emphasized that the prediction that vaporization, rather than heat conduction, is the dominant energy loss mechanism is strongly dependent upon the assumption that the evaporation coefficient for H_2O is unity. If it were 0.033, as mentioned in Section II conduction could dominate vaporization. This point is discussed in some detail in the next section.

FIGURE CAPTIONS

Figs. 5 - 9 The Rise in Droplet Temperature Above Ambient vs. Time. $I\alpha = 2.7 \times 10^5$ cal/cc-sec, R = 0.5, 1., 3., 5., 10. μm, respectively. Ambient conditions are $T = 293^oK$, $X_v = 2.1 \times 10^{-2}$.

Figs. 10 - 14 The Rise in Gas Temperature Above Ambient vs. Radius at Times of 1, 3, 5 msec. Initial conditions the same as in Figs. 5 - 9, respectively.

Figs. 15 & 16 The Rise in Water Vapor Mole Fraction Above Ambient vs. Radius at Times of 1, 3, 5 msec. $I\alpha = 2.7 \times 10^5$ cal/cc-sec, R = 1., 10. μm respectively. Ambient conditions are $T = 293^oK$, $X_v = 2.1 \times 10^{-2}$.

Figs. 17 - 20 The Rise in Droplet Temperature Above Ambient vs. Time. $I\alpha = 2.7 \times 10^6$ cal/cc-sec, R = 0.5, 1., 3., 5. μm respectively. Ambient conditions are $T = 293^oK$, $X_v = 2.1 \times 10^{-2}$.

Figs. 21 - 24 The Rise in Gas Temperature Above Ambient vs. Radius. Initial conditions are the same as in Figs. 17 - 20, respectively.

Figs. 25 - 29 Cumulative Energy Deposition vs. Time. R = 5 μm, $I\alpha = 2.7 \times 10^4$, 8.1×10^4, 2.7×10^5, 8.1×10^5, 2.7×10^6 cal/cc-sec, respectively. Shown are the total absorbed energy and the amounts lost to heat conduction, heat convection and vaporization.

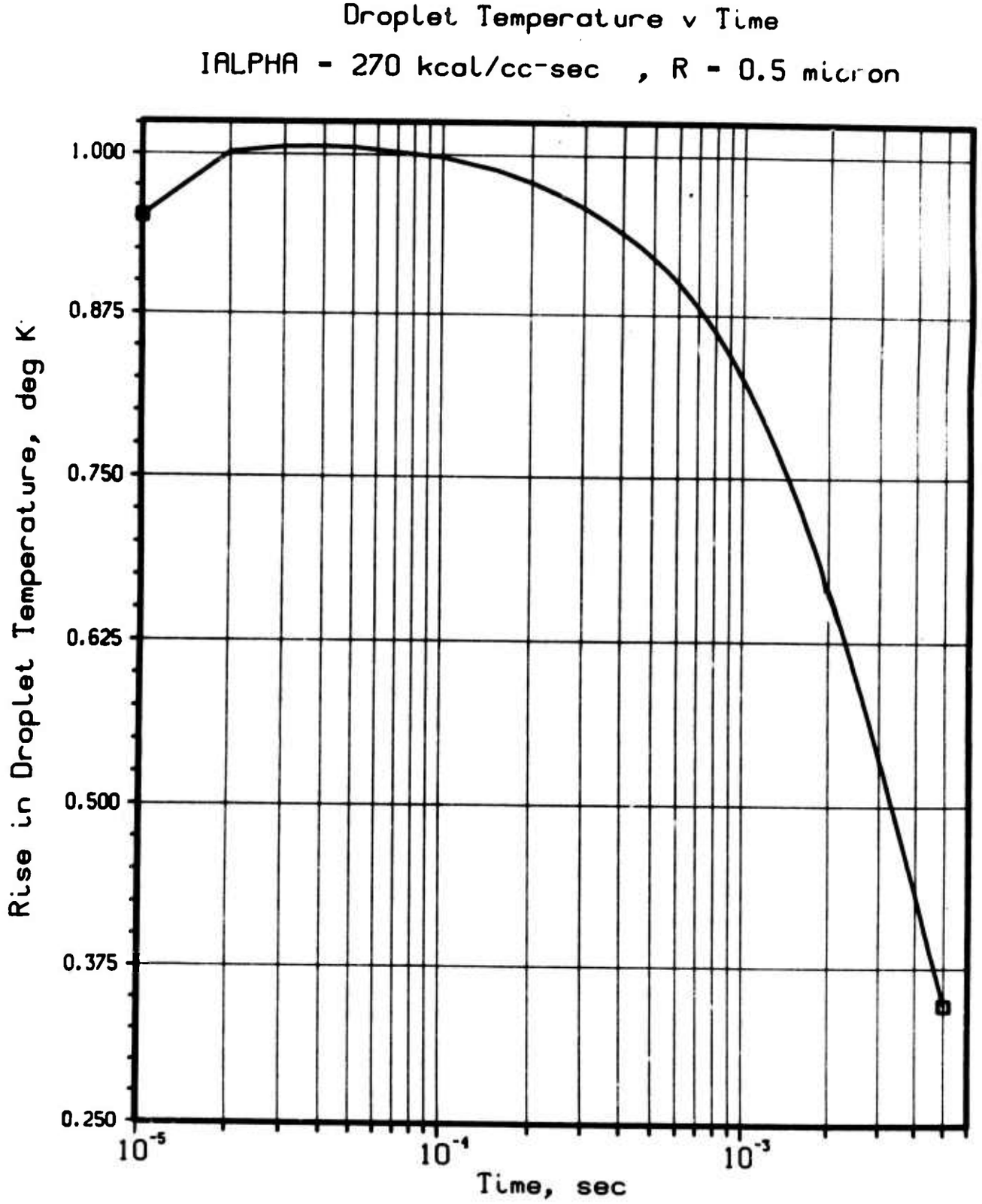
Droplet Temperature v Time
IALPHA - 270 kcal/cc-sec , R - 0.5 micron
Rise in Droplet Temperature, deg K
1.000
0.875
0.750
0.625
0.500
0.375
0.250
10^{-5}
10^{-4}
10^{-3}
Time, sec

Fig. 5

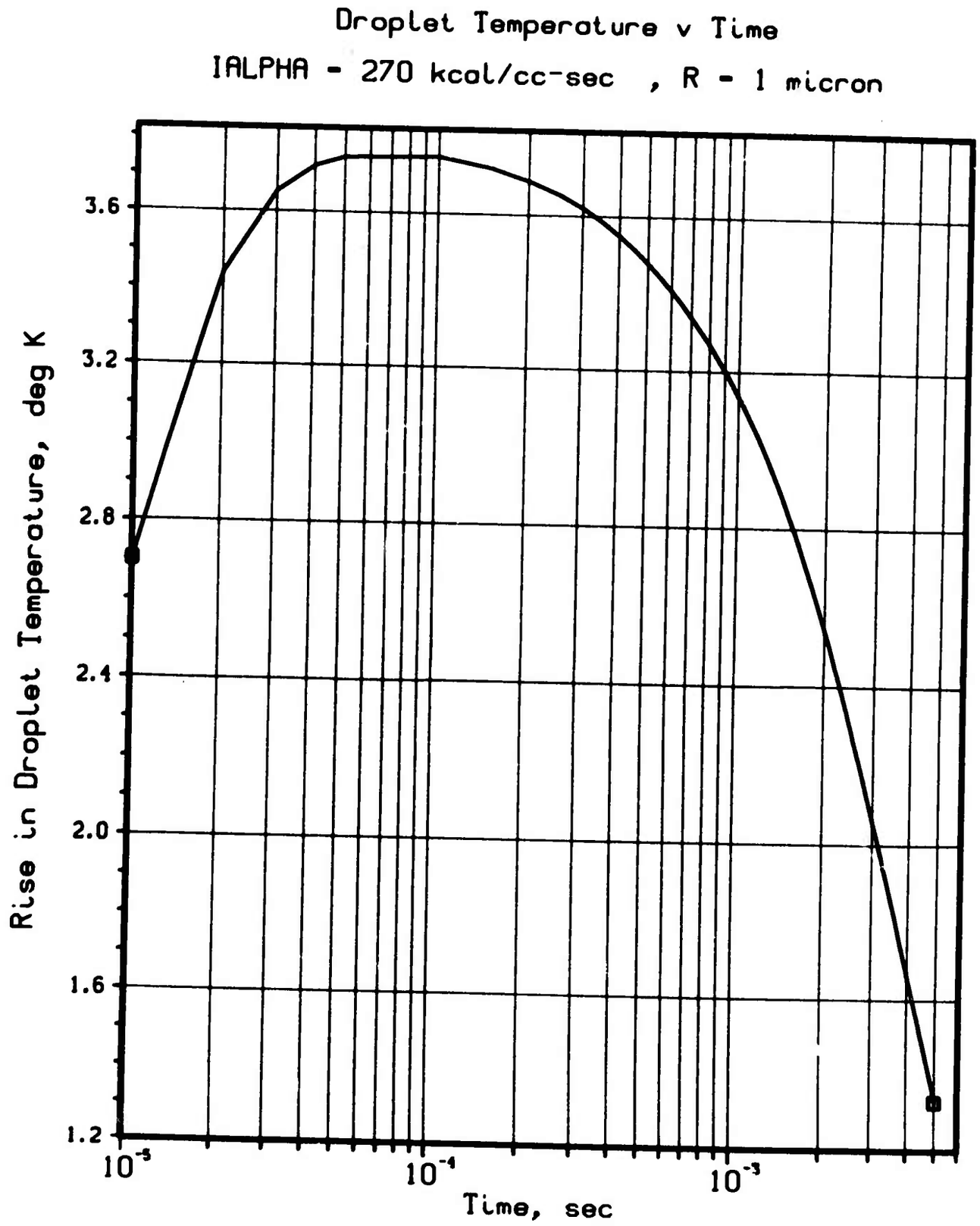
Droplet Temperature v Time
IALPHA - 270 kcal/cc-sec , R - 1 micron
Rise in Droplet Temperature, deg K
3.6
3.2
2.8
2.4
2.0
1.6
1.2
10^{-5}
10^{-4}
10^{-3}
Time, sec

Fig. 6

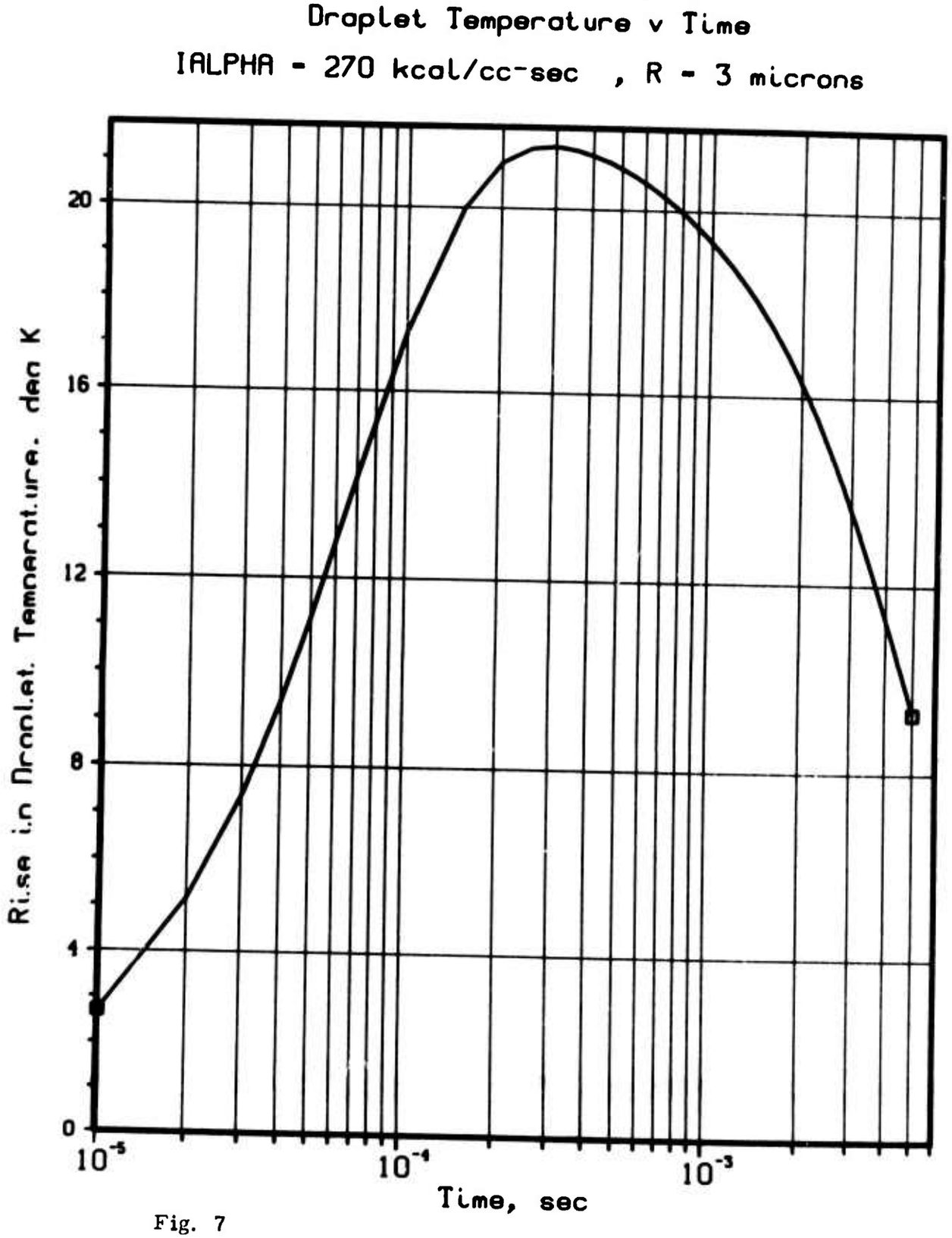
Droplet Temperature v Time
IALPHA - 270 kcal/cc-sec , R - 3 microns
Rise in Droplet Temperature, deg K
20
16
12
8
4
0
10^{-5}
10^{-4}
10^{-3}
Time, sec

Fig. 7

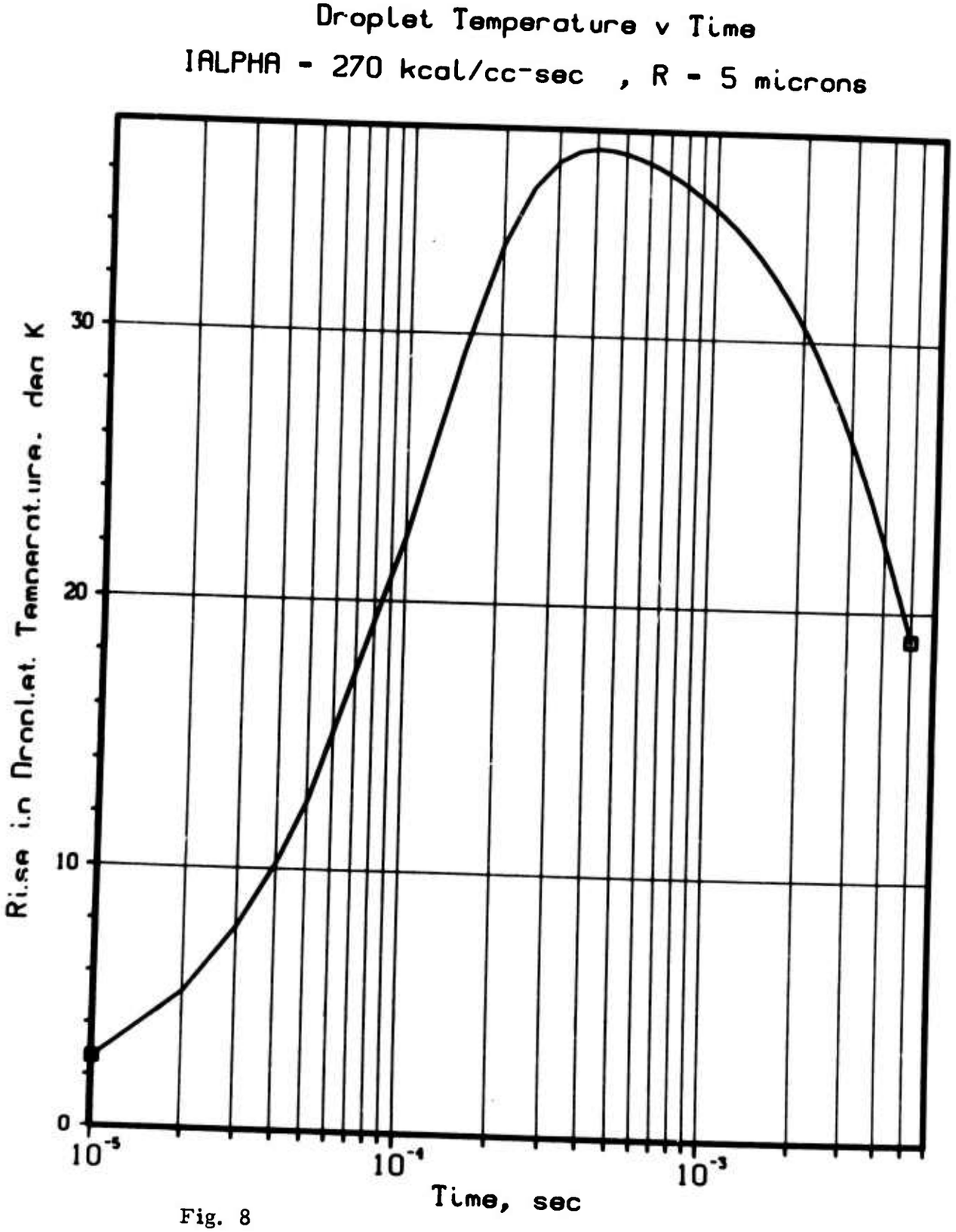
Droplet Temperature v Time
IALPHA - 270 kcal/cc-sec , R - 5 microns
Rise in Droplet Temperature, deg K
30
20
10
0
10^{-5}
10^{-4}
10^{-3}
Time, sec

Fig. 8

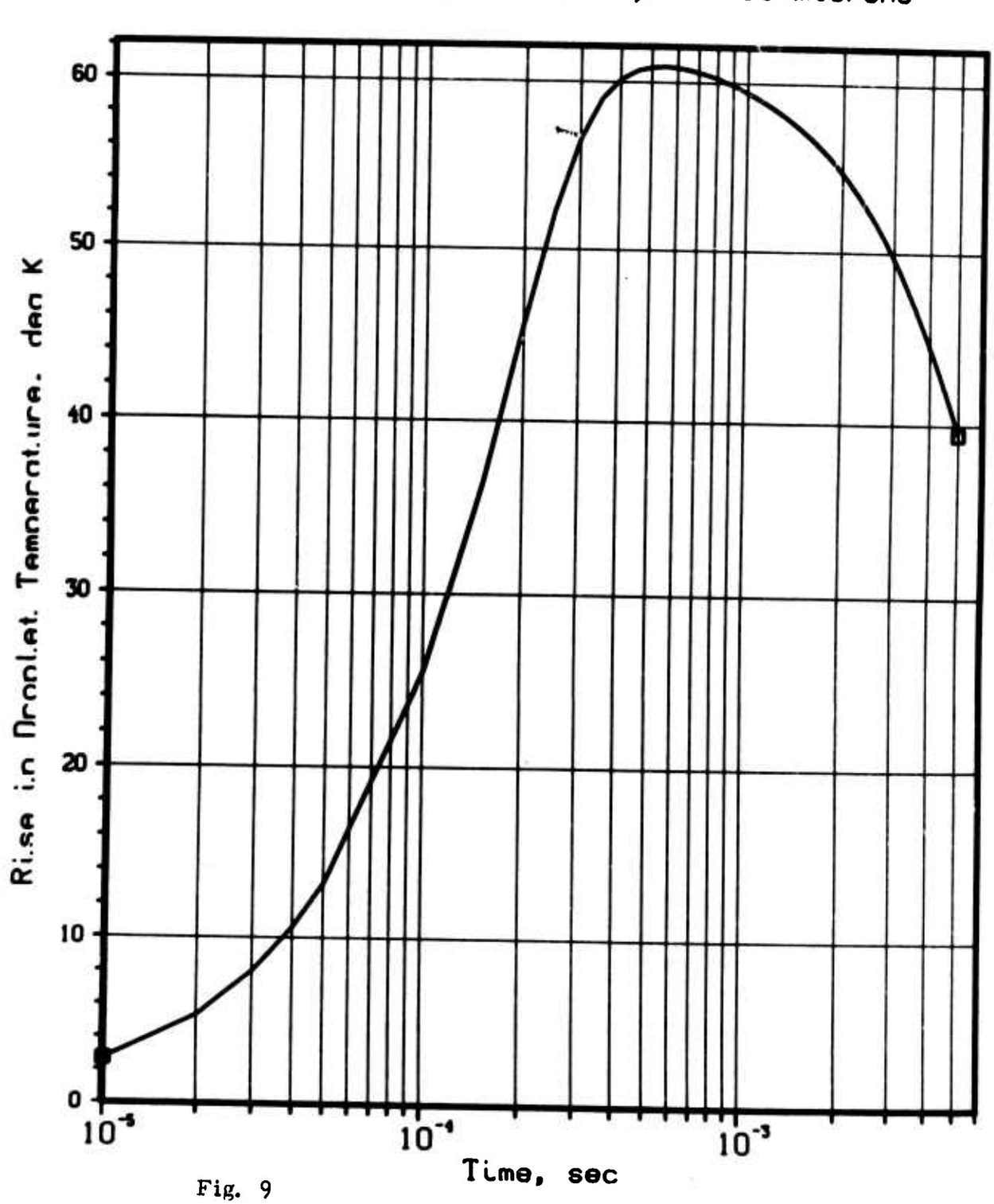
Droplet Temperature v Time
IALPHA - 270 kcal/cc-sec , R - 10 microns
Rise in Droplet Temperature, deg K
60
50
40
30
20
10
0
10^{-5}
10^{-4}
10^{-3}
Time, sec

Fig. 9

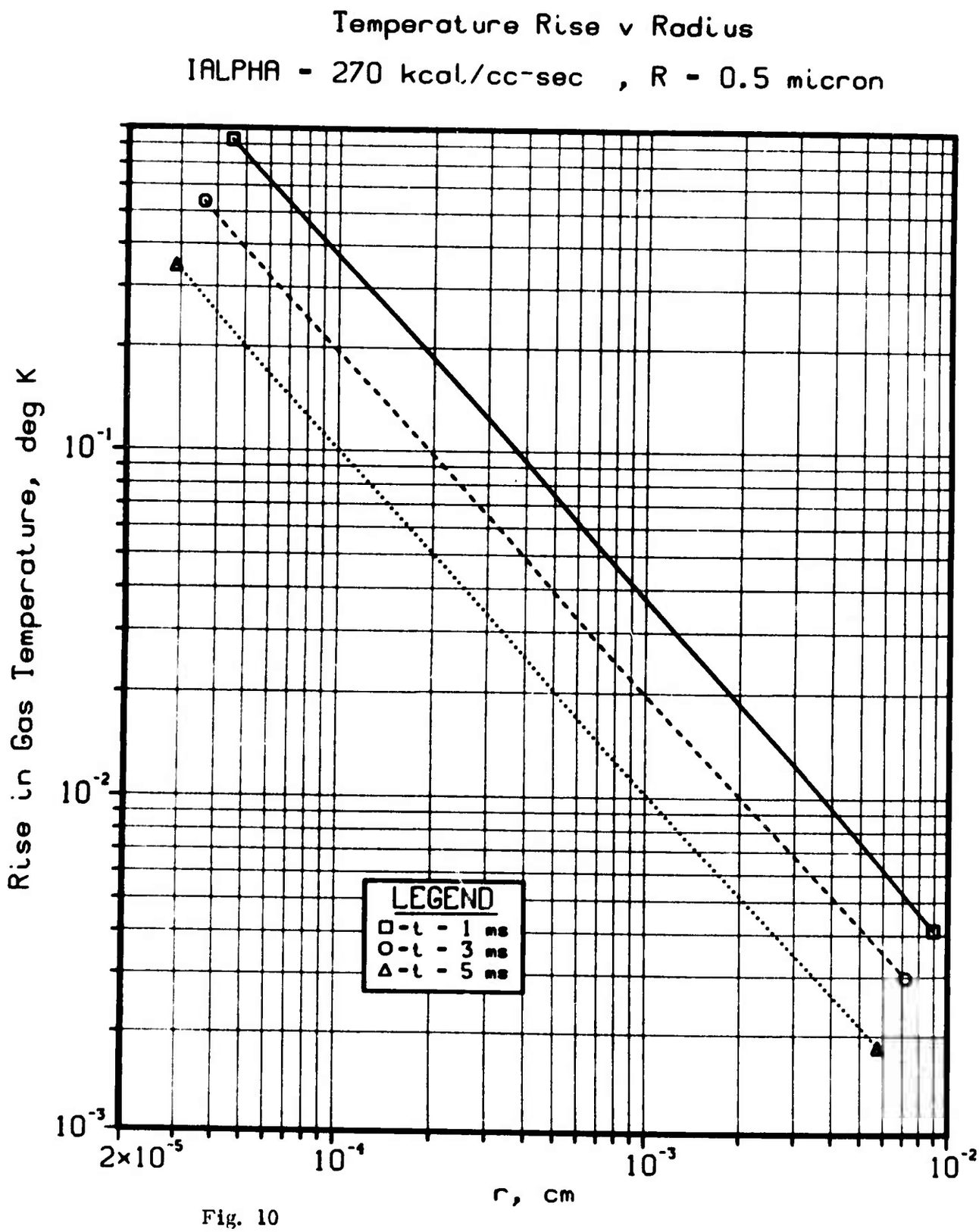
Temperature Rise v Radius
IALPHA - 270 kcal/cc-sec , R - 0.5 micron
Rise in Gas Temperature, deg K
10^{-1}
10^{-2}
10^{-3}
2×10^{-5}
10^{-4}
10^{-3}
10^{-2}
r, cm
LEGEND
□-t - 1 ms
○-t - 3 ms
△-t - 5 ms

Fig. 10

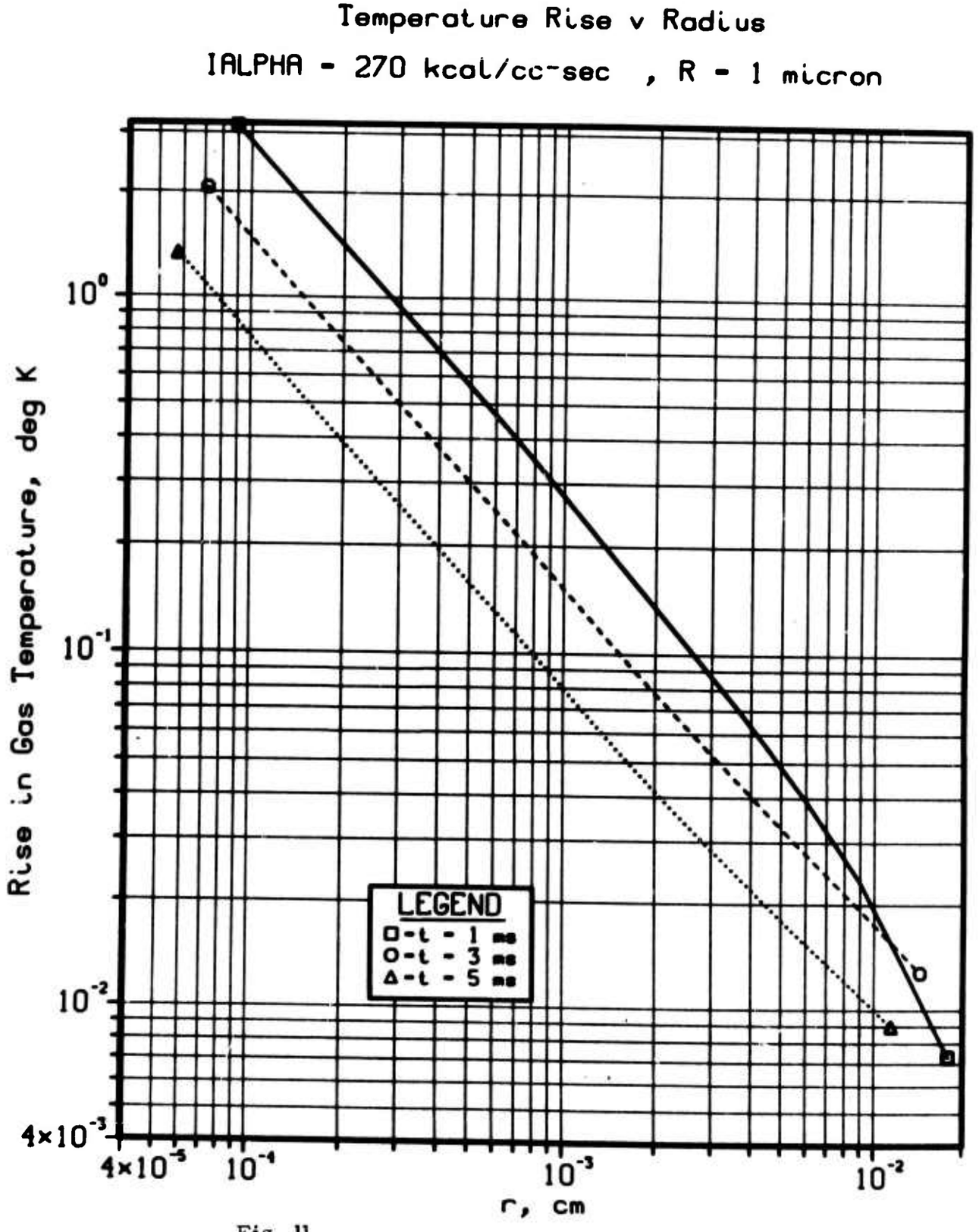
Temperature Rise v Radius
IALPHA - 270 kcal/cc-sec , R - 1 micron
Rise in Gas Temperature, deg K
10^{0}
10^{-1}
10^{-2}
4×10^{-3}
4×10^{-5}
10^{-4}
10^{-3}
10^{-2}
r, cm
LEGEND
□-t - 1 ns
○-t - 3 ns
△-t - 5 ns

Fig. 11

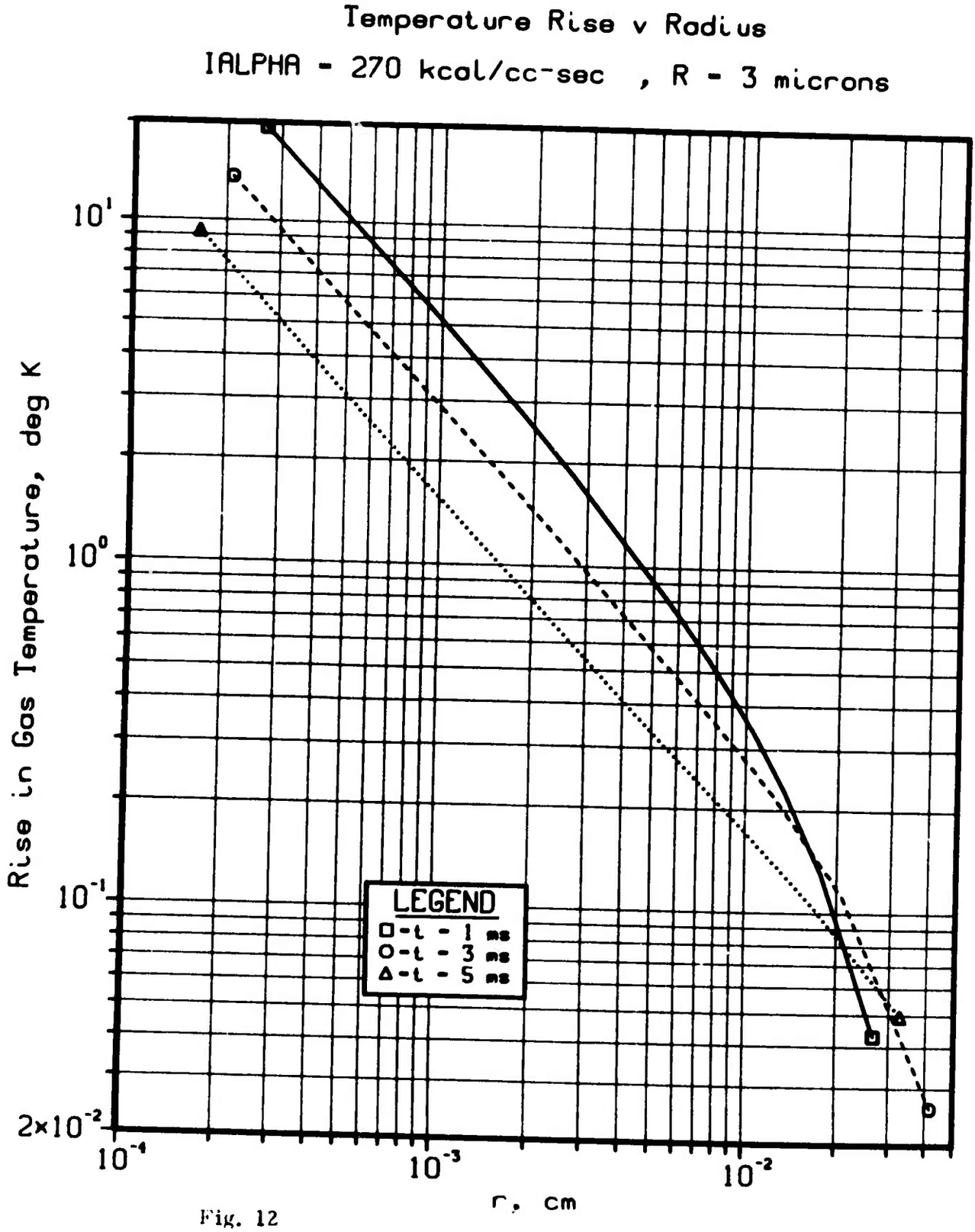
Temperature Rise v Radius
IALPHA - 270 kcal/cc-sec , R - 3 microns
Rise in Gas Temperature, deg K
r, cm
LEGEND
□-t - 1 ms
○-t - 3 ms
△-t - 5 ms
10^1
10^0
10^-1
2x10^-2
10^-4
10^-3
10^-2

Fig. 12

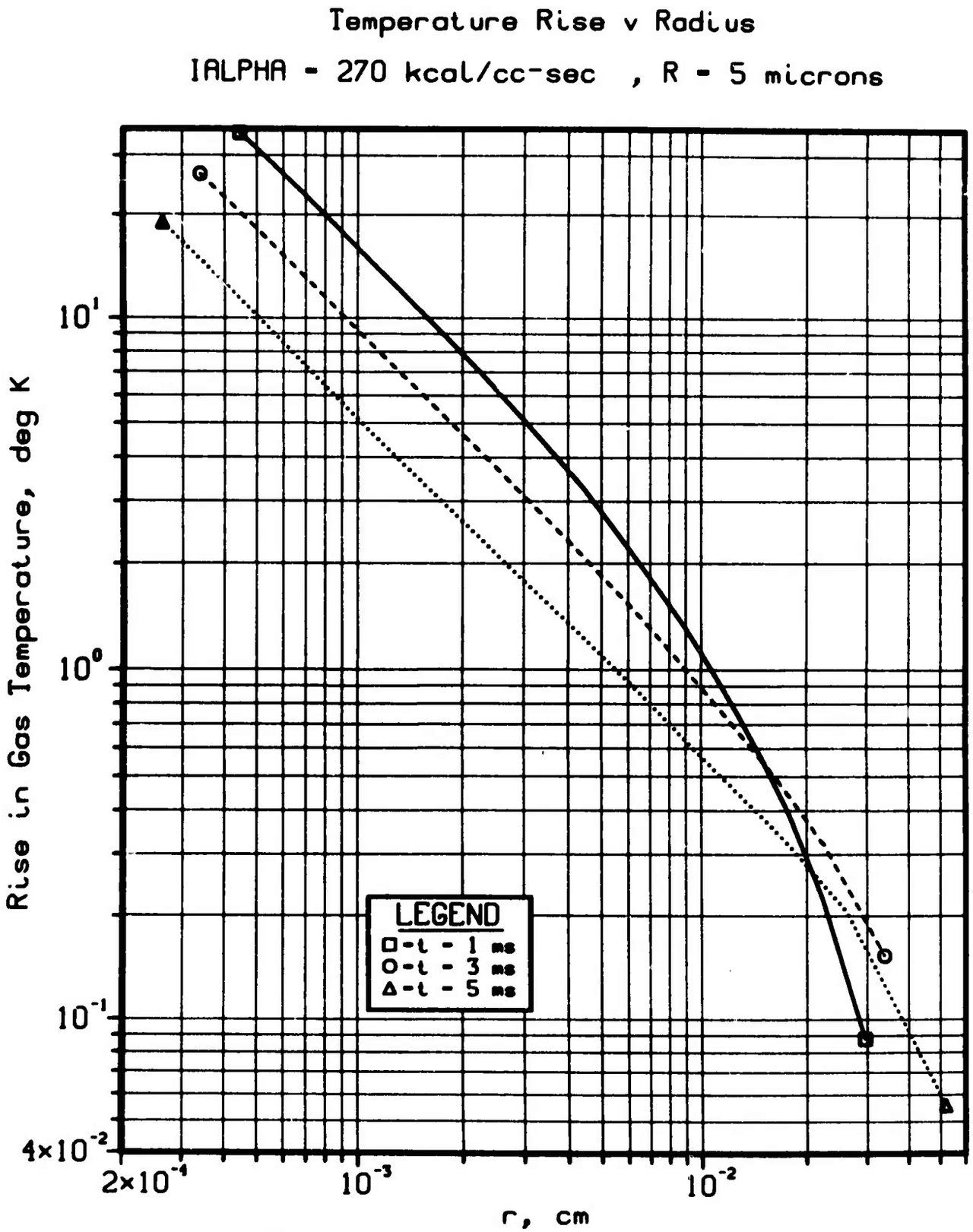
Temperature Rise v Radius
IALPHA - 270 kcal/cc-sec , R - 5 microns
Rise in Gas Temperature, deg K
10^1
10^0
10^-1
4x10^-2
2x10^-4
10^-3
10^-2
r, cm
LEGEND
□-t - 1 ms
○-t - 3 ms
△-t - 5 ms

Fig. 13

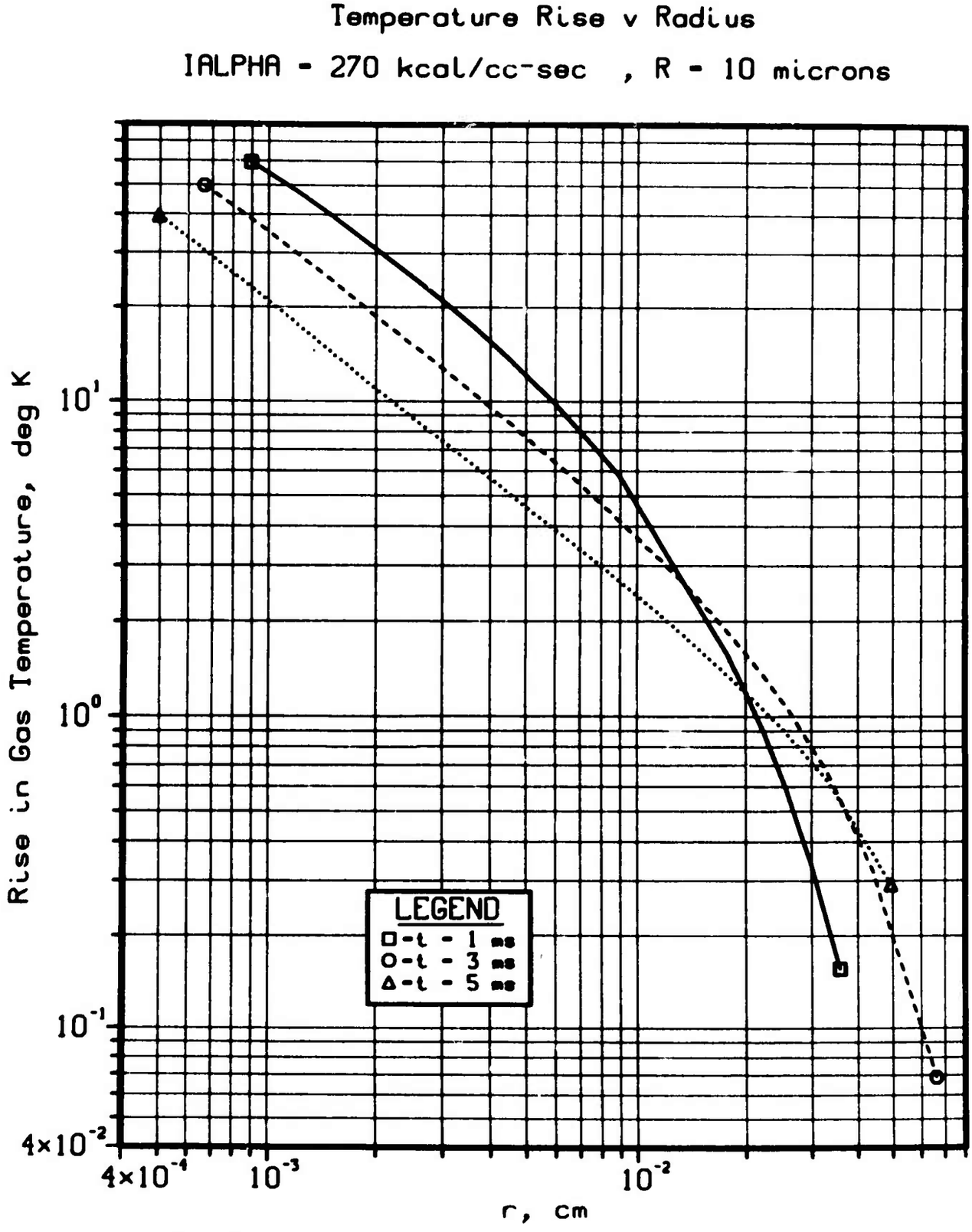
Temperature Rise v Radius
IALPHA - 270 kcal/cc-sec , R - 10 microns
Rise in Gas Temperature, deg K
10^1
10^0
10^{-1}
4×10^{-2}
4×10^{-4}
10^{-3}
10^{-2}
r, cm
LEGEND
□-t - 1 ms
O-t - 3 ms
Δ-t - 5 ms

Fig. 14

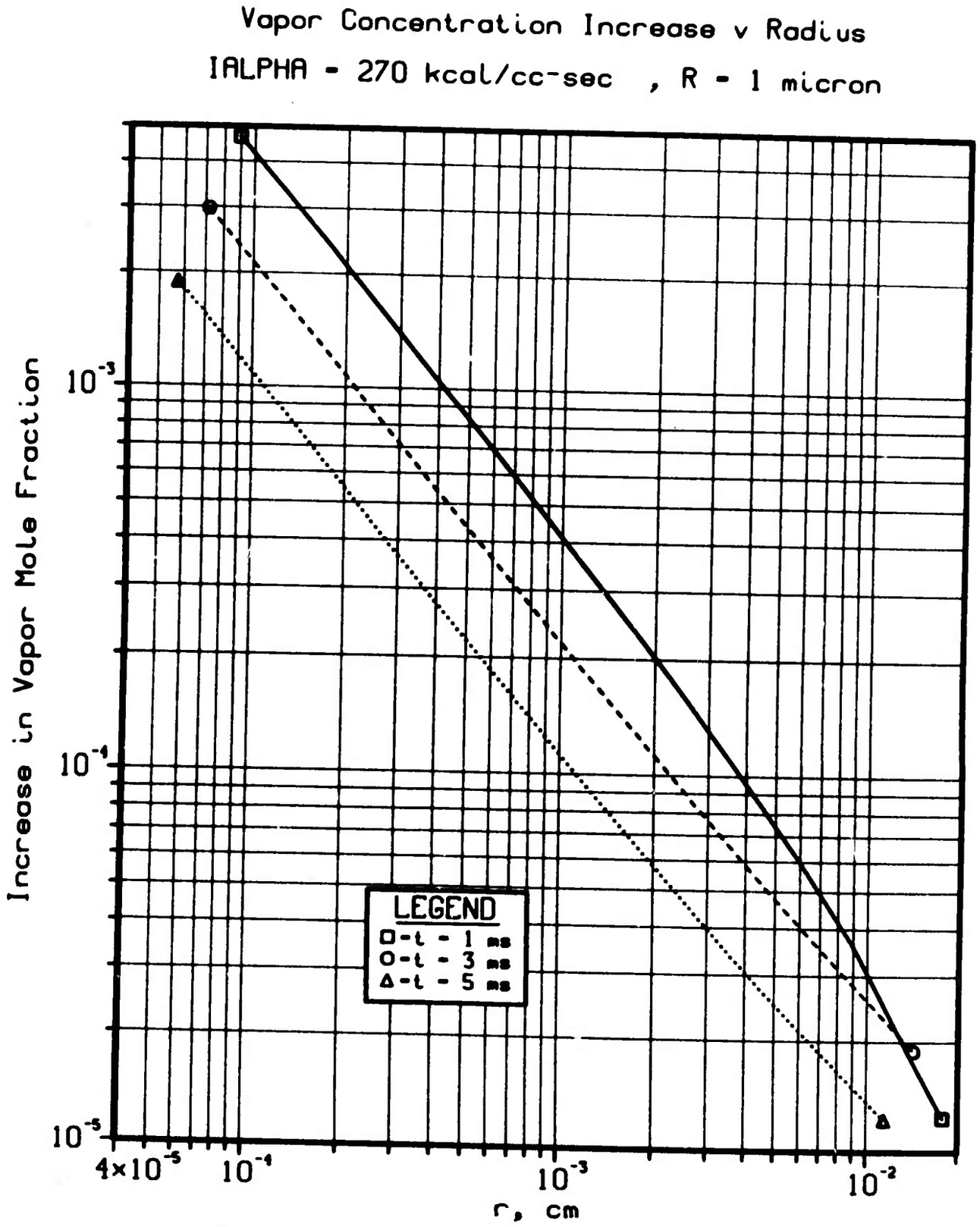
Vapor Concentration Increase v Radius
IALPHA - 270 kcal/cc-sec , R - 1 micron
Increase in Vapor Mole Fraction
10^{-3}
10^{-4}
10^{-5}
4×10^{-5}
10^{-4}
10^{-3}
10^{-2}
r, cm
LEGEND
□-t - 1 ms
○-t - 3 ms
△-t - 5 ms

Fig. 15

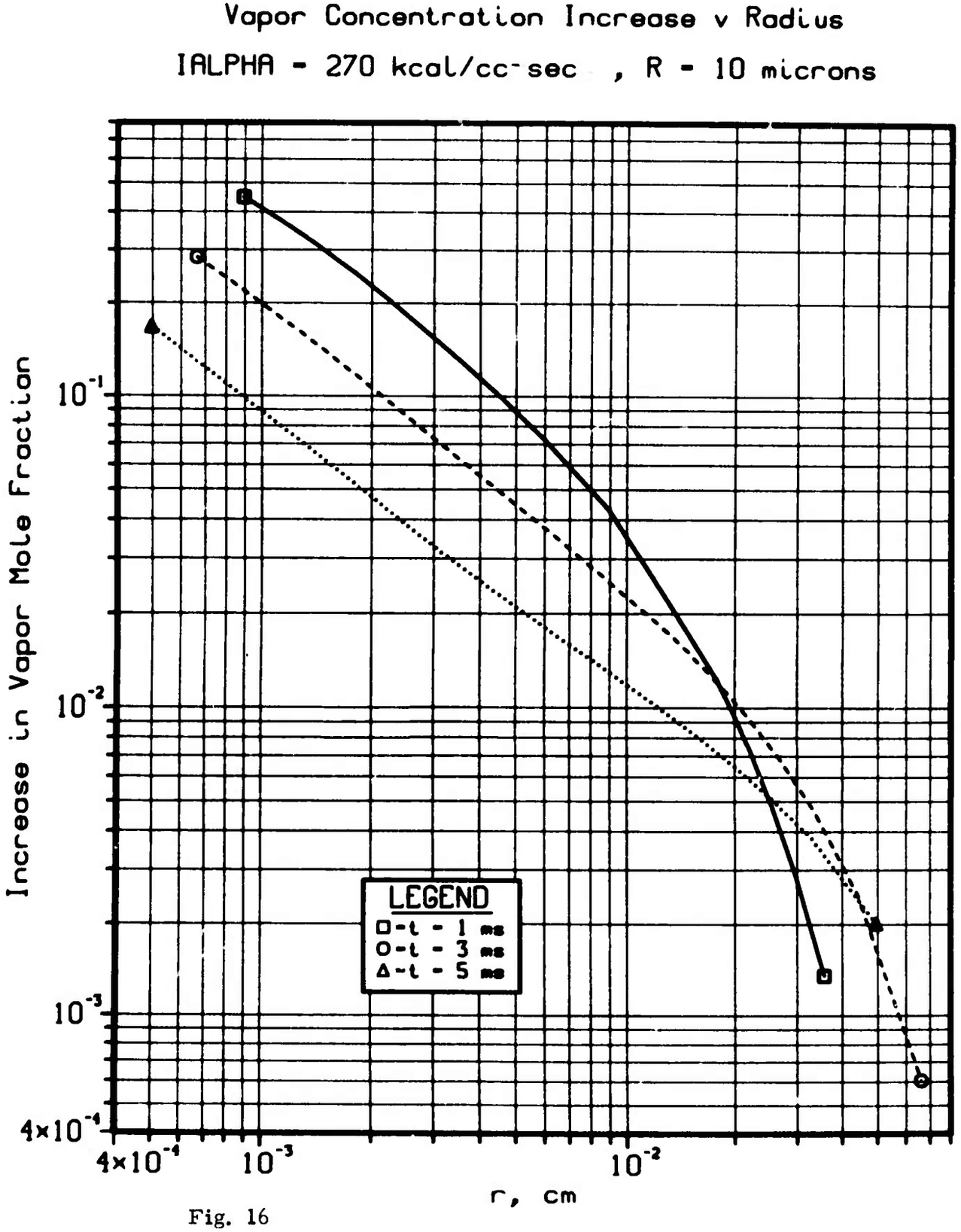
Vapor Concentration Increase v Radius
IALPHA - 270 kcal/cc-sec , R - 10 microns
Increase in Vapor Mole Fraction
10^{-1}
10^{-2}
10^{-3}
4×10^{-4}
4×10^{-4}
10^{-3}
10^{-2}
r, cm
LEGEND
□-t - 1 ms
○-t - 3 ms
Δ-t - 5 ms

Fig. 16

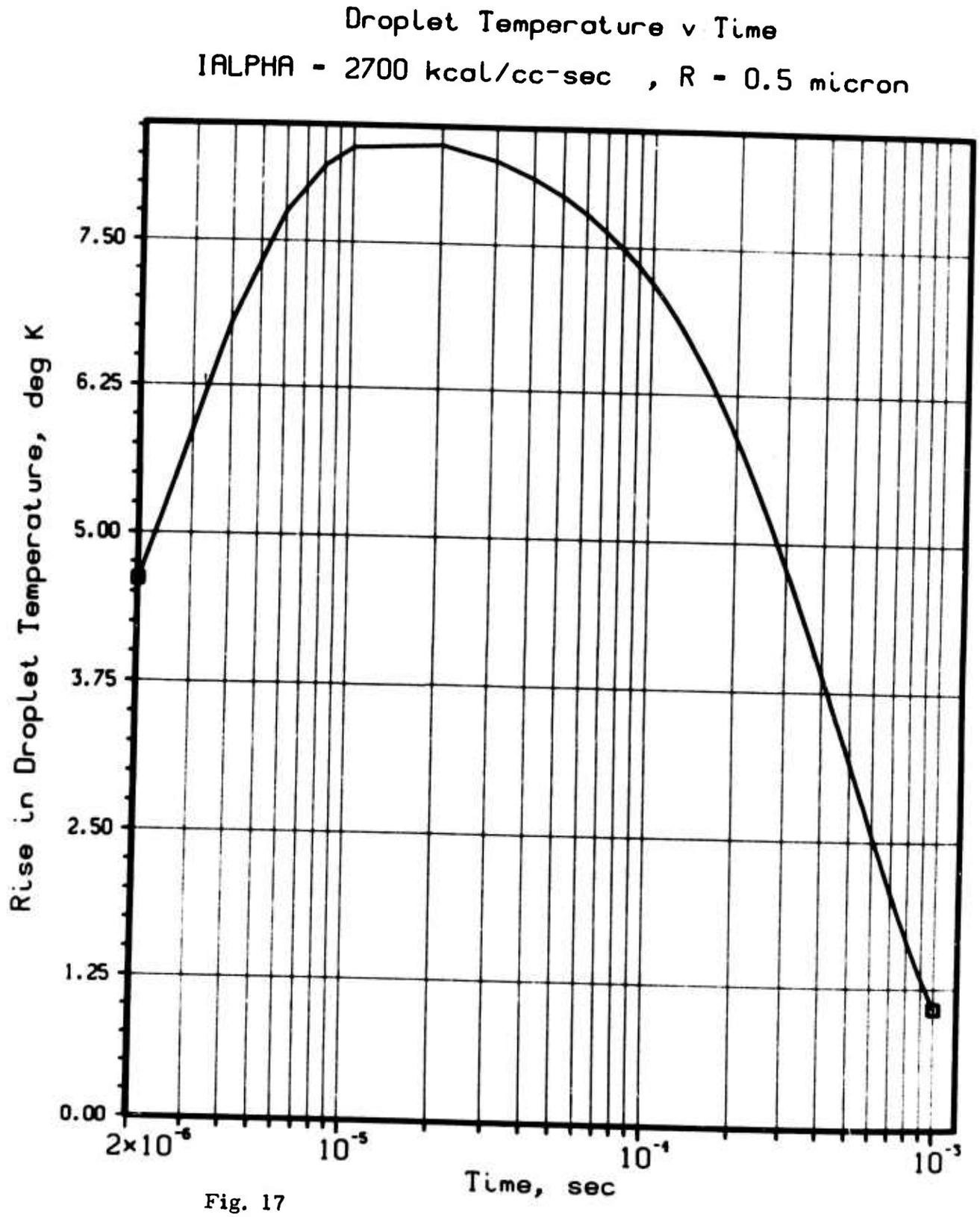
Droplet Temperature v Time
IALPHA - 2700 kcal/cc-sec , R - 0.5 micron
Rise in Droplet Temperature, deg K
7.50
6.25
5.00
3.75
2.50
1.25
0.00
2×10⁻⁶
10⁻⁵
10⁻⁴
10⁻³
Time, sec

Fig. 17

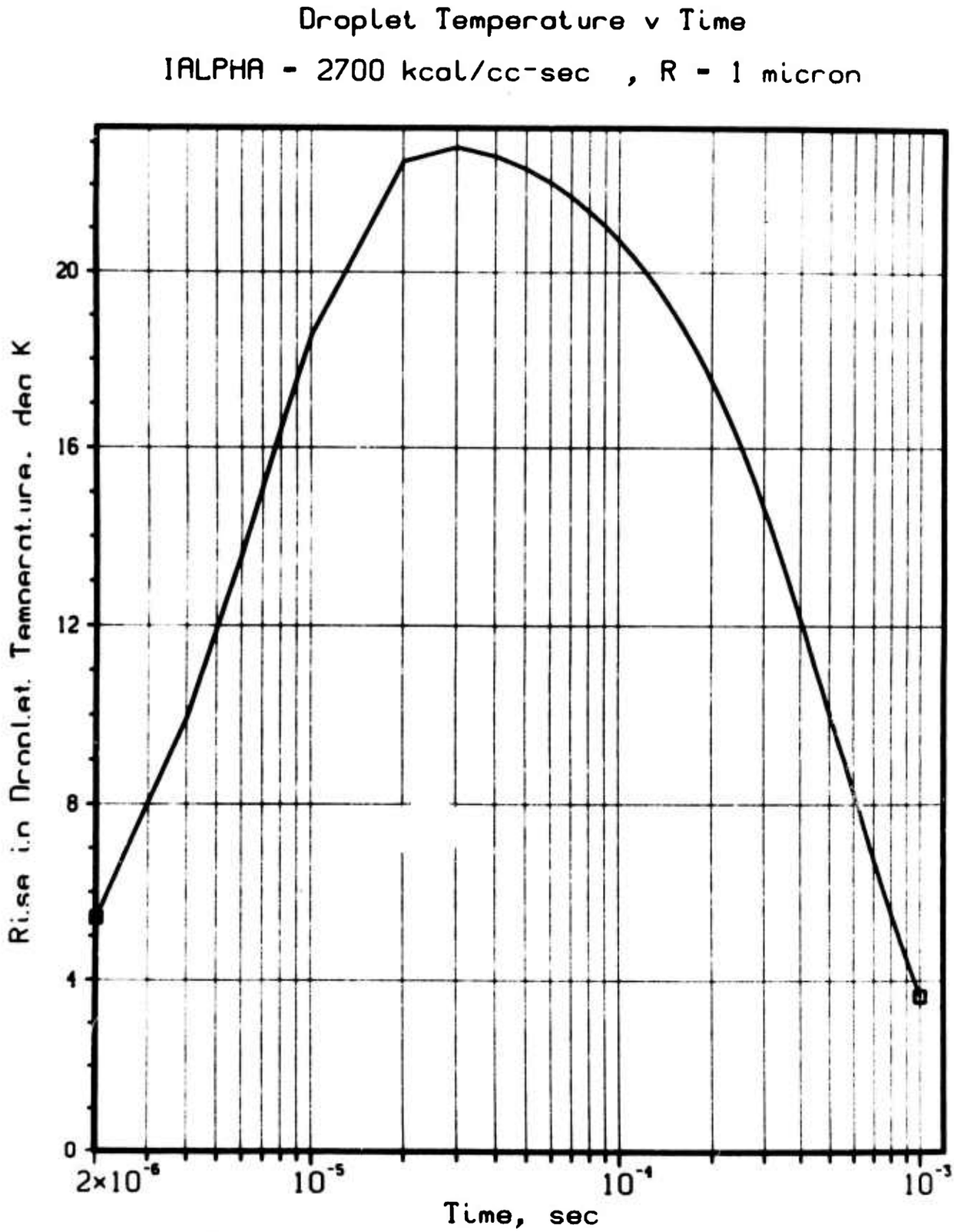
Droplet Temperature v Time
IALPHA - 2700 kcal/cc-sec , R - 1 micron
Rise in Droplet Temperature, deg K
0
4
8
12
16
20
2×10⁻⁶
10⁻⁵
10⁻⁴
10⁻³
Time, sec

Fig. 18

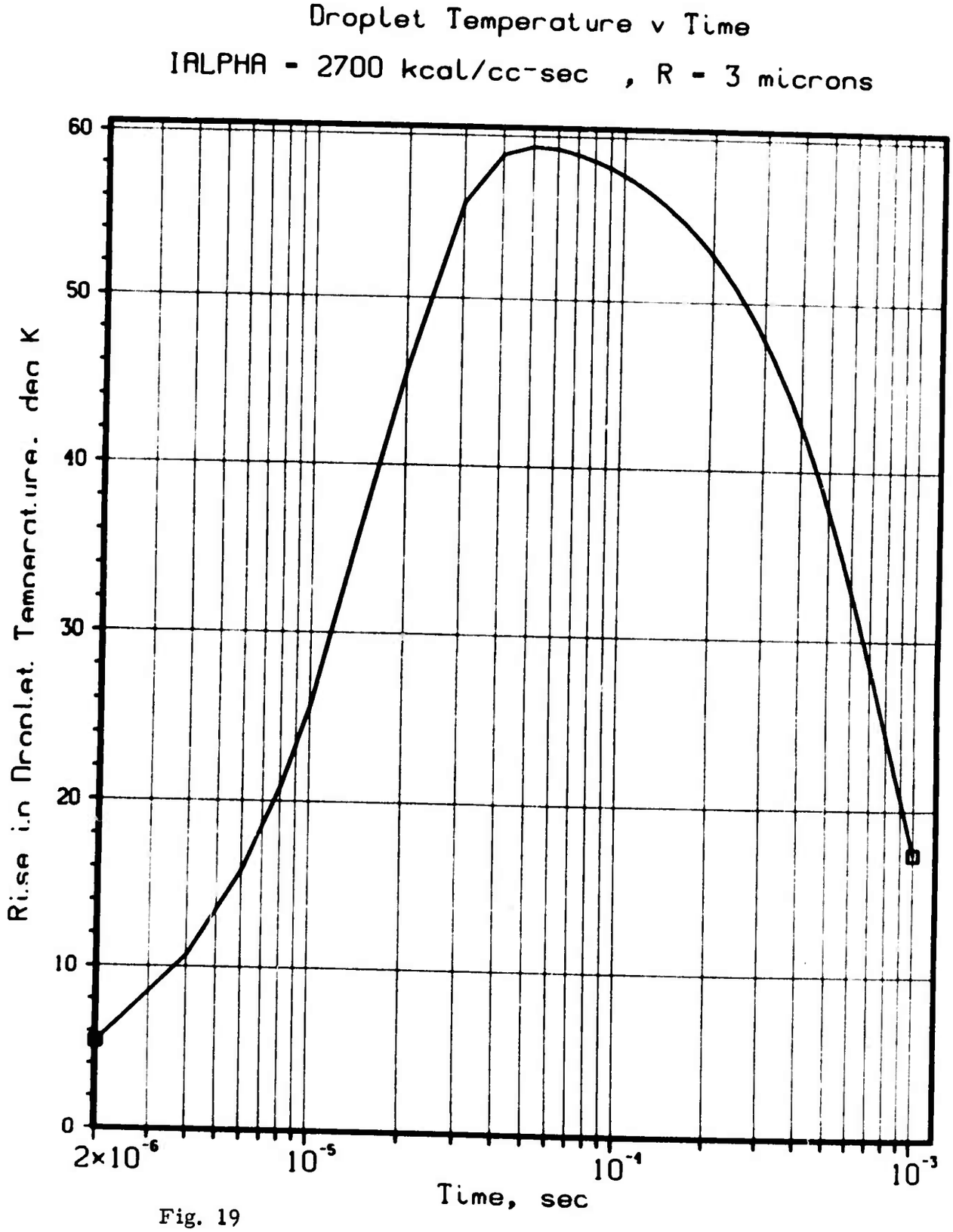
Droplet Temperature v Time
IALPHA - 2700 kcal/cc-sec , R - 3 microns
Rise in Droplet Temperature, deg K
60
50
40
30
20
10
0
2×10⁻⁶
10⁻⁵
10⁻⁴
10⁻³
Time, sec

Fig. 19

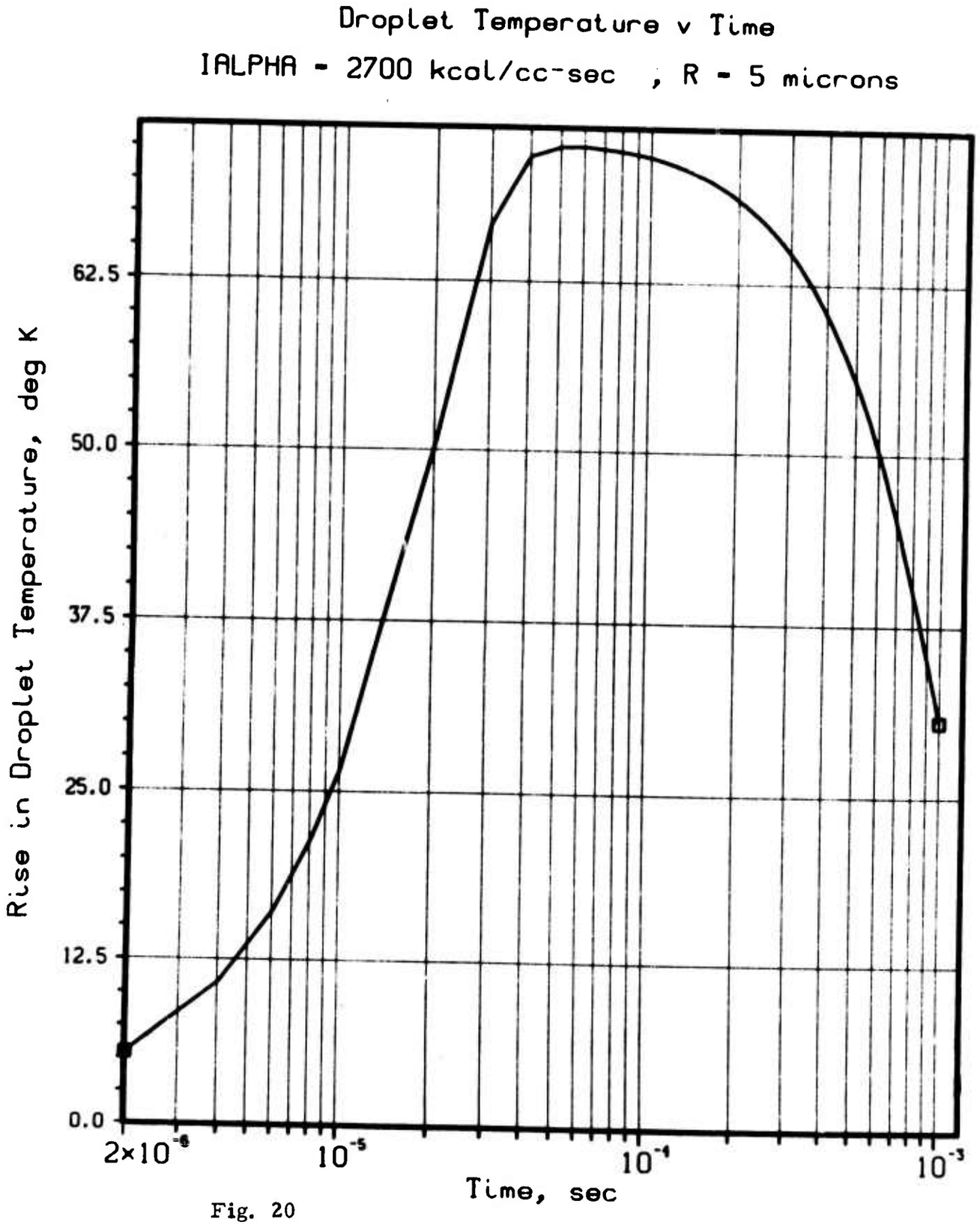
Droplet Temperature v Time
IALPHA - 2700 kcal/cc-sec , R - 5 microns
Rise in Droplet Temperature, deg K
62.5
50.0
37.5
25.0
12.5
0.0
2×10⁻⁶
10⁻⁵
10⁻⁴
10⁻³
Time, sec

Fig. 20

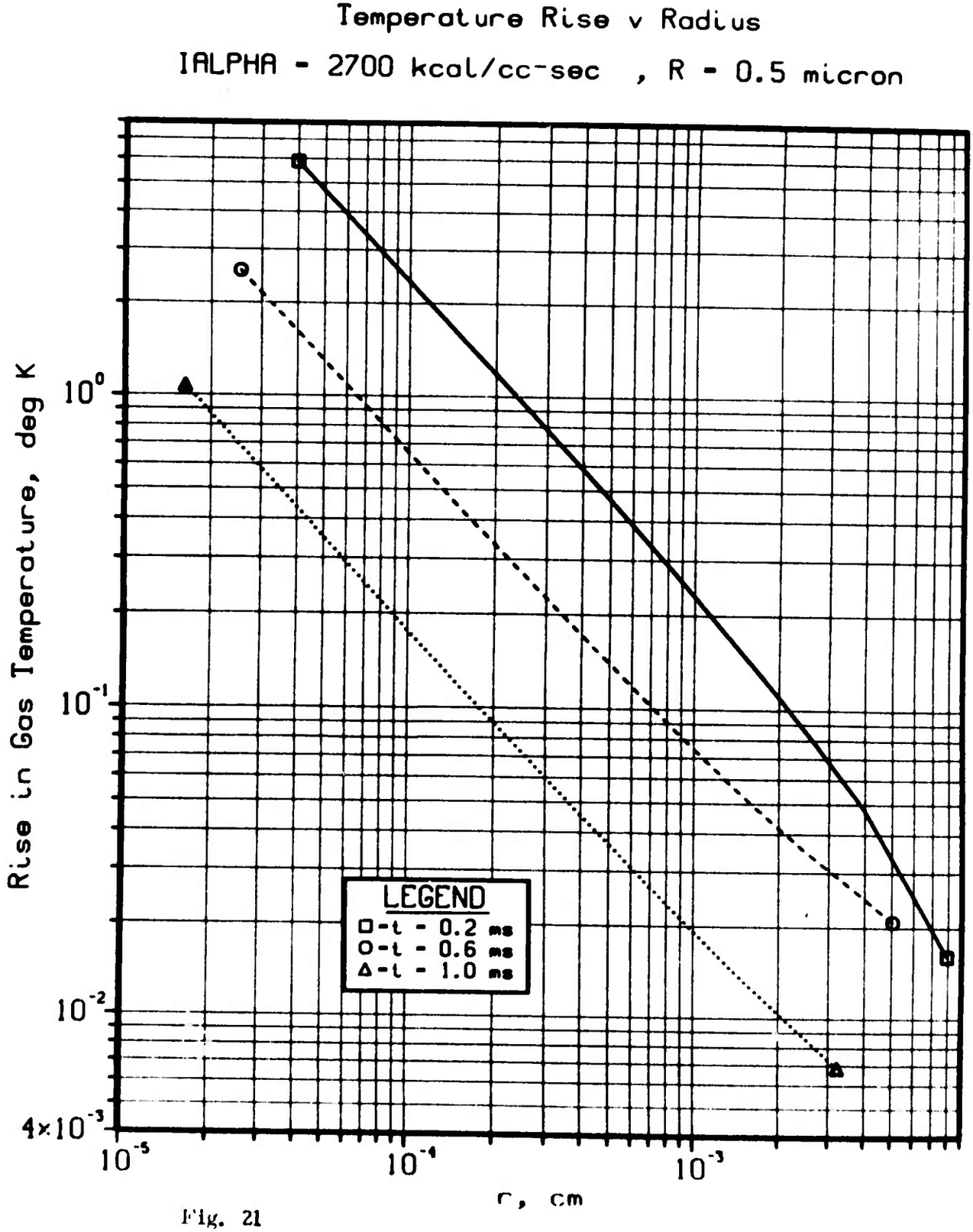
Temperature Rise v Radius
IALPHA - 2700 kcal/cc-sec , R - 0.5 micron
Rise in Gas Temperature, deg K
10^{0}
10^{-1}
10^{-2}
4×10^{-3}
10^{-5}
10^{-4}
10^{-3}
r, cm
LEGEND
□-t - 0.2 ms
○-t - 0.6 ms
△-t - 1.0 ms

Fig. 21

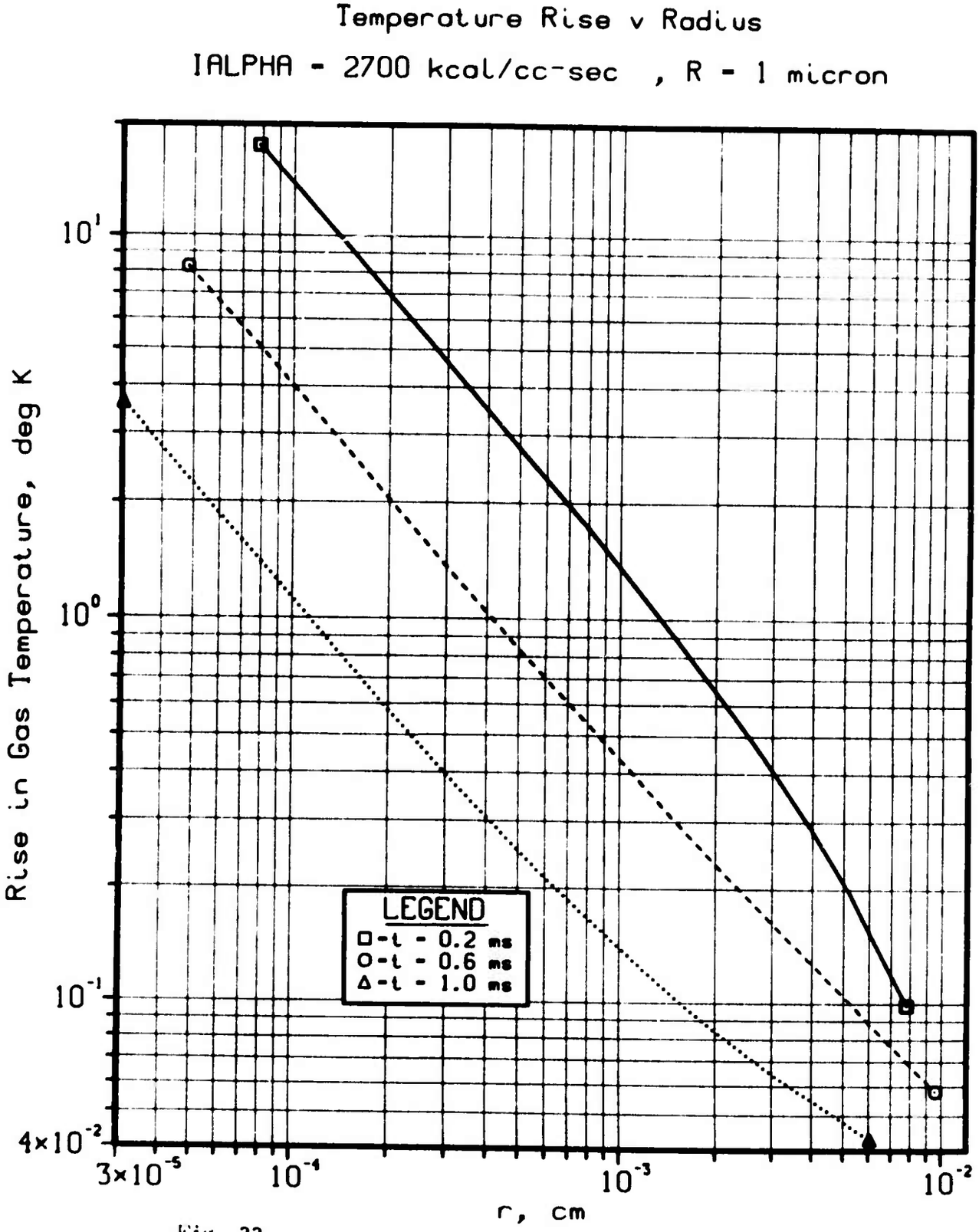
Temperature Rise v Radius
IALPHA - 2700 kcal/cc-sec , R - 1 micron
Rise in Gas Temperature, deg K
r, cm
LEGEND
□-t - 0.2 ms
○-t - 0.6 ms
△-t - 1.0 ms

Fig. 22

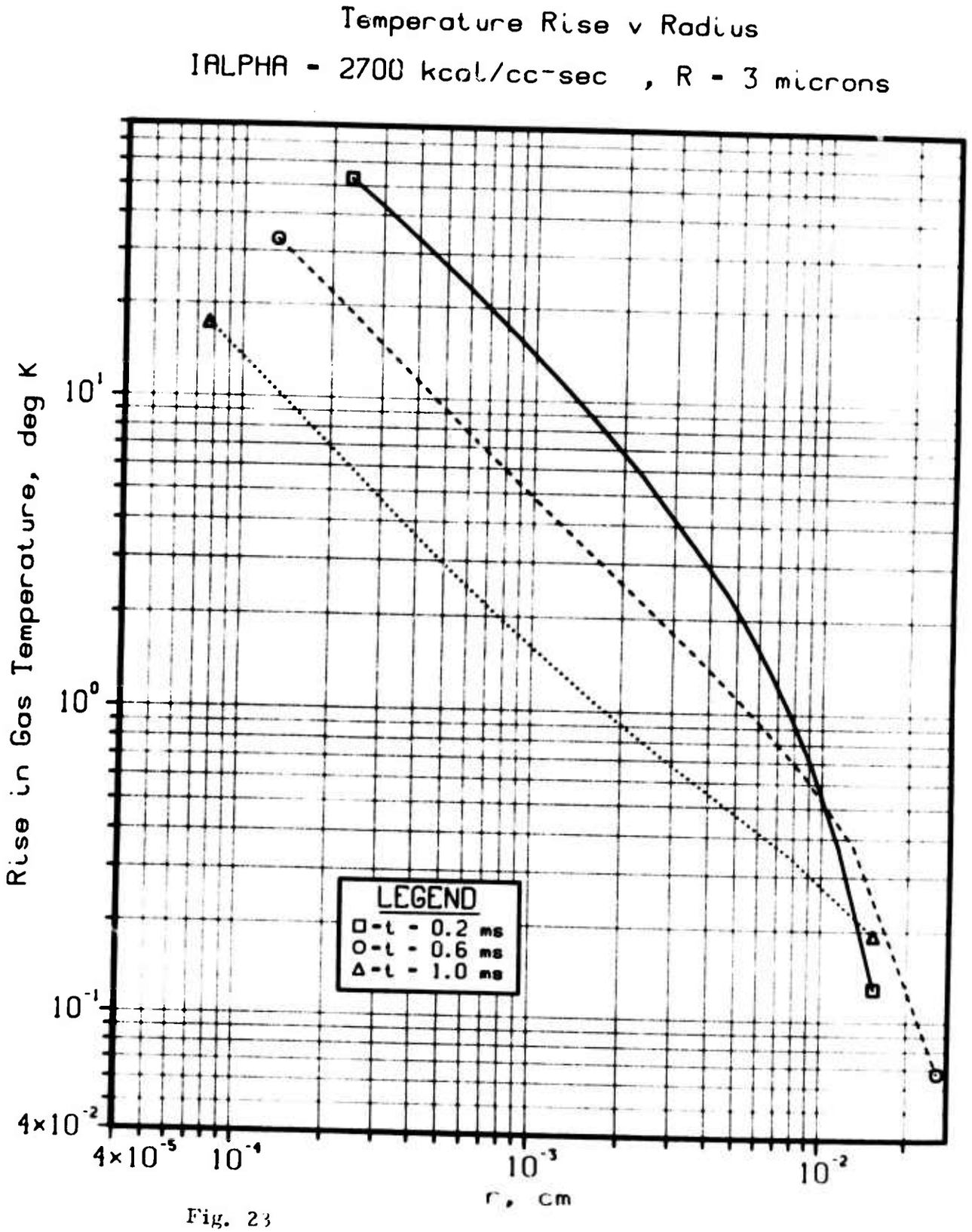
Temperature Rise v Radius
IALPHA - 2700 kcal/cc-sec , R - 3 microns
Rise in Gas Temperature, deg K
10^1
10^0
10^{-1}
4×10^{-2}
4×10^{-5}
10^{-4}
10^{-3}
10^{-2}
r, cm
LEGEND
□-t - 0.2 ms
O-t - 0.6 ms
Δ-t - 1.0 ms

Fig. 23

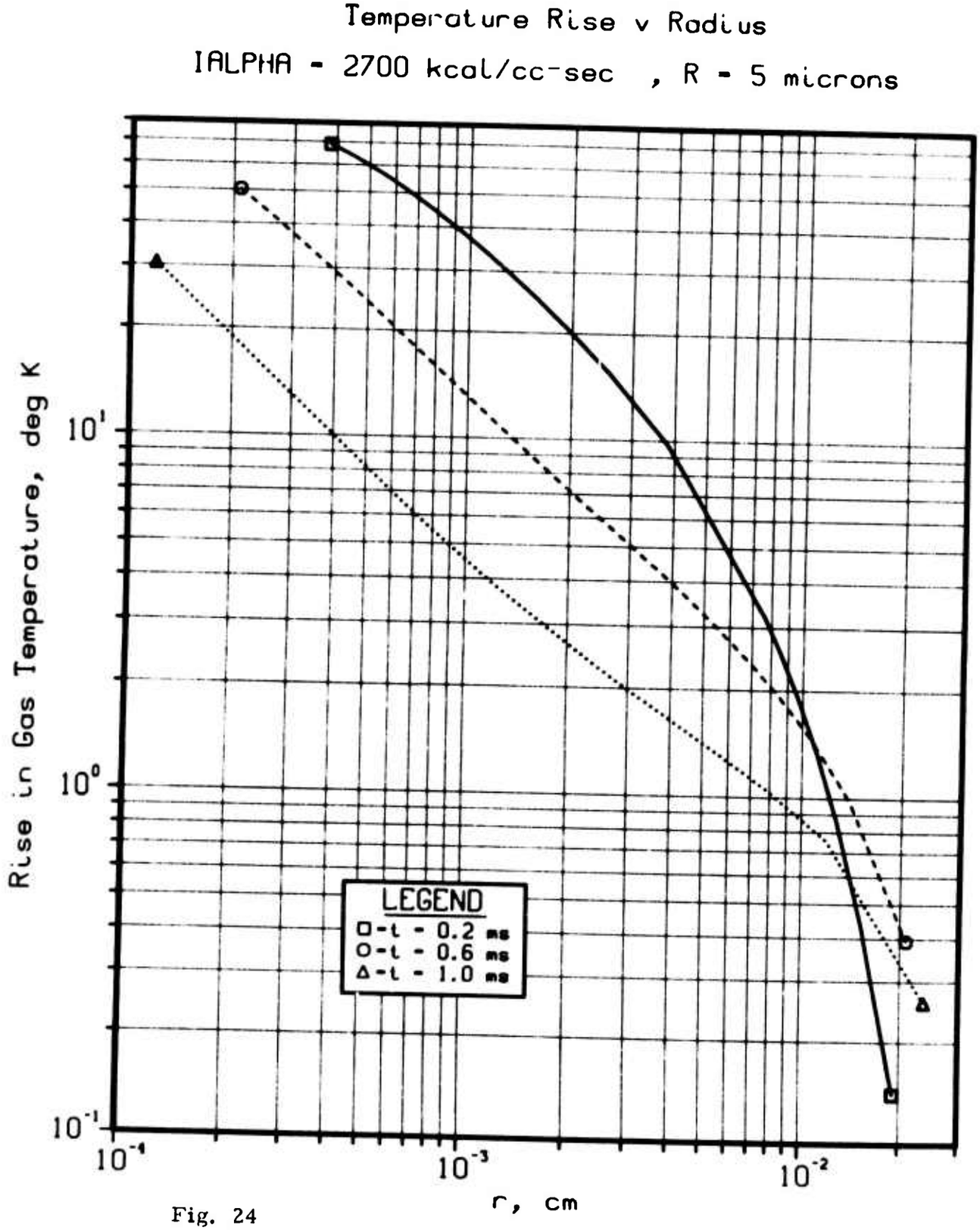
Temperature Rise v Radius
IALPHA - 2700 kcal/cc-sec , R - 5 microns
Rise in Gas Temperature, deg K
10^1
10^0
10^{-1}
10^{-4}
10^{-3}
10^{-2}
r, cm
LEGEND
□-t - 0.2 ms
○-t - 0.6 ms
△-t - 1.0 ms

Fig. 24

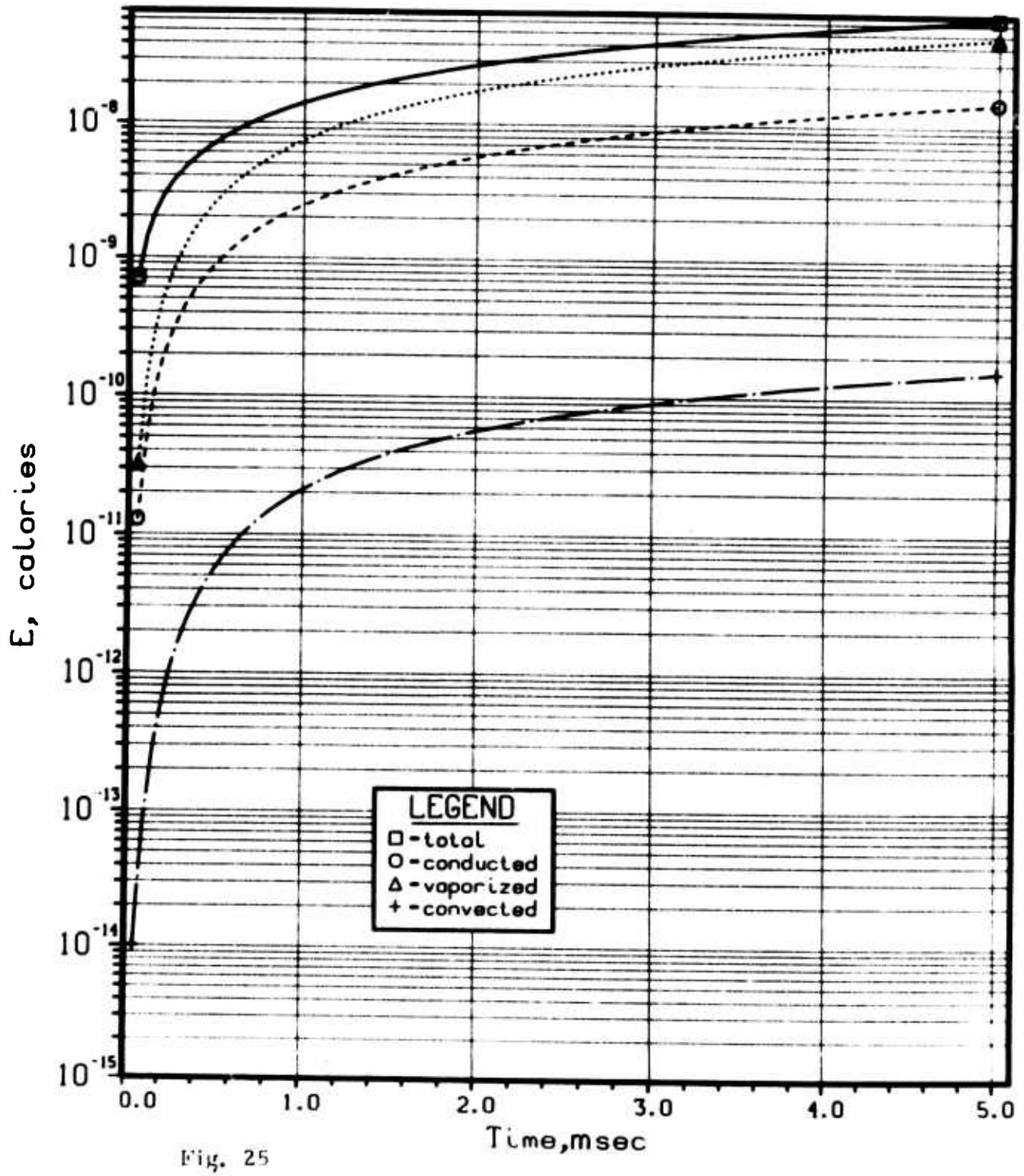
Cumulative Energy Deposition
IALPHA - 27 kcal/cc-sec , R - 5 microns
E, calories
10^-8
10^-9
10^-10
10^-11
10^-12
10^-13
10^-14
10^-15
0.0
1.0
2.0
3.0
4.0
5.0
Time,msec
LEGEND
□ - total
O - conducted
Δ - vaporized
+ - convected

Fig. 25

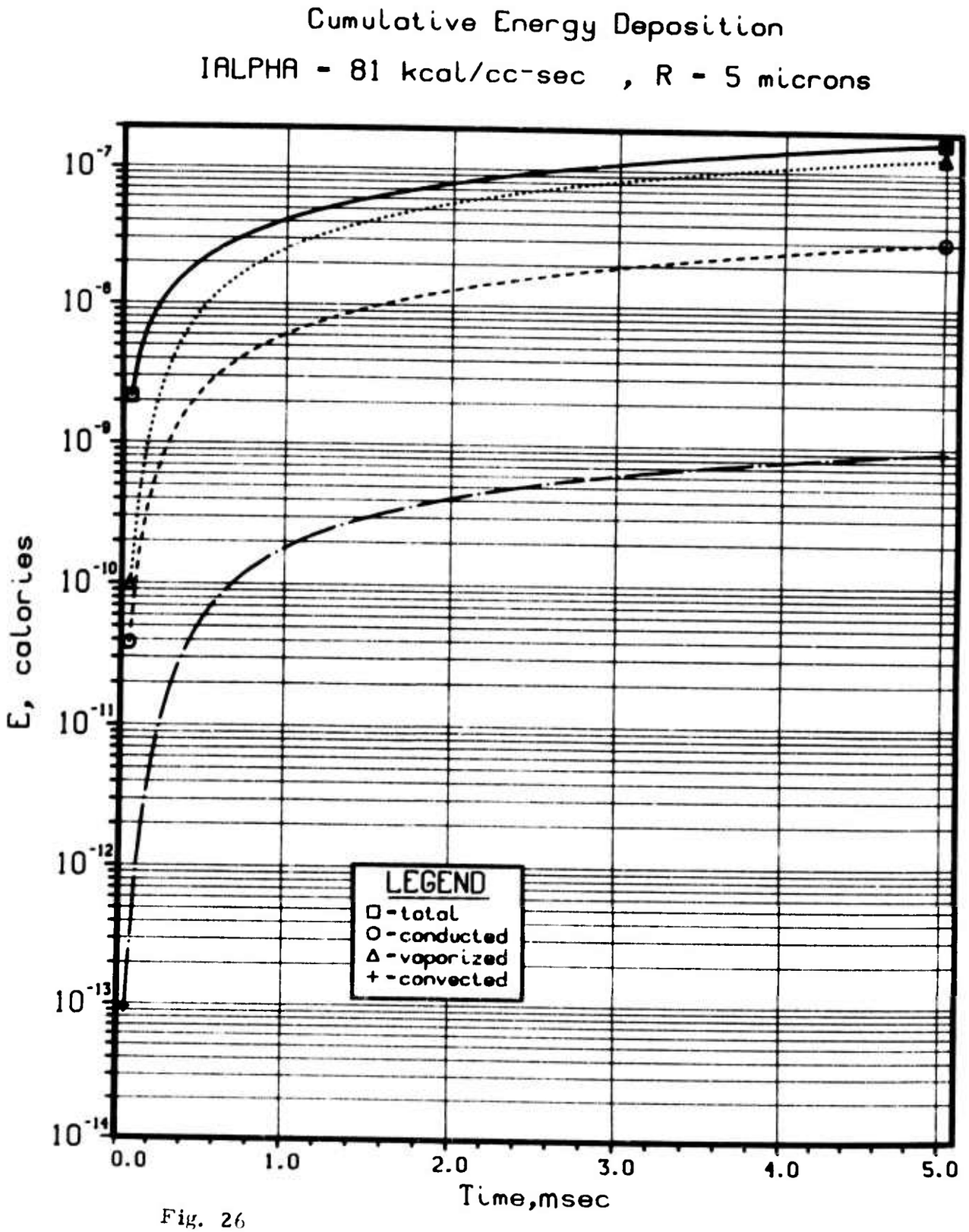
Cumulative Energy Deposition
IALPHA - 81 kcal/cc-sec , R - 5 microns
E, calories
Time,msec
LEGEND
□ - total
O - conducted
Δ - vaporized
+ - convected

Fig. 26

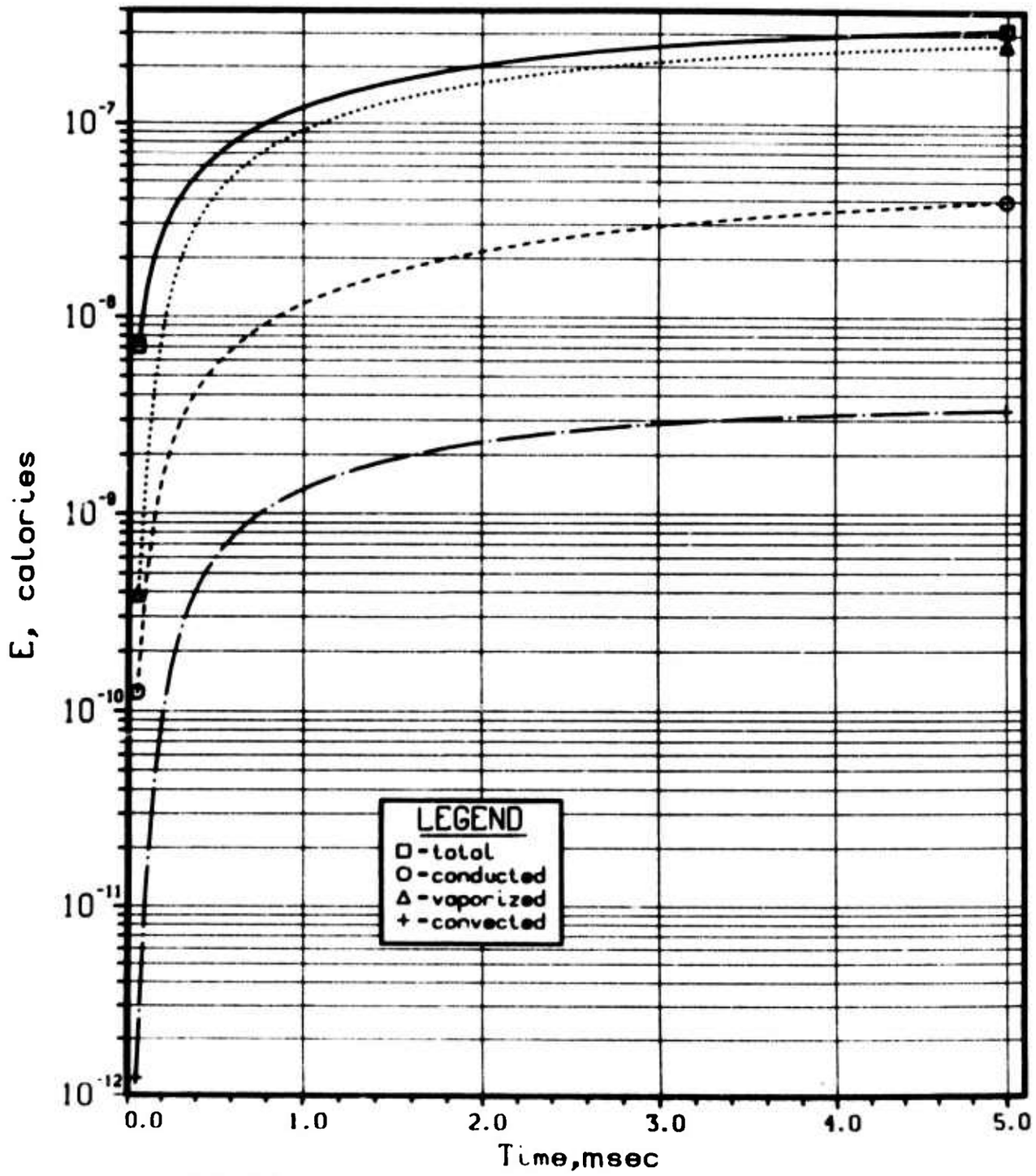
Cumulative Energy Deposition
IALPHA - 270 kcal/cc-sec , R - 5 microns
E, calories
Time,msec
LEGEND
□ - total
O - conducted
Δ - vaporized
+ - convected
10^-7
10^-8
10^-9
10^-10
10^-11
10^-12
0.0
1.0
2.0
3.0
4.0
5.0

Fig. 27

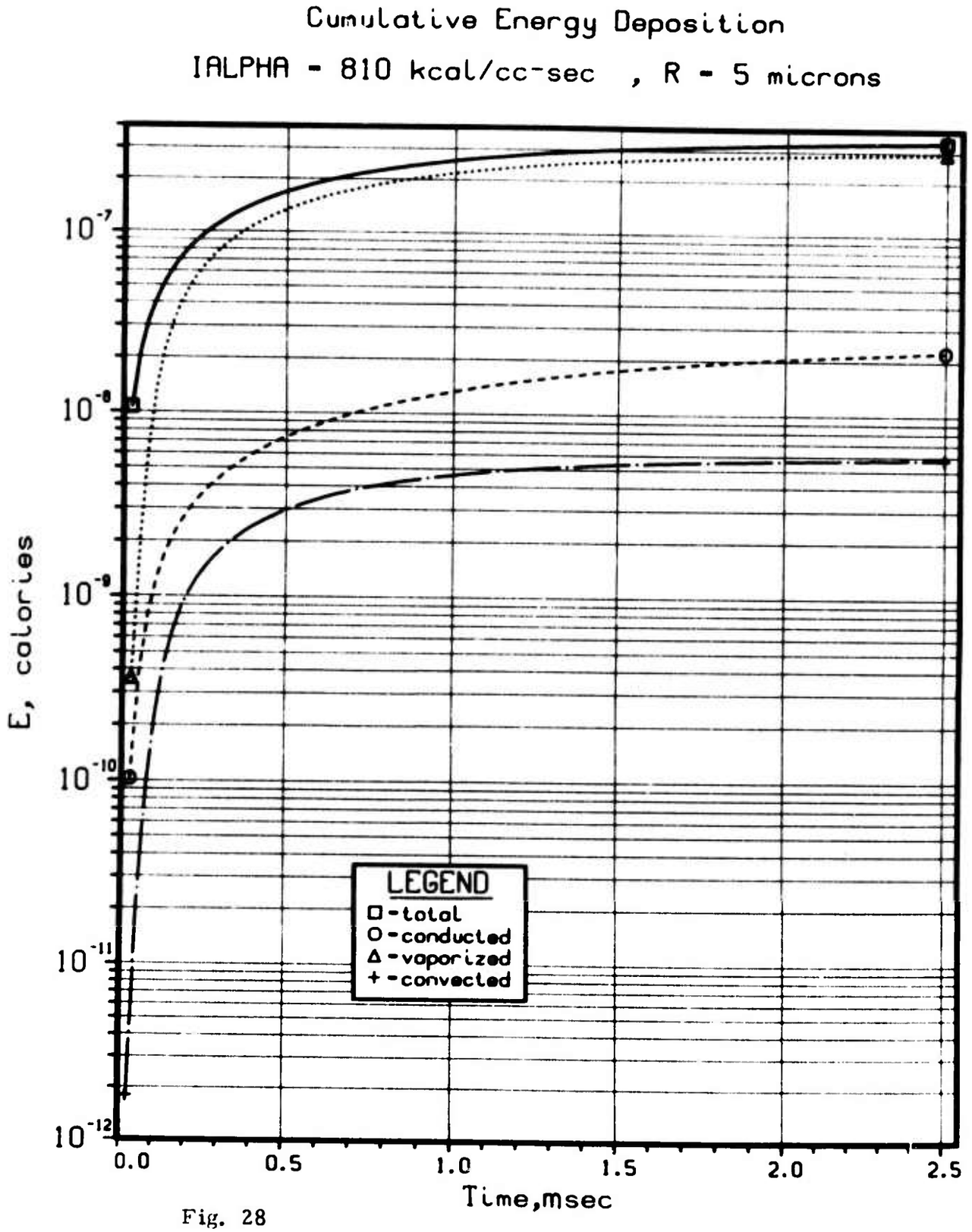
Cumulative Energy Deposition
IALPHA - 810 kcal/cc-sec , R - 5 microns
E, calories
10^{-7}
10^{-8}
10^{-9}
10^{-10}
10^{-11}
10^{-12}
0.0
0.5
1.0
1.5
2.0
2.5
Time,msec
LEGEND
□ - total
O - conducted
Δ - vaporized
+ - convected

Fig. 28

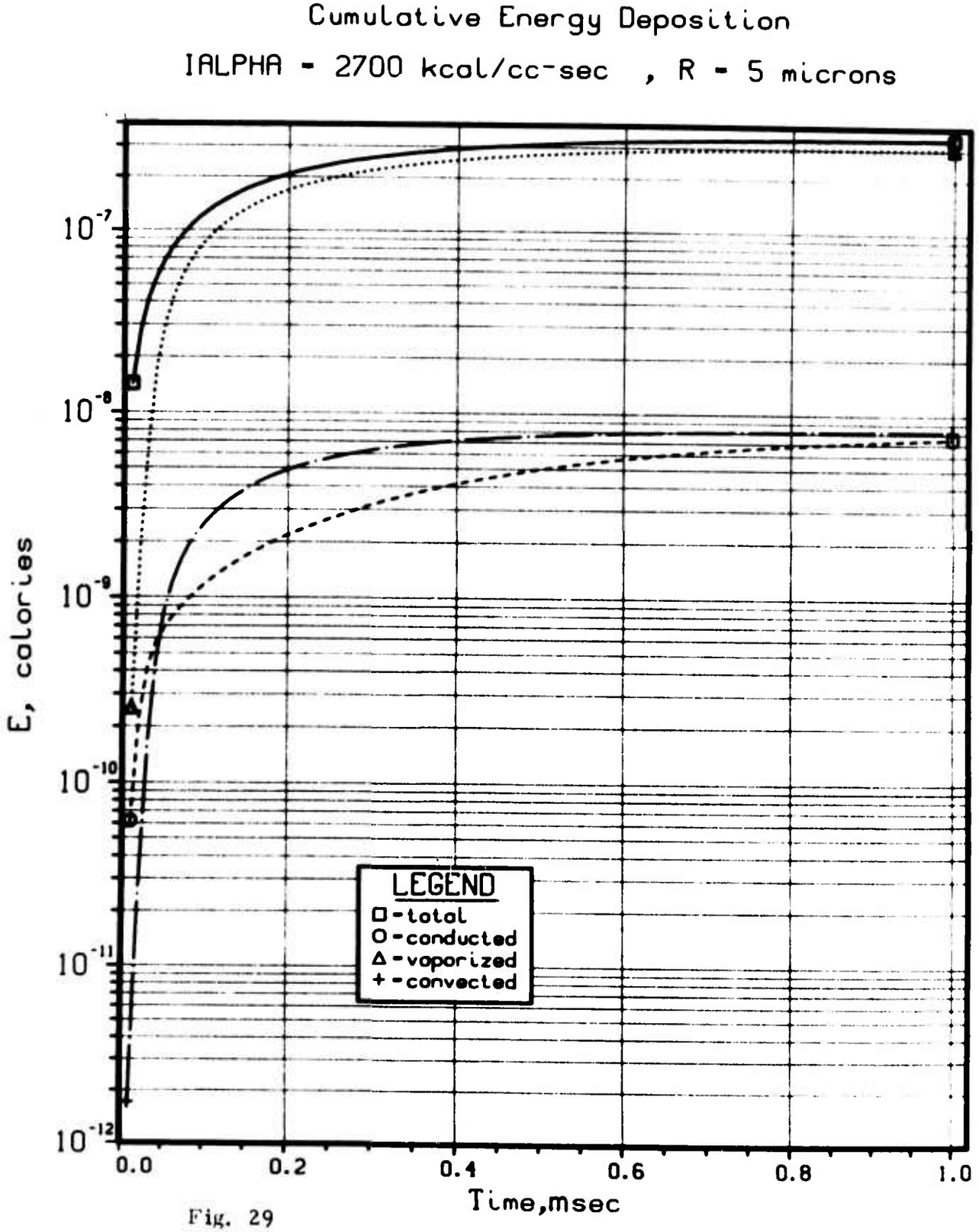
Cumulative Energy Deposition
IALPHA - 2700 kcal/cc-sec , R - 5 microns
E, calories
10^{-7}
10^{-8}
10^{-9}
10^{-10}
10^{-11}
10^{-12}
0.0
0.2
0.4
0.6
0.8
1.0
Time,msec
LEGEND
□ - total
O - conducted
Δ - vaporized
+ - convected

Fig. 29

V. "NON-IDEAL" DROPLET EFFECTS

The modeling discussed in the previous sections has been limited to the ideal case of a pure water droplet undergoing volume absorption. As alluded to in Section II there are a number of effects pertaining to real aerosol properties which either were not included in the model or were included in an approximate manner. Some of these effects are considered in detail in this section. These include consideration of non-uniform absorption and heating, vaporization, solution effects and droplet ebullition.

A. Nonuniform Heating

1. Ray Optics

The calculations discussed in Sections III and IV have all been based on the concept of "volumetric absorption", which is something of a mathematical fiction. From a ray optics viewpoint, it assumes that all rays pass through the irradiated volume without deflection and with negligible attenuation; the energy deposition along a ray bundle of area dA is $I\alpha\, dA\, dr$, or $I\alpha$ watts per unit volume at all points within the irradiated volume, regardless of its shape.

Ray optics can be used to examine the water droplet more realistically, choosing a droplet size for which the theory is applicable, without at this point specifying how large that size must be. From the sketch below it is clear that most of the rays have longer path lengths within the droplet than they would have if they were not deflected by refraction at the droplet surface. For refractive index n, Snell's law yields $\sin\theta = n \sin\phi$, and if an absorption coefficient α cm^{-1} is assumed then $I(s) = I_o e^{-\alpha s}$, where s is measured along the ray from its intersection with the droplet surface. The resultant energy deposition

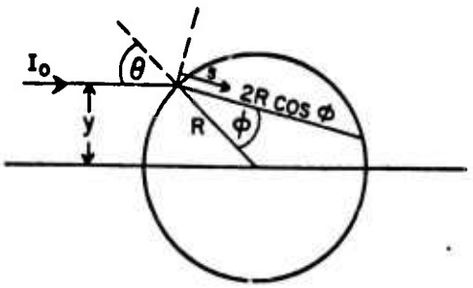

rate within the droplet relative to the volumetric absorption rate can be expressed by the ratio

$$A_R = \frac{\int_0^R 2\pi y\, dy \int_0^{2R\cos\phi} I\, ds}{\int_0^R 2\pi y\, dy\, (I_0 2R\cos\theta)} \tag{44}$$

Making the substitutions $z = y^2 / R^2 = \sin^2\theta$, and $\cos\phi = \sqrt{1 - z/n^2}$ one obtains

$$A_R = \frac{\int_0^1 dz\, \frac{1}{\alpha}\left[-e^{-\alpha s}\right]_0^{2R\sqrt{1-z/n^2}}}{\int_0^1 dz\, 2R\sqrt{1-z}}$$

$$= \frac{\int_0^1 \left[1 - \exp\left(-2\alpha R\sqrt{1 - z/n^2}\right)\right] dz}{2\alpha R\int_0^1 \sqrt{1-z}\, dz}$$

$$= \frac{3}{4\alpha R}\left[1 - 2\left(\frac{n}{2\alpha R}\right)^2 \left\{\left(1 + 2\alpha R\sqrt{1 - 1/n^2}\right)\exp\left(-2\alpha R\sqrt{1 - 1/n^2}\right) - (1 + 2\alpha R)\exp(-2\alpha R)\right\}\right] \tag{45}$$

This expression has several interesting limiting values. For instance, when $n = 1$,

$$A_R = \frac{3}{4\alpha R}\left[1 - \frac{1 - (1+2\alpha R)\exp(-2\alpha R)}{2\alpha^2 R^2}\right]$$

$$\rightarrow 1 - 3\alpha R/4 \qquad \text{as } \alpha R \rightarrow 0 . \tag{46}$$

Thus ray optics recovers the volumetric rate ($A_R = 1$) when $\alpha R \rightarrow 0$, and the correction for finite absorption is obtained in the case where rays are not deflected.

For finite n, and $\alpha R \rightarrow 0$, Eq. 45 takes the form

$$A_R = n^2\left[1 - \left(1 - 1/n^2\right)^{3/2}\right], \tag{47}$$

yielding $A_R = 1.275$ when $n = 1.364$. Finally, for large values of αR, $A_R \rightarrow 3/4\alpha R$, which is independent of n. This implies a correction to the volumetric rate; i. e.

$$\text{total energy deposited} = \frac{4}{3}\pi R^3 I_o \alpha A_R = \pi R^2 I_o . \tag{48}$$

Thus for large α the incident radiation is entirely absorbed within the droplet surface, and refraction is irrelevant.

For $n = 1.364$ and $\alpha = 112.4\ \text{cm}^{-1}$, Eq. 45 has been used to evaluate A_R as a function of R, and values of $A_R\alpha$ are shown in Fig. 2. $A_R\alpha$ is thus an effective absorption coefficient and it may be compared with the absorption coefficient obtained from Mie theory, as discussed in Section II, and shown in Fig. 2. It is clear that the ray optics value of effective absorption coefficient is excellent for $R \geq 50\ \mu m$, but rather seriously in error (as would be expected) for $R \leq 20\ \mu m$.

Knowing the focusing effect of a spherical refracting surface, one can be sure that the heating within a droplet of $R \geq 50\ \mu m$ is highly nonuniform. For smaller droplets, Mie theory establishes that the total absorption becomes much higher than the volumetric rate, but no statement can be made about the spatial nonuniformity of the energy deposition at this time. This can only be established by using Mie theory to evaluate the fields and their derivatives within the droplet, and this effort does not appear justified at present. However, it is worthwhile to revert to the ray optics and ascertain the local energy deposition rate as a function of position within the droplet. Establishing the location of contours of constant absorption rate is a straight-forward bookkeeping problem on a computer, and two cases have been evaluated. Figure 30 shows the location of contours for $M = 3$, 4, 5 and 10, where M is the ratio of local absorption rate to the volumetric absorption rate. Along the droplet centerline M increases monotonically from 1.0 near the front face to slightly over 4 at the rear face. Higher absorption rates are found in a cusp-shaped region where ray-crossing occurs. Beyond this region lies almost 20% of the sphere volume which receives no energy input at all. The results are displayed more quantitatively in Fig. 31. The curve of M versus P shows what percentage (P) of the sphere volume is contained within any given M-value contour. Corresponding to any P is a value N which represents the mean energy deposition rate (relative to the volumetric rate) for the entire volume within the M(P) contour. Thus the curves show that 2% of the volume lies within the $M = 5$ contour, while the mean rate within this 2% volume is $N = 8.8$ times volumetric.

As long as $\alpha R \lesssim .01$ there is negligible attenuation along a ray, and the results labeled "no absorption" are applicable for all values of R for which ray optics is valid. Unfortunately, for $R \geq 50\ \mu m$ the attenuation is appreciable, so a separate calculation has been carried out for the $R = 50\ \mu m$ case, and plotted in Fig. 31. Although

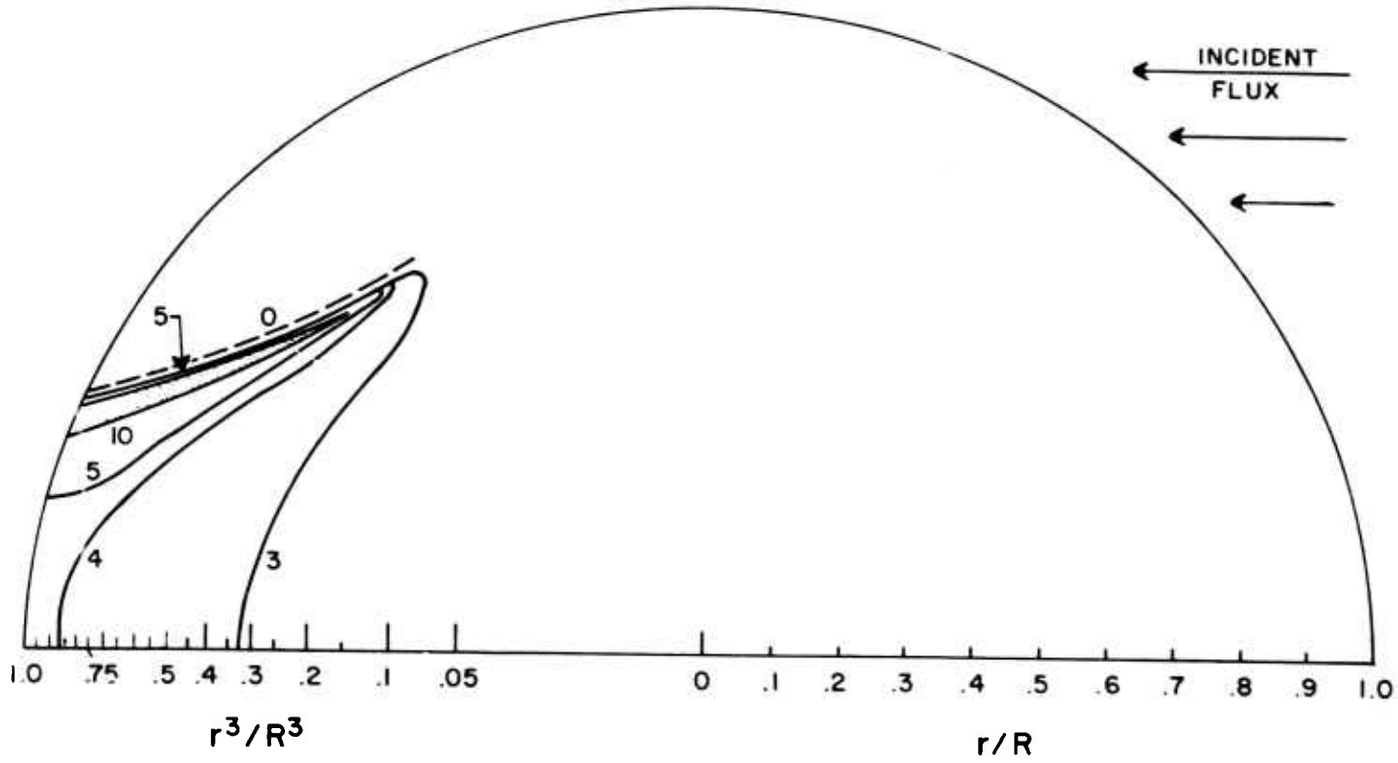

Fig. 30 Nonuniform Absorption Within Droplet. Focusing effect at rear of droplet is shown by contours of local absorption rate normalized by the volumetric absorption rate. Calculations are based on ray optics, with no attenuation of the incident beam.

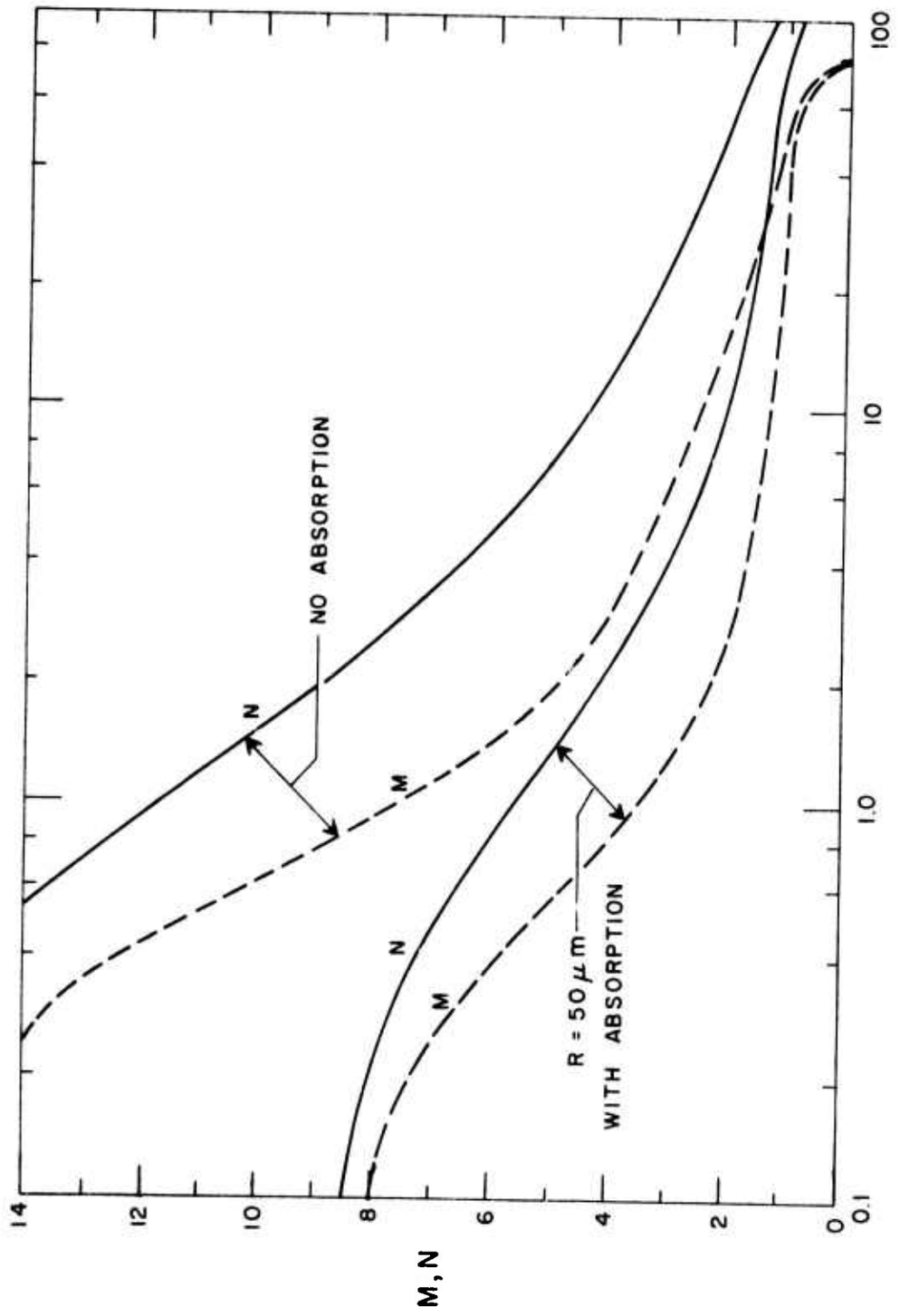

Fig. 31 Nonuniform Absorption Within Droplet. Symbols are described in the text. Calculations are based on ray optics, with $n = 1.364$ and $\alpha = 0$ or $\alpha = 112.4\ cm^{-1}$.

the focusing effects are less dramatic, one still finds 1% of the sphere volume within the $M = 3.5$ contour, and an average rate of 5.6 times volumetric within that contour.

2. Temperature Gradients Within a Droplet

Although at this point no simple way of determining the magnitude of the nonuniformities in heating rates within the smaller droplets ($R \lesssim 20\ \mu m$) has been established, it would appear that nonuniformities will exist. Thus it is important to assess the effects of internal temperature gradients caused by these nonuniformities.

It has already been pointed out that even the uniform absorption requires a nonuniform temperature distribution within the droplet, since heat must flow toward the droplet surface for removal by conduction and vaporization. For a heating rate of $I_o \alpha_o$ the steady-state difference in temperature between droplet center and surface was shown to be $\Delta T_o = \frac{I_o \alpha_o R^2}{6k_D}$, where $k_D \approx 1.4 \times 10^{-3}$ cal/cm-sec^o K is the thermal conductivity of water. The value of ΔT_o is plotted in Fig. 4 as a function of $I_o \alpha_o R^2$. In the two examples which follow the effect of nonuniform heating on $\Delta T = T_{center} - T_{surface}$ is examined, and the results expressed at $\Delta T/\Delta T_o$. For simplicity, both cases considered preserve the spherical symmetry, and steady-state conditions are assumed.

For the first example a uniform heating rate $I\alpha$ cal/cm^3 - sec within a radius $r < R$ is assumed, while the remainder of the droplet is taken to be heated at the primary rate $I_o \alpha_o$. Then it can be shown that

$$\frac{\Delta T}{\Delta T_o} = 1 + \left(\frac{I\alpha}{I_o \alpha_o} - 1\right)\left(\frac{r}{R}\right)^2 \left(3 - \frac{2r}{R}\right) \qquad (49)$$

and this function is plotted in Fig. 32. The curves indicate that if ~ 1% of the central volume of the droplet had a heating rate of 10 times the volumetric rate, then the ΔT value would be doubled. This localized heating need not be restricted to the focusing, of course; this analysis is equally valid for the case of an insoluble nucleus having a large absorption coefficient within the droplet for which $\alpha >> \alpha_o$.

Fig. 30 showed that the focusing effects generated high heating rates much closer to the surface than to the center. Search for a solution of an asymmetric heating problem of this type is not justified at this time, but a spherically symmetric case of some relevance can be readily set up. This is illustrated in Fig. 33, where now the higher heating rate $(I\alpha)$ is confined to a spherical shell $r_1 < r < r_2$, while the basic rate $I_o \alpha_o$ applies to the regions $0 < r < r_1$ and $r_2 < r < R$. In this case the steady state solution is

$$\frac{\Delta T}{\Delta T_o} = 1 + \left(\frac{I\alpha}{I_o \alpha_o} - 1 \right) \left[\frac{3\left(r_2^2 - r_1^2\right)}{R^2} - \frac{2\left(r_2^3 - r_1^3\right)}{R^3} \right] \qquad (50)$$

The effect of varying the position of the $r_1 r_2$ shell is best displayed by keeping the shell volume constant. Thus Fig. 33 shows values of $\Delta T/\Delta T_o$ plotted versus r_1/R, for shell volumes of 5, 10 and 15% of the droplet volume. As $r_1 \to 0$ the values of $\Delta T/\Delta T_o$ are identical with those obtained from Fig. 32 with $(r/R)^3 = .05, .10$ and $.15$ respectively. Thus the curves of Fig. 33 show the decrease obtained in $\Delta T/\Delta T_o$ as the region with higher heating rate is displaced from the center. Nevertheless it is clear that the possible increases in $T_{center} - T_{surface}$ are still appreciable, and this can be an important factor once T_{center} approaches the boiling point, as will be discussed later.

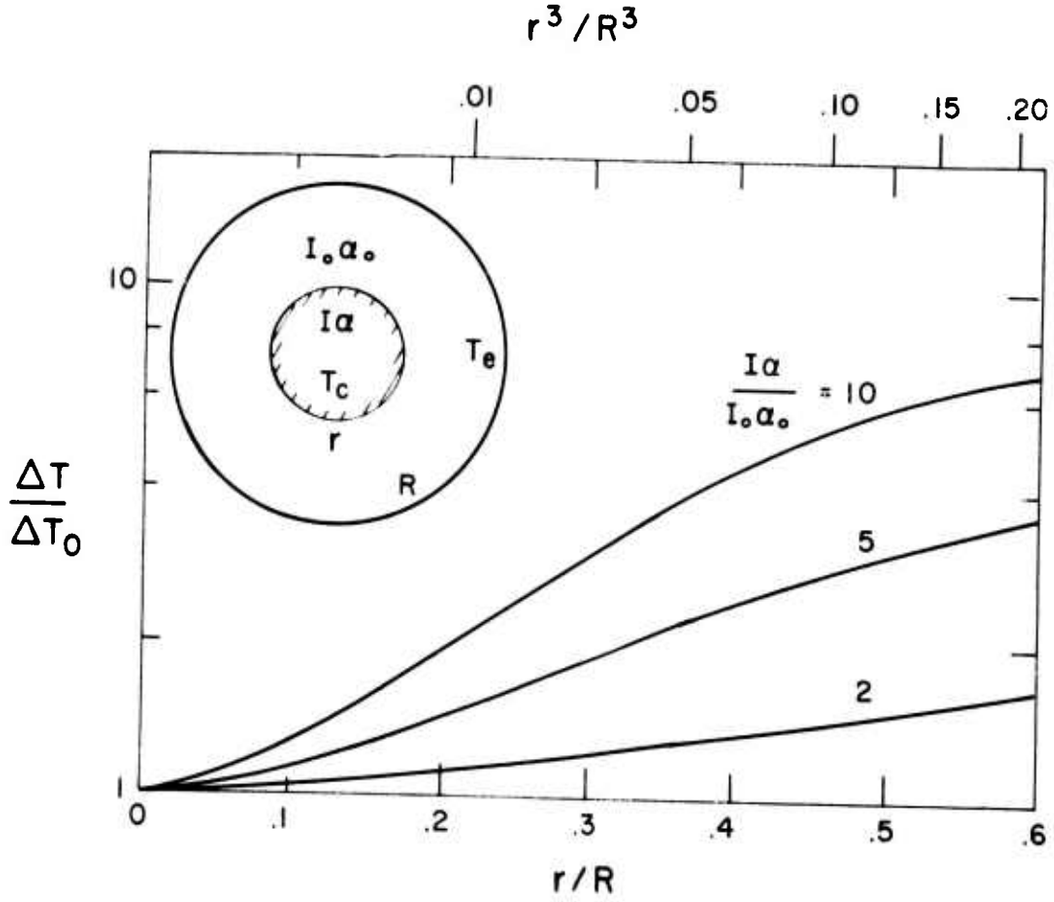

Fig. 32 Differential Heating at Center of Droplet. The temperature difference $\Delta T = T_c - T_e$ is shown for various values of the volumetric absorption rate $I\alpha$ which applies to the inner spherical region, radius r.

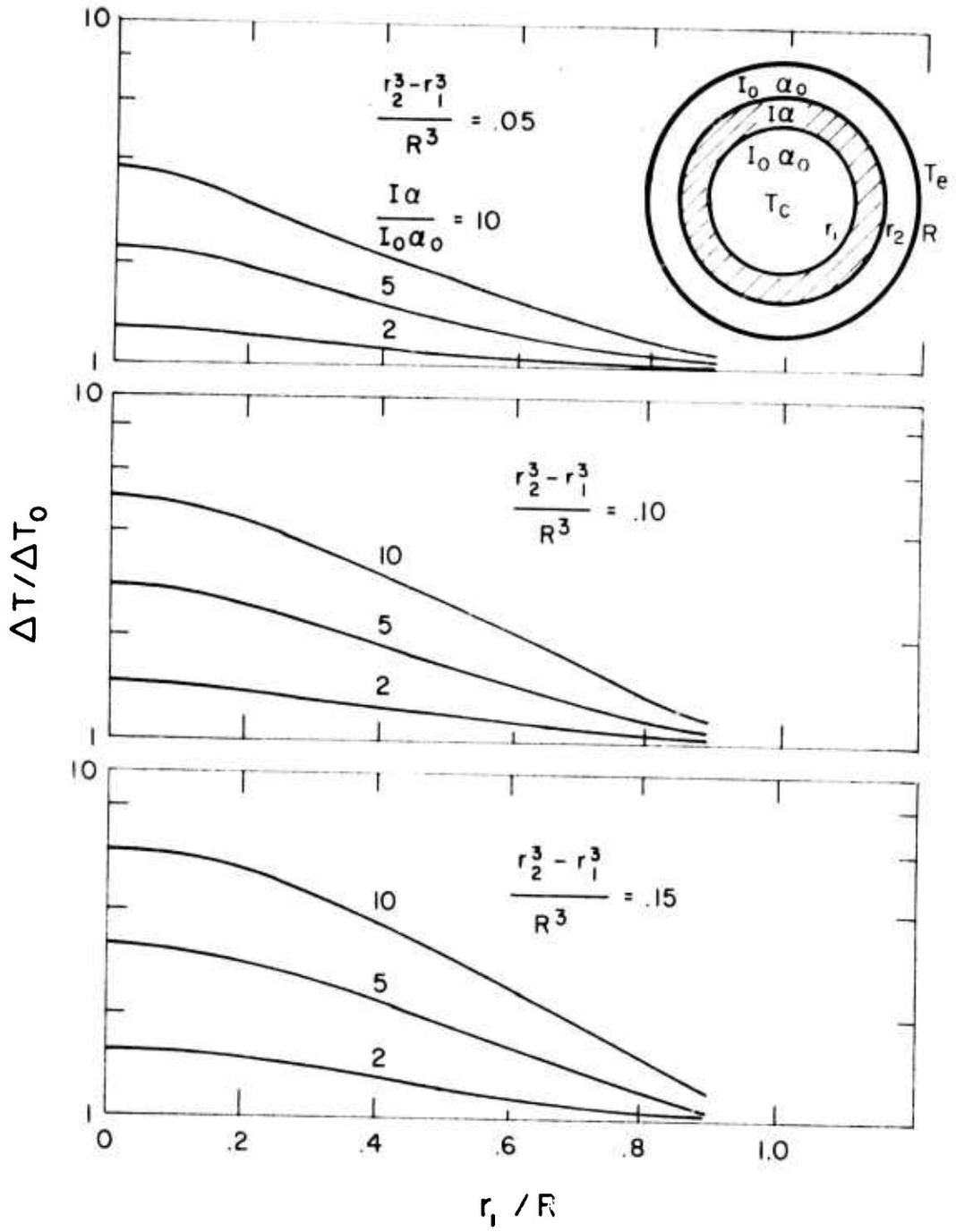

Fig. 33 Differential Heating Within Spherical Shell. The volumetric absorption rate $I\alpha$ applies to the region $r_1 < r < r_2$. Values of $\Delta T = T_c - T_e$ are shown as functions of r_1 for shell volumes of 5, 10 and 15% of the total sphere volume.

B. Vaporization Coefficient

In all the cases shown in this report the mass loss calculations are based on diffusion with a driving vapor pressure concentration at the droplet surface assumed to be the saturated vapor pressure at the surface temperature. This assumption has limitations which have been known for many years. To assess the effect of these limitations, one may examine the steady state diffusive evaporation of a droplet, following the analysis given by Fuchs.[27] The straightforward Maxwell solution for vaporization in the absence of temperature gradients gives the diffusive flux as

$$J = 4\pi r D \left\{ c(r) - c_\infty \right\} \quad g/sec \tag{51}$$

where D is the diffusion coefficient (cm^2/sec), and water vapor concentrations c (r) and c_∞ are in g/cm^3. Near the droplet the flux may also be written as

$$J = 4\pi R^2 (c_o - c_1) \nu \alpha_v, \tag{52}$$

where c_o is the concentration at the surface R, c_1 the concentration at a distance Δ above the surface, $\nu = \sqrt{kT/2\pi m}$ cm/sec, and α_v is the vaporization coefficient for the liquid, usually set equal to the condensation coefficient for the vapor. In the region $R < r < R + \Delta$, where Δ is roughly two or three times the gaseous mean free path, the concentration gradient is much steeper than in the region where steady state diffusion is established. Since Eq. (51) gives $J = 4\pi (R + \Delta) D (c_1 - c_\infty)$, we may use Eq. (52) to eliminate c_1 and obtain

$$J = \frac{4\pi R D (c_o - c_\infty)}{\left(\frac{R}{R + \Delta} + \frac{D}{R \nu \alpha_v} \right)} \tag{53}$$

Thus, the Maxwell flux obtained by setting r = R in Eq. (51) is reduced by the factor in the denominator of Eq. (53). Now at sea level the mean free path is $\approx$ 0.06 μm, so that the term $R/(R + \Delta)$ does not differ appreciably from unity unless $R < 0.5\ \mu m$, which is approximately the lower limit of interest for the present study. The other term may be approximated as

$$\frac{D}{R\nu\alpha_v} \approx \frac{1}{6\alpha_v}\,(10^4/R) \tag{54}$$

and at the start of the present study it was felt that this term could be neglected for $R \gtrsim 0.5\ \mu m$, since the most recent experimental evidence[22-24] indicated that $\alpha_v \approx 1$. Under these circumstances the two terms in the denominator of Eq. (53) tend to be self-compensating, and their sum remains close to unity.

However, recent work[25] has tended to revive the justification for using $\alpha_v = .033$ for water condensation, so that the term

$$\frac{D}{R\nu\alpha_v} \approx 5\ (10^{-4}/R) \tag{55}$$

which does not become negligible until $R >> 5\ \mu m$. Even for much larger drops, when the reduction factor approaches unity, one still finds a significant effect on the vaporization process if $\alpha_v << 1$.

As pointed out in Section IV the diffusion solution is only valid for values of $R^2 I\alpha$ where vaporization is not strongly dominant and convection terms may be neglected. For small droplets which do not reach the boiling point (as an example from Fig. 4 for droplets with $R \lesssim 3\ \mu m$ for a nominal value of $I\alpha = 2.7 \times 10^5$ cal/cm^3-sec) the diffusion solution, Eq. (53), is appropriate. From Eq. (55) it can be seen that the vaporization rate will be considerably smaller than that predicted in Section IV if $\alpha_v = 0.033$ rather than unity. Indeed the quantity $1 + D/(R\nu\alpha_v)$ may be envisioned as a correction to the diffusion coefficient at the droplet surface, i.e.

$$D_s = \frac{D}{1 + \frac{D}{R \nu \alpha_v}} \tag{56}$$

In Section IV it was shown that the ratio of the absorbed energy going into conduction to that going into vaporization was inversely proportional to the diffusion coefficient at the surface for droplet sizes with steady state temperatures $\lesssim 40^{\circ}$ C (see Eq. (33)). If Eq. (56) is used for this diffusion coefficient, with $\alpha_v = 0.033$, Eq. (33) would predict that conduction strongly dominates vaporization for these particle sizes. As discussed in Section IV the opposite would be true if α_v were unity. A corollary to this increased conduction would, of course, be that the predicted steady state temperatures of these droplets would approach those predicted for the case of heat conduction alone as shown in Fig. 4.

An additional consequence of Eq. (52) occurs at large droplet sizes or laser intensities where vaporization dominates. It was pointed out in Section IV that in this limit

$$J = - dm/dt = 4/3 \pi R^3 I \alpha / \Delta H_v \tag{34}$$

Since it is known from Eq. (52) that this mass efflux is kinetically limited, Eq. (34) must put a constraint on the surface vapor concentration. The modeling presented so far was developed under the constraint of a constant pressure gas. It is a necessary but obviously not sufficient criterion that

$$(c_o - c_l) R_v T < 10^6 \text{ dynes/cm}^2 \tag{57}$$

for the gas to be at constant pressure. (Actually this quantity should be considerably less than 10^6 dynes/cm^2 since $r_l = R + \Delta \sim R$). If Eq. (52) and Eq. (34) are equated it can be readily seen that the constraint (57) will only be satisfied if

$$R I\alpha < \frac{3 \times 10^6 \alpha_v \Delta H_v}{(2 \pi R_v T)^{1/2}} \tag{57}$$

or for $\alpha_v = 0.033$, and $T = 373^\circ$ K,

$$R I\alpha < 600 \text{ cal/cm}^2\text{-sec} \tag{58}$$

For a nominal value of $I\alpha = 2.7 \times 10^5$ cal/cc-sec this corresponds to $R < 22$ μm. Thus, it would appear that if $\alpha_v = 0.033$, significant overpressure (probably leading to shock formation) could occur at relatively moderate particle sizes and laser intensities. The isobaric vaporization modeling developed in this report would not be valid in such situations.

C. Solution Droplets

All of the work presented above has been explicitly concerned with pure H_2O droplets, although it is well recognized that all naturally occurring aerosol droplets contain original nucleus material, which may be entirely in solution or remain partially insoluble. Junge and McLaren[28] claim that very few aerosol nuclei contain less than 25% soluble material, and cite measurements for which 70% of the cases contained more than 50% soluble material.

1. Droplet Growth

Much work on growth of solution droplets has been carried out by cloud physicists, and an extensive literature is largely applicable to the present situation. The equilibrium vapor pressure p'_r at the surface of a droplet of radius R is expressed relative to the vapor pressure p_∞ over a plane H_2O (pure) surface at the same temperature. It will be shown that

$$\frac{p r'}{p_\infty} = (a_w)^{\rho_w/\rho'_D} \exp\left(\frac{2\sigma'}{R\,\rho'_D\,R_v\,T}\right) \tag{59}$$

where a_w is the activity of the solvent and σ', ρ'_D are, respectively, the surface tension and density of the solution.

Variants of this equation exist in the literature: the present discussion combines the approaches of Mason[10] and Low[29]. The change in free energy when an elemental mass dm of H_2O is transferred from a solution droplet to the plane water surface is

$$\Delta G = \sigma' d A - \Pi dv = dm/\rho'_D (2\sigma'/R - \Pi) \tag{60}$$

where $\Pi = -R_v T \rho_w \ln a_w$ is the osmotic pressure expressed in terms of the activity of the solvent, which itself in turn is a function of solute concentration. The vapor pressure is obtained by noting that the relationship

$$\Delta G = dm\, R_v T \ln (p'_r/p_\infty) \tag{61}$$

expresses the change in free energy to vaporize water at p'_r, compress to p_∞, and condense back to liquid. Equating the two expressions for ΔG results in

$$\ln p'_r/p_\infty = \frac{\rho_w}{\rho'_D} \ln a_w + \frac{2\sigma'}{R\,\rho'_D\,R_v\,T} \tag{62}$$

which is equivalent to Eq. (59).

The solvent activity a_w is generally tabulated as a function of molality of the solution. Low[29] provides tables for eight common electrolytes which are found in aerosols. To obtain the molality for a solution containing m' gm of solute of molecular weight M' one first obtains the H_2O mass, $\frac{4\pi}{3} R^3 \rho'_D - m'$. The molality, m_s (moles of solute per kg of H_2O), is then

$$m_s = \frac{1000\, m'/M'}{\frac{4}{3}\pi R^3 \rho'_D - m'} \tag{63}$$

An important aspect of the application of Eq. (59) is the fact that for a given mass of solute one can in general find a droplet radius consistent with a value of p'_r which yields p'_r/p_∞ equal to the prevailing relative humidity. Note that this can never happen for pure H_2O droplets for which $a_w = 1$, since an equilibrium droplet then always requires supersaturated surroundings. This was to some extent a drawback in the pure H_2O calculation of droplet evaporation; if the surface tension term is neglected and the R.H. maintained at 100% a pure H_2O droplet remains in equilibrium, but if a lower R.H. were specified then evaporation would be in process before the droplet was laser-irradiated.

For the solution droplets, however, this drawback does not exist. Considering a 10^{-13} gm particle of NaCl in a saturated solution ($\sim$ 26% NaCl by mass, molality $\sim$ 6), one obtains $\rho'_D = 1.194$ gm/cc (also a weak function of concentration), $R = 0.425\ \mu m$, and thus from Eq. (59) $p'_r/p_\infty \approx 0.80$, so that such a droplet would be in equilibrium at RH = 80%. At higher humidity the droplet would increase in radius and decrease in salt concentration until it established a new equilibrium. Such curves are shown in Fig. 34, the shape of the radius vs. RH being very close to the empirical expression given by Hodges[4]. This is shown explicitly in Fig. 35 where the predicted droplet radius vs. relative humidity as determined by the variation of activity with molality is displayed for a NaCl particle of 10^{-13} gm. The droplet size shown is normalized by the droplet size at saturation (which occurs at R.H. $\approx$ 80%). Larger salt particles would exhibit the same growth law, however, as the salt particle size is decreased surface tension effects can become important and these would modify the growth law. Shown for comparison is the growth law of Hodges[4], Eq. (2), normalized by the value of F at 80% R.H. The comparison is quite good.

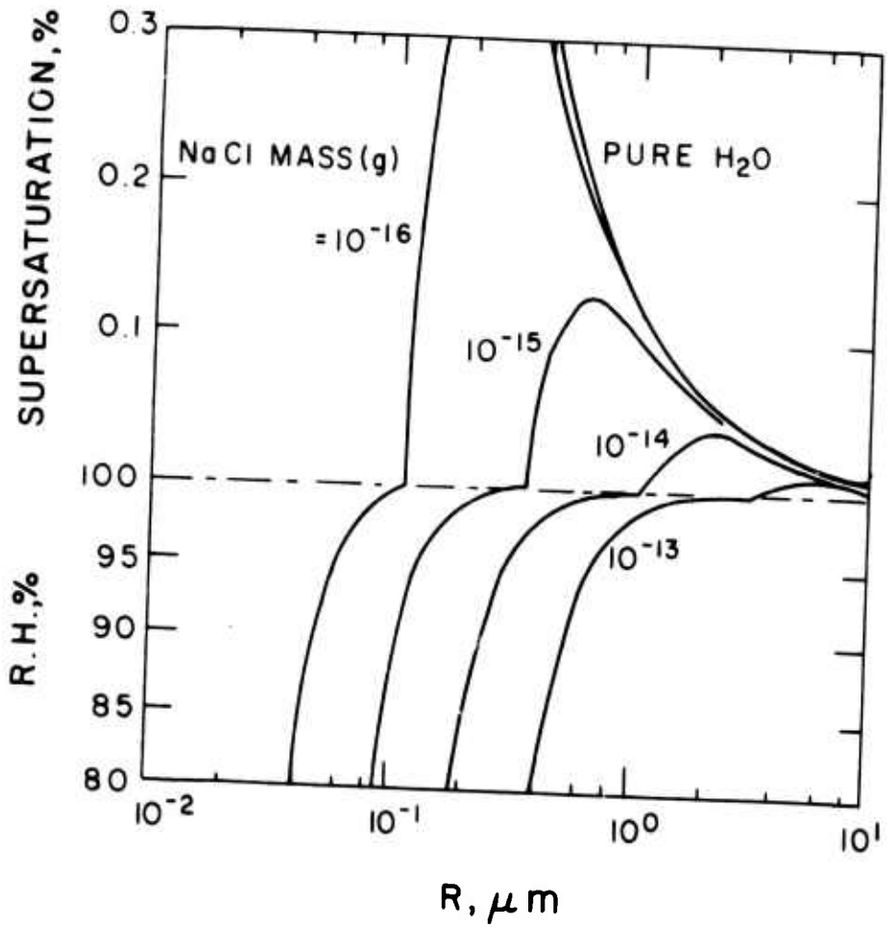

Fig. 34 Equilibrium Radii of Salt Solution Droplets as a Function of Relative Humidity or Supersaturation (note scale change above R.H. = 100%). Curves are reproduced from Ref. 10.

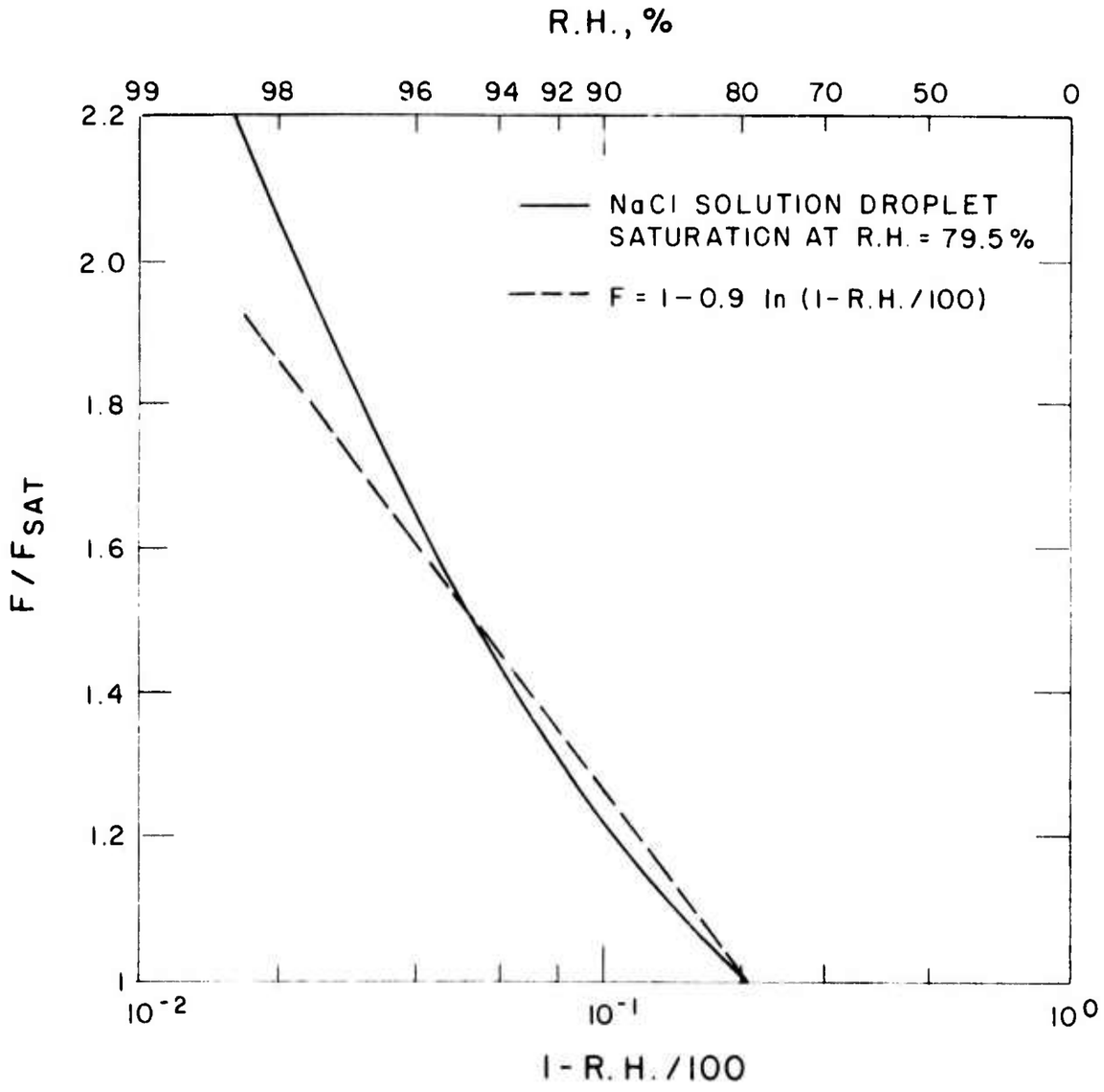

Fig. 35 Growth Curve for Equilibrium Radius of Salt Solution Droplet as a Function of Relative Humidity. Solid curve is calculated as in Fig. 34, valid for NaCl mass $\geq 10^{-13}$ g; dashed curve is taken from Ref. 4.

Unfortunately, the present analysis cannot be used at relative humidities below the saturation limit. The determination of p'_r/p_∞ is equally direct for a mixture of solutes, as Chen[30] has pointed out that the water activity can still be established from the individual solvent-solute values of a_w, with appropriate weighting over the molality of each solute component.

The major effect of inclusion of solution properties into the modeling of aerosol heating would be to reduce the vapor pressure at the droplet surface, making the diffusion boundary condition a function of both surface temperature and salt concentration in the droplet. As vaporization proceeded, the solute concentration would increase, and the vapor pressure would become an even smaller fraction of the saturated vapor pressure.

2. Solute Concentration Gradients within the Droplet

The evaporation of the solvent (H_2O) occurs at the droplet surface, so that solute must diffuse towards the center of the droplet to restore uniformity of concentration. In practice this will almost certainly not occur on a sufficiently fast time scale, and it will be necessary to compute or approximate the concentration gradients. A rough estimate of the behavior can be obtained as follows: consider a droplet of radius R_o, with solute concentration c_o gm/cc at the surface. If the solution density is ρ_D gm/cc at the surface, then the H_2O concentration there is $(\rho_D - c_o)$ gm/cc. As water leaves the surface, one can imagine it being replaced by water flowing from the center of the droplet. This is not quite the physical situation of the evaporating droplet, and to make a steady state situation one must postulate a source flow of H_2O at the droplet center. The solute then has a positive gradient, and attempts to diffuse back to the center against the convective velocity of the water. The solute concentration at radius r is then given by $\ln (c/c_o) = A\,(1/R - 1/r)$, and the H_2O flux is $4\pi R^2 D \rho_D \frac{\partial \ln c}{\partial r} = 4\pi D \rho_D A$ gm/sec. The constant A may be established by specifying the radius r' at which c/c_o is some convenient fraction, say, an e-folding distance, so that $-1 = A\,(1/R - 1/r')$, and the flux $= 4\pi D \rho_D R/(R/r' - 1)$ gm/sec. Now, as can be seen

from Eq. (34), one can equate the H_2O mass loss to $\beta 4\pi R^3 I\alpha / 3\Delta H_v$ g/sec, where β is the fraction of absorbed laser energy which goes into vaporization. Equating the two fluxes results in

$$\frac{R}{r'} - 1 = \frac{3\Delta H_v D \rho_D}{\beta R^2 I \alpha} \tag{64}$$

Inserting $D = 0.6 \times 10^{-5}$ cm^2/sec and $\rho_D = 1.2$ g/cc for NaCl solutions,

$$\frac{R}{r'} - 1 = \frac{.0123}{\beta R^2 I \alpha} \tag{65}$$

For small values of laser flux $R/r' >> 1$, which implies that concentration gradients are very small. But for $R^2 I \alpha \approx 1$ we have $R/r' = 1 + \frac{.0123}{\beta}$. The gradients within the droplet will thus depend critically on the fraction of energy going into vaporization; if $\beta \approx .1$, say, then the e-folding location will be very close to the droplet surface. Under such circumstances a real droplet would develop very high solute concentrations near the surface, probably reaching saturation level. Even supersaturation is a possibility, since the recrystalization process would require nucleation and could well be kinetically limited.

3. Ebullition

The possibility of nonuniform heating as well as the relatively large temperature differences which can exist within the droplet, i.e. Eq. (43), dictate that the possibility of boiling within a droplet be considered. If a bubble of vapor were to exist within a droplet, instantaneously in mechanical equilibrium, and also in thermal equilibrium with the parent liquid, then the pressure within the bubble would be $p^* = P + 2\sigma/r^*$, where P is the hydrostatic droplet pressure. Taking $\sigma = 58.9$ dynes/cm at $T \sim 100^\circ$ C, results in

$$p^*/p = 1 + 1.178\,(10^{-4}/r^*) \tag{66}$$

Thus, even a bubble of radius 1.2 μm would require a saturation vapor pressure of 2 atm to sustain itself, and this would require a liquid temperature of ~121° C. A smaller bubble in water at that temperature would collapse, while a larger one would grow. The size for a self-sustaining bubble is so large that it seems extremely unlikely that such bubbles could spontaneously appear within a 20-50 μm droplet with no solid present to act as a nucleation site. The same statement can be made even more strongly for a solution droplet with no insoluble nucleus, since the solute elevates the boiling point, and raises the requirement for superheat.

However, if a supersaturated solution began to crystallize, or if an insoluble nucleus were present in the droplet it is clear that nonuniform heating could lead to internal temperatures which would yield vapor bubbles inside the droplet. Indeed, an insoluble nucleus with high absorption coefficient could enhance the nonuniform heating within the droplet to the extent depicted in Fig. 32. Thus, this aspect of the ebullition question merits further study.

D. Summary of Droplet Effects

All the effects discussed which relate to surface vaporization of the droplet can contribute to reducing the mass loss and thereby increasing the transfer of heat to the surrounding air by conduction. These effects include use of an evaporation coefficient $\alpha_v = .033$ instead of $\alpha_v \approx 1$, and lowering of vapor pressure at the surface of solution droplets. Focusing of the laser radiation and nonuniform heating effects tend to increase the heat transfer to the droplets relative to the volumetric absorption rates, and to lead to possibilities of ebullition which could in turn lead to droplet shattering.

VI. BEAM PROPAGATION EFFECTS

This section is concerned with the resultant effects of aerosol heating and vaporization on laser beam quality. "Blooming" of the laser beam can be caused by two separate effects. The first of these is that the heated air around the aerosol will have a different index of refraction from ambient. The changes in the index of refraction across the beam width can be a complicated function of both laser intensity and the aerosol size distribution function. In general, the phase shift produced in a wave propagating through this nonuniform medium will depend upon these variables and thus there will be variations in beam refraction across the laser beam width. Along with the temperature variation around the aerosols there will also be a variation of water vapor concentration. Although the amount of water vapor vaporized from the aerosols will be insignificant compared to the ambient vapor concentration the former will be sharply peaked around the aerosols and in that region can provide a major part of the total index of refraction. While the index of refraction of water vapor is different from that of air there do not appear to be any measurements of n_{H_2O} for infrared wavelengths.[31] It is clear, however, that n_{H_2O} would have to be significantly different from n_{air} for the water vapor perturbations to be as important as the temperature perturbations (note at $\lambda = 0.8\ \mu m$ the ratio $(n_{H_2O} - 1)/(n_{air} - 1) \approx 0.9$). Only the effect of temperature/density variations will be considered in the following analysis.

The prediction of beam propagation through the temperature fields caused by heated, vaporizing aerosols is a very complex problem which will not be treated in detail in this section. However, crude estimates of the resulting phase shifts will be made. Both Cook and Butts[2] and Lencioni and Kleiman[3] have examined beam propagation through the temperature

fields resulting from the heating of nonvaporizing aerosols. Cook and Butts[2] applied the first Born approximation to the wave equation to predict the average scattering cross section of an aerosol particle. They concluded that scattering from the hot bubbles would only be important at large irradiation times ($t \gtrsim 1$ sec. for $I = 10^4$ W/cm^2).

Lencioni and Kleiman performed a similar analysis for the scattering cross section but also predicted the average phase shift a wave experiences in propagating through the hot air bubble about a heated nonvaporizing aerosol. In this analysis they used the analytical heat conduction solution and included beam shape effects. They made the interesting point that there is a hydrodynamic sphere outside the heated sphere which has a positive density gradient resulting from the gas which had been convected outside of the heated bubble at the speed of sound. The inner radius of this hydrodynamic sphere occurs somewhere beyond $r \sim \sqrt{4 k_A t/\rho C_{P_A}}$, the point where the conduction solution falls off, and the outer radius is, of course, given by ct.

Their main conclusion is that to first order for short times the average phase change a wave undergoes in traversing the hydrodynamic bubble is equal and opposite to that experienced within the heated bubble. This results because of mass conservation, i.e. the increase in mass above ambient in the hydrodynamic bubble must balance the decrease in mass in the heated bubble.

A complication in this is that the hydrodynamic bubble is not well defined. For the continental distribution described in Section II the average spacing between aerosols is ~ 2 mm. The heated bubbles at times of msecs are typically a few hundred μm in radius and thus will not overlap; however, at a time of 1 msec the outer radius of the hydrodynamic bubbles will be 30 cm which is of the order of the laser beam width. Thus, not only will there be a strong overlap between the hydrodynamic bubbles of neighboring aerosols but also much of the excess mass will have passed outside of the beam extent.

Because of this one could conclude that the phase shift encountered on passing through the heated bubble should provide a reasonable, albeit somewhat crude estimate of the total phase shift encountered by the wave after an irradiation time $\gtrsim$ 1 msec[3]. In any event in the case of a vaporizing molecule mass is added to the gas at the expense of the droplet and the constraint of gaseous mass conservation does not apply even at short times.

Predictions of the phase shift induced in a wave propagating through a heated air bubble can be readily performed. The index of refraction near the droplet is changed due to the change in air temperature. This change in index of refraction will cause a position dependent phase shift for rays passing through the heated air. At constant pressure the index of refraction, n, at temperature T is related to the ambient index of refraction, n_∞, at temperature T_∞ by:

$$\frac{n - 1}{n_\infty - 1} = \frac{T_\infty}{T} \tag{67}$$

The present analysis will be restricted to cases where $T - T_\infty$ is much less than T_∞. Then expanding Eq. (67) in a binomial series and keeping only the first two terms results in

$$n \tilde{=} n_\infty - \frac{(n_\infty - 1)\,\Delta T}{T_\infty} \tag{68}$$

where $\Delta T = T - T_\infty$. This index of refraction will be used to calculate the optical path through a heated air bubble.

The optical path length of a ray is defined by

$$OP = \int_C nds \tag{69}$$

where the ray is taken to follow a curve C through the medium and ds is the differential element along this curve C. Given an expression for the temperature field about the droplet Eq. (68) and (69) can be combined to evaluate OP. As discussed in Section IV the radial temperature distribution about a heated aerosol droplet at moderate laser intensities such that convection could be neglected was given by

$$\Delta T(r) \cong \frac{\Delta T(R)\, R}{r} \tag{25}$$

for the regime $R < r < r_o$, where R is the aerosol droplet radius, r is the radial distance from the droplet center, and r_o is a characteristic heat conduction length, $\sqrt{4 k_A t/\rho C_{P_A}}$. Combining Eq. (25) with (68) results in

$$\begin{aligned} n &= n_\infty - \frac{(n_\infty - 1)\,\Delta T(R)\, R}{T_\infty\, r} && R \leq r \leq r_o \\ &\approx n_\infty && r > r_o \\ &= 1.36 && r \leq R \end{aligned} \tag{70}$$

In general in calculating the total path length the shape of the curve C must also be evaluated. In the following analysis C will be taken as a straight line and it will be seen that the increase in path length over ambient, ΔOP, is sufficiently small to justify this.

A heated air bubble of radius r_o is sketched below. If a ray

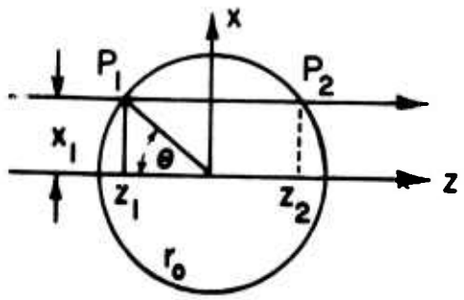

enters at point P_1 and exits at point P_2 it can readily be shown from Eqs. (69) and (70) that

$$OP \approx n_\infty (z_2 - z_1) + \frac{2 (n_\infty - 1) \Delta T (R) R}{T_\infty} \ln[\tan(\theta/2)] \qquad (71)$$

providing that $x_1 > R$. (Entry points P_1 corresponding to $x_1 < R$ will be excluded from the analysis). Thus

$$\Delta OP = \frac{2 (n_\infty - 1) \Delta T (R) R}{T_\infty} \ln [\tan (\theta/2)] . \qquad (72)$$

Note that the quantity ΔOP is not independent of bubble size since $\theta = \sin^{-1} (x_1/r_o)$.

A detailed phase shift prediction would require tracing a wave propagating through an ensemble of such heated bubbles, as expected from a typical aerosol distribution, including the wave refraction and random entry sites, x_1, at each bubble. Instead the average phase shift encountered in propagating through a bubble will be calculated as an estimate of the actual solution.

The quantity $\ln [\tan (\theta/2)]$ can vary considerably for values of x_1/r_o between R/r_o and unity. However, it can be shown that the average value of ΔOP defined by

$$\overline{\Delta OP} = \frac{\int_R^{r_o} \Delta OP \, 2\pi x_1 \, dx_1}{\pi (r_o^2 - R^2)} \qquad (73)$$

is given by

$$\overline{\Delta OP} \approx \frac{2\,(n_\infty - 1)\,\Delta T(R)\,R}{T_\infty} \tag{74}$$

So far this analysis is similar to that of Lencioni and Kleiman[3]; however, in the case of a water droplet the quantity $\Delta T(R)$ will no longer be linearly proportional to $I\alpha$ for values of $R^2 I\alpha \gtrsim 10^{-2}$-$10^{-1}$ cal/cm^3-sec.

As a specific example of the average phase shift encountered by a wave propagating through an atmospheric aerosol distribution consider the case of the standard continental distribution, Eq. (1), at an R.H. of 98%. The average phase shift is given by

$$\langle \phi \rangle = z \pi r_o^2 \frac{2\pi}{\lambda} \int_{R_1}^{R_2} \overline{\Delta OP} \frac{dN_A}{dR}\, dR \tag{75}$$

where z is the range in cm and dN_A/dR is the aerosol distribution given by

$$\frac{dN_A}{dR}\,(\text{R.H.} = 98\%) \approx \frac{3.5 \times 10^{-11}}{R^4},\ \text{part/cm}^4 \tag{76}$$

for $0.5\ \mu\text{m} < R < 100\ \mu\text{m}$.

From reference to Fig. 4 it can be seen that

$$\Delta T(R) \approx \frac{R^2 I\alpha}{9 k_A} \quad ; \quad R^2 I\alpha \leq 4.5 \times 10^{-2}\ \text{cal/cm-sec}$$

$$\simeq 80^\circ\,\text{K}; \quad R^2 I\alpha > 4.5 \times 10^{-2}\ \text{cal/cm-sec} \tag{77}$$

or approximately 1/3 of the heat conduction solution for $R^2 I\alpha \leq 4.5 \times 10^{-2}$ cal-cm-sec. Considering as a specific example $I = 10^4$ watts/cm^2 and $\alpha = 113$ cm^{-1}, then $R^2 I\alpha = 4.5 \times 10^{-2}$ cal/cm-sec at $R = 4\,\mu$m. Therefore, coupling Eqs. (74) - (76) and the definition that $r_o^2 = 4 k_A t/\rho C_{P_A}$ results in

$$\langle\phi\rangle = \frac{16\pi^2 z k_A t (n_\infty - 1)}{\rho C_{P_A} \lambda T_\infty}\left[\int_{0.5\times10^{-4}}^{4\times10^{-4}} \frac{3.4\times10^{-11} I\alpha}{9 k_A R}\, dR + \int_{4\times10^{-4}}^{10^{-2}} \frac{3.5\times10^{-11}\times 80}{R^3}\, dR\right] \tag{78}$$

For this particular case the dominant contribution is provided by the first integral, for which $0.5 \leq R \leq 4\,\mu$m, and the result may be approximated as

$$\langle\phi\rangle \approx \frac{1.3\times10^{-9} z t (n_\infty - 1) I\alpha}{\rho C_{P_A} \lambda T_\infty} \tag{79}$$

Inserting $I\alpha = 2.7 \times 10^5$ cal/cm^3-sec, $n_\infty - 1 = 3 \times 10^{-4}$ and $\lambda = 3.8\,\mu$m yields

$$\langle\phi\rangle/z \approx 300\, t \text{ km}^{-1}, \tag{80}$$

corresponding to phase shifts of order unity at times of msecs and ranges of $\sim$ 1 km.

As long as the only droplets which can reach the boiling point come from the tail of the aerosol distribution function, the above result (Eq. (79)) is not strongly affected by the uncertainties discussed in previous sections

of this report. For instance, use of a vaporization coefficient of $\alpha_v = .033$ would raise the value of ΔT (R) in Eq. (77) by at most a factor of 3. On the other hand, at higher laser intensities the vaporization limit is approached at smaller droplet radii, and the details of the boiling phenomenon become more important in the determination of beam quality.

It should be emphasized that there is no justification for adding and averaging the phase shifts in the above analysis. This was done only in order to provide a gross estimate of the effect of aerosol heating on beam quality. More realistic predictions must await a more detailed analysis.

Furthermore, phase shifts resulting from molecular absorption can be larger, particularly if the H_2O vapor continuum absorption is as strong as it appears to be. However, as pointed out in Section II aerosol mass loadings higher than the standard continental distribution are commonly observed and can be the dominant absorbers. It should be emphasized that the functional form of Eq. (79) is similar to that resulting from uniform absorption because the individual phase shifts were averaged. This is functionally the same as averaging the density change in the gas.

VII. SUMMARY

A detailed model has been developed to predict the temperature and vapor fields resulting from the laser irradiation of small water droplets. The water droplets are considered to be representative of hygroscopic aerosols at high relative humidities. The model includes the effects of vaporization, heat conduction and convection. The model was developed under the assumption of a constant pressure gas and thus is valid only up to the isobaric vaporization limit.

Both steady state and time dependent solutions for the model have been discussed in some detail. It was shown that the predicted profiles of increase in gas temperature and water vapor scale inversely with distance from the droplet for moderate laser intensities and particle sizes. For larger laser intensities and/or particle sizes convection began to dominate conduction and diffusion resulting in more bowed profiles. It was demonstrated that the model was specifically valid only if the evaporation coefficient for water α_v approached unity. It was pointed out that recent evidence suggests that α_v is considerably smaller than unity and if this is so, the model must be modified accordingly.

A number of effects corresponding to real aerosol properties not included in the model were discussed in some detail. These include nonuniform absorption and heating, solution effects including recrystallization and ebullition. It is concluded such phenomena could be important under extreme conditions corresponding to heavy vaporization and/or droplet superheating. Estimates of the characteristic phase shifts a wave will encounter in propagating through a heated aerosol distribution were also presented.

There are several areas of this problem which warrant further study:

a) The estimates of characteristic phase shifts are sufficiently large to require that a more accurate prediction be performed.

b) Model predictions should be made for the case of $\alpha_v = 0.33$. Furthermore, a firmly established value of this quantity would be valuable.

c) The absorption coefficient of liquid water near 3.8 μm should be re-examined along with its temperature dependence in order to clear up present uncertainties.

d) Lastly, the water vapor continuum absorption coefficient and index of refraction near 3.8 μm should be measured near room temperature.

ACKNOWLEDGEMENTS

The authors are grateful to Drs. P. N. Nebolsine and K. L. Wray for their contributions during many useful discussions on the subject matter of this report.

REFERENCES

1. G. H. Canavan, "Thermal Blooming Due to the Heating of Aerosols", AFWL Laser Digest, AFWL-TR-73-273, p. 66, December 1973.

2. R. J. Cook and R. R. Butts, "Aerosol Induced Thermo-Optical Degradation of a High Intensity Laser Beam," AFWL Laser Digest, AFWL-TR-73-272, p. 69, December 1973.

3. D. E. Lencioni and H. Kleiman, "Effects of Aerosol Particle Heating on Laser Beam Propagation", Lincoln Lab. Project Rept. LTP 27, July 22, 1974.

4. J. A. Hodges, "Aerosol Extinction Contribution to Atmospheric Attenuation in Infrared Wavelengths", Appl. Opt. 11, 2304 (1972).

5. A. D. Wood, M. Camac and E. T. Gerry, "Effects of 10.6 μ Laser Induced Air Chemistry on the Atmospheric Refractive Index", Appl. Opt. 10, 1877 (1971).

6. P. B. Ulrich, J. N. Hayes, J. H. Hancock and J. T. Ulrich, "Documentation of PROP E, A Computer Program for the Propagation of High Power Laser Beams Through Absorbing Media", Naval Research Lab. Rpt. 7681, May 29, 1974.

7. G. E. Caledonia and K. L. Wray, "Aerosol Propagation Effects, Mid-Contract Report", Physical Sciences Inc. Rpt. PSI TR-6, June 1, 1974.

8. W. A. Proctor, "A Short Descriptive Survey of Atmospheric Aerosols," AFWL Laser Digest AFWL-TR-73-131, pp. 69-77 (1973).

9. E. A. Barnhardt and J. L. Streete, "A Method for Predicting Atmospheric Aerosol Scattering Coefficients in the Infrared" App. Opt. 9, 1337 (1970).

10. B. J. Mason, "The Physics of Clouds", Clarendon Press, Oxford, 1971.

11. S. Tsunogai, O. Saito, K. Yamada, S. Nakaya, "Chemical Composition of Oceanic Aerosol", JGR 77, 5283 (1972).

12. E. deBary, K. Bullrich, R. Eiden, G. Eschelback and G. Hanel, "Research on Atmospheric Optical Radiation Transmission", Johannes Gutenberg University, Mainz Germany, published as AFCRL-72-0180, February 1972.

13. G. M. Hidy, "Theory of Formation and Properties of Photochemical Aerosols", presented at Summer Institute, Battelle Seattle Research Center June 18-29, 1973.

14. H. C. Van de Hulst, "Light Scattering by Small Particles", John Wiley and Sons, New York, 1957.

15. G. M. Hale and M. R. Querry, "Optical Constants of Water in the 200 nm to 200 μm Wavelength Region", App. Opt. 12, 555 (1973).

16. P. S. Ray, "Broadband Complex Refractive Indices of Ice and Water", App. Opt. 11, 1836 (1972).

17. R. A. McClatchey and J. E. A. Selby, "Atmospheric Attenuation of HF and DF Laser Radiation," AFCRL Report 72-0312, May 23, 1972.

18. D. F. Burch, Ford Aeronutronic Report U-4784, January 1970.

19. G. W. Sutton, "Fog Dispersal by High Power Lasers" AIAA J. 8, 1907 (1970).

20. S. L. Glickler, "Propagation of a 10.6 Micron Laser through a Cloud Including Droplet Vaporization", App. Opt. 10, 644 (1971).

21. F. A. Williams, "On Vaporization of Mist by Radiation", Int. J. Heat and Mass Transfer 8, 575 (1965).

22. C. S. Chen, "Evaluation of the Water Vapor Diffusion Coefficient in the Drop Growth Equation", J. Atm. Sci. 31, 845 (1974).

23. A. F. Mills, "The Condensation of Steam at Low Pressures", Tech. Rept., NSF Grant GP-2520, Series No. 6, Issue No. 39, Space Science Laboratory, Univ. of California, Berkeley (1965).

24. H. A. Duyuid and J. F. Stampfer, Jr. "The Evaporation Rates of Small, Freely Falling Water Drops", J. Atmos. Sci. 28, 1233 (1971).

25. N. Chodes, J. Warner and A. Gayin, "A Determination of the Condensation Coefficient of Water from the Growth Rate of Small Cloud Droplets, J. Atmos. Sci. 31, 1351 (1974).

26. H. S. Carslaw and J. C. Jaeger, "Conduction of Heat in Solids", Oxford at the Clarendon Press, 1959.

27. N. A. Fuchs, "Evaporation and Droplet Growth in Gaseous Media", Pergamon Press, London, 1959.

28. C. Junge and E. McLaren, "Relationship of Cloud Nuclei Spectra to Aerosol Size Distribution and Composition," J. Atm. Sci. 28, 382 (1971).

29. R. D. H. Low, "A Generalized Equation for the Solution Effect in Droplet Growth," J. Atm. Sci. 26, 608 (1969).

30. C. S. Chen, "Evaluation of the Vapor Pressure Over an Aerosol Particle", J. Atm. Sci. 31, 847 (1974).

31. S. Nir, S. Adams and R. Rein, "Polarizability Calculations on Water, Hydrogen, Oxygen and Carbon Dioxide", J. Chem. Phys. 59, 3341 (1973).